1-1-1971

Viscoelastic properties of blends of high molecular weight polymers.

William Marchan Prest
University of Massachusetts Amherst

VISCOELASTIC PROPERTIES

OF

BLENDS OF HIGH MOLECULAR WEIGHT POLYMERS

A Dissertation Presented

By

William Marchant Prest, Jr.

Submitted to the Graduate School of the
University of Massachusetts in
partial fulfillment of the requirements for the degree of

DOCTOR OF PHILOSOPHY

November 1971

Major Subject: Polymer Science and Engineering

VISCOELASTIC PROPERTIES

OF

BLENDS OF HIGH MOLECULAR WEIGHT POLYMERS

A Dissertation

By

William Marchant Prest, Jr.

Approved as to style and content by:

R S Porter
(Chairman of Committee)

R S Porter
(Head of Department)

Richard S. Stein
(Member)

Stanley Middleman
(Member)

November 1971

Dedicated to the women in my life

Edie, Peggy, and Eelo

ACKNOWLEDGMENT

I would like to express my thanks and appreciation to those professors, students, and professionals whose discussions helped to formulate the ideas developed in this thesis.

Specific gratitude is extended to my thesis advisor, Professor Roger S. Porter, for his encouragement, support, and direction.

I am also indebted to the members of the Polymer Physics Branch of the General Electric Research and Development Center, and in particular to Dr. James M. O'Reilly, for introducing me to the field of Polymer Science and giving me invaluable encouragement in my initial endeavors.

Fellowship and research support from the Plastic Institute of America and the Paint Research Institute were sincerely appreciated. Special thanks for their encouragement, aid, and direction are extended to Dr. A. Meyer and Dr. R. Meyers.

PREFACE

This thesis consists of four related manuscripts concerning the viscoelastic properties of blends of high molecular weight polymers. The manuscripts are presented as submitted for publication. Extended discussions of related subjects are presented in the appendices.

Chapter I is based on data obtained at the General Electric Research and Development Center with Dr. J.M. O'Reilly, who originally suggested the form of analysis. The first author subsequently developed this idea in conjunction with Dr. Roger S. Porter. Raw data obtained for papers II-IV is on file with Dr. Roger S. Porter at the University of Massachusetts.

TABLE OF CONTENTS

CHAPTER I

Non-Newtonian Flow and the Steady State Shear Compliance

W. M. Prest, Jr. and Roger S. Porter
Polymer Science and Engineering Program
University of Massachusetts
Amherst, Massachusetts 01002

and

J. M. O'Reilly
Xerox Research Laboratories
Webster, New York

SYNOPSIS

A survey of viscoelastic data on amorphous polymer melts indicates that the steady state shear compliance, J_e^o of many systems can be approximated from a knowledge of their flow response. For systems with monomodel molecular weight distributions, the absolute value of the reduced complex viscosity, η^*/η_o is found to equal 0.67 ± 0.03 at the frequency ω, where $\omega\eta_o J_e^o = 1$. This result applies to a variety of polymer systems and to a wide range of molecular weights and distributions as long as the highest molecular weight dispersion of the distribution constitutes more than 20 weight percent of the sample. This relationship determines J_e^o from non-Newtonian flow data and thus provides a consistent way to relate differently shaped reduced variable curves and to calculate compliances from characteristic times reported in the literature. The connection between some commonly used times and J_e^o is given. The method of calculating J_e^o is successfully applied to capillary measurements of melt viscosities

and to characteristic times determined from steady state shear measurements of concentrated polymer solutions.

INTRODUCTION

Different forms for characteristic times, τ, have been used to classify the non-Newtonian response of polymeric systems. In simple models, a time τ is defined as the ratio of the zero-shear viscosity to the elastic modulus, or equivalently the product of η_o with the steady state shear compliance, J_e^o. The region of the onset of non-Newtonian flow is then characterized by a τ which is determined by the elastic properties of the system. More complex models involve multiple τ's which can be combined in prescribed ways to calculate the total compliance and viscosity. These measurable quantities, however, can only be used to determine an average characteristic time for non-Newtonian flow. When only a viscosity measurement is available a τ is customarily determined by fitting data to standard viscosity-shear rate curves or by finding a form of reduced variables which produce one curve from all data[1]. Average times determined in this manner should depend on the elastic properties of the system. This study attempts to empirically relate measured elastic properties to the shape of the viscosity-shear rate curve. This correction would provide a consistent method for describing non-Newtonian flow and would open data in the literature to the analysis of elastic properties.

In this study, the non-Newtonian response of several different types of polymer melts, with differing molecular weights and molecular weight

distributions, is correlated with the measured steady state shear compliance, J_e^o. This compliance is defined as the low frequency limit of the storage compliance, J'. The viscoelastic properties of these melts were measured at the General Electric Research and Development Center using a Weissenberg Rheogoniometer equipped with a version of the Birnboim[2] Ultra Low Frequency Phase Meter. The result of this correlation is then tested with capillary flow measurements of the melt viscosities of narrow distribution polystyrenes and with the reported characteristic times of concentrated solutions of linear polystyrenes and branched polyvinyl acetates.

Analysis:

Two of these authors[3] have formerly reported the approximately equal compliances for high molecular weight, commercial polydimethylsiloxanes with similar molecular weight distributions. It was noted that the reduced viscosity, the first normal stress difference and the shear storage modulus of these samples could be superimposed if the time scale for each sample was multiplied by the zero shear viscosity, η_o. The equal compliances of these samples makes this data reduction equivalent to using an average characteristic time, $\eta_o J_e^o$, as the reduced variable.

Dynamic data for seven polystyrene samples with weight to number average ratios from 1.06 to 2.6 were compared as a function of $\omega\eta_o J_e^o$, where ω is the frequency of the dynamic measurement. It was noted that the absolute value of the reduced complex viscosity, η^*/η_o of each sample is generally 0.67 at $\omega\eta_o J_e^o = 1$. This agreement is apparently

independent of the differences in the shapes of the viscosity curves. The value of 0.67 for the reduced viscosity corresponds to the point where the Bueche[4] theoretical curve crosses the Bueche-Harding[1] standard curve, shown in Fig. 1 of reference 1. Table I gives typical data on these samples. Figure 1 gives a comparison of η^*/η_o for two samples with approximately the same M_w but with different molecular weight distributions. The reduced complex viscosities of a series of narrow distribution polystyrenes with molecular weights from 4,800 to 411,000 and a tetra-branched star polystyrene with M_w = 205,000 are shown in Figure 2, where the time scales have been arbitrarily shifted for display purposes. The dot marks the point at which $\omega\eta_o J_e^o = 1$ and the dashed line corresponds to $\eta^*/\eta_o = 0.67$. This same relationship is found for a variety of commercial melts as is shown in Figure 3. These are samples of high density polyethylene, polypropylene, polydimethylsiloxane, polyisobutylene, poly-carbonate, and Silly Putty with compliances from 2.5×10^{-5} to 2.2×10^{-7} cm^2/dyne. The compliances used to calculate the value of $\omega\eta_o J_e^o = 1$ are defined to within $\pm$ 15%. On the curves presented this corresponds to $\eta^*/\eta_o = 0.67 \pm 0.03$. For most of the samples $\eta^*(\omega)$ coincides with the apparent steady shear viscosity $\eta_a(\dot{\gamma})$, until the onset of steady state flow instabilities. In cone and plate measurements this instability appears as a break in the free surface of the sample which creates an abnormally low apparent viscosity because of the reduced size of the sample. Many other experimenters[5-9] have reported the equivalent of $\eta_a(\dot{\gamma})$ and $\eta^*(\omega)$. This observation was used to verify and in some cases determine η_o from $\eta^*(\omega)$.

Figure 4 presents the distribution of the values of the reduced viscosity at $\omega\eta_o J_e^o = 1$ for 52 experiments on 32 different polymer melts. The average reduced viscosity is 0.67. The standard deviation of these measurements is 0.023, in agreement with the uncertainties expected from the experimental determination of J_e^o.

Measurements on the samples used in this study gave well defined values of the zero shear viscosity. This necessarily excluded samples with molecular weight distribution containing a broad, high molecular weight tail because η_o could not be determined. This class of materials would test the extent of the applicability of the correlation since the high molecular weight components are the first to contribute to non-Newtonian flow and have the greatest affect on J_e^o. The difficulty in measuring η_o can be circumvented using blends of well defined samples to simulate the extreme effect of different molecular weight distributions. The correlation between non-Newtonian flow and J_e^o was tested in this manner with the binary blends of high molecular weight polydimethylsiloxanes which were previously used to study the molecular weight distribution dependence of J_e^o [10]. The non-Newtonian behavior of the blends was used to calculate a compliance $J_{e\tau}^o$ defined as $(\omega\eta_o)^{-1}$ where ω is the frequency at which $\eta^*/\eta_o = 0.67$. These results are compared with the measured compliances, which are shown as lines, in Fig. 5. The apparent agreement of $J_{e\tau}^o$ with J_e^o is deceptive. When samples contain small amounts of high molecular weight material, the calculated compliance $J_{e\tau}^o$, is less than J_e^o. This difference is not apparent in Fig. 5 because of the high dependence of J_e^o on M_w in this region. The sign of this deviation reverses near the maximum in the compliance, see Fig. 5, where the calculated compliance is

greater than J_e^o. Importantly, beyond the maximum, where the high molecular weight components comprise more than 20 weight percent of the system, $J_{e\tau}^o$ is found to be within 15% of J_e^o. These results imply that the correlation is not applicable to solutions of polymers with concentration less than 0.2. The correlation may also not apply to samples with molecular weight distributions containing a small amount of very high molecular weight polymer.

Alternatively the correlation appears to apply to systems in which the compliance is primarily controlled by the high molecular weight components. (i.e. in Fig. 5, M_w above the maximum in J_e^o). Experimentally this included all melts which had measurable zero shear viscosities, with the exception of the extreme binary blends. It is concluded that the compliance of a polymer melt can be calculated from the measured non-Newtonian response, provided the high molecular weight components of the system comprise more than 20 weight percent of the sample.

Applications:

Calculation of J_e^o from Reported Characteristic Times

The connection between J_e^o and the non-Newtonian response provides a consistent method for relating the characteristic times of different viscosity-shear curves. The point at which the reduced viscosity becomes 0.67 is some fraction ζ of the particular time τ such that:

$$\eta_o J_{e\tau}^o = \zeta\tau \qquad (1)$$

Values of ζ for commonly used τ's are given in Table II. Calculations of compliances from these τ's require that the original data fit the

master curve at the point where the reduced viscosity equals 0.67. Note that ζ_{Bueche} is not twice ζ_{Rouse} as would otherwise be expected from the explicit forms of the characteristic times. This reflects the differences in the shapes of the Bueche[14] and Rouse[11] theoretical curves. Direct calculations from the Rouse theory yield $\zeta_{Rouse} = 0.658$. This corresponds to a reduced viscosity of 0.65, within the standard deviation of the observed result.

The correspondence of $\eta^*(\omega)$ with $\eta_a(\dot{\gamma})$ permits compliances to be calculated from characteristic times for steady flow reported in the literature. Graessley, Hazleton and Lindeman[12] find that concentrated solutions of narrow distribution polystyrenes obey equation 2,

$$\tau_R/\tau_o = \frac{(1 + \beta cM)}{A} \qquad (2)$$

where $\tau_R = \frac{6}{\pi^2} \frac{\eta_o M}{cRT}$ is the Rouse relaxation time, and τ_o is the characteristic time of the system found by fitting the experiments $\eta_a(\dot{\gamma})$ data to Graessley's[13] theoretical master curve. The experimental constants A and β were determined by a least square fit of the data. These results can be used to test the correlation since the concentration of the polystyrene component comprises no less than 20% of the sample. Equation 3 is the compliance calculated from Eqn. 1 and 2.

$$J^o_{e\tau} = \frac{6\zeta MA}{\pi^2 cRT (1 + \beta cM)} \qquad (3)$$

Graessley and Segal[14] find $A = 2.0$ and $\beta = 0.962 \times 10^{-5}$ by fitting data to a master curve which assumes that the polystyrene samples can be represented by a Schultz-Zimm distribution with $M_w/M_n = 1.09$. For

this curve $\zeta = 0.64$. The compliances of bulk polymers (c = 1) predicted with these constants, are represented by the solid line in Fig. 6 and are in good agreement with the measured melt compliance of the Pressure Chemical polystyrene samples determined previously by these authors[15,16]. The brackets on the data cover the results of several measurements. The point represents the best value of these measurements. The dashed portion of the curve is the extrapolation of Eqn. 3 outside the experimental region of Eqn. 2. The measured compliances in this low molecular weight region[16] are in approximate agreement with the predictions of the Rouse theory[11]. The difference between the dashed line and the data results from A = 2.0 which keeps Eqn. 2 from reducing to Rouse type behavior for $\beta cM << 1$. This reflects the different types of polymeric behavior at high and low molecular weights.

The compliance of each solution can be estimated from the reported characteristic time,[14]

$$\tau_N \equiv \frac{15\ \eta_o\ M_w^2}{2\pi^2\ M_z\ M_{z+1}} \lim_{\dot{\gamma} \to o} \frac{P_{11} - P_{22}}{\dot{\gamma}^2\ \eta^2} \tag{4}$$

which is based on measurements of $P_{11} - P_{22}$, the first normal stress difference. This can be written in terms of a compliance where

$$J^o_{eN} \equiv \lim_{\dot{\gamma} \to o} \frac{P_{11} - P_{22}}{2\ \dot{\gamma}^2\ \eta^2} \tag{5}$$

The theory of second order viscoelastic fluids[17] implies that the steady state shear compliance J^o_e, equals the compliance defined from

normal stress measurements, J^o_{eN}. Graessley and Segal[14] find that equation 2 represents the concentration-molecular weight dependence of τ_N when τ_N is used in place of τ_o. A least squares fit of τ_R/τ_N data gives A = 2.2 and $\beta = 1.92 \times 10^{-5}$. These coefficients are not as well defined as those found for τ_R/τ_o because the τ_N data is scattered at high values of cM. The compliance estimated from these constants, J^o_{eN}, has a different functional form than $J^o_{e\tau}$ since the coefficient β is twice that found from the τ_R/τ_o measurements. At the lowest experimental point ($cM = 3.05 \times 10^5$) J^o_{eN} is 18% less than $J^o_{e\tau}$ and is distinctly less than the measured melt compliances. Values of τ_R/τ_N calculated from the measured melt compliance for $M = 4.11 \times 10^5$ and $M = 8.60 \times 10^5$ fall below the given least squares line. These values are in approximate agreement with the concentrations-molecular weight dependence of the τ_R/τ_o data (i.e. $\beta \simeq 1 \times 10^{-5}$). This is what would have been found for the τ_R/τ_N data if the three lowest concentrations of the $M = 8.60 \times 10^5$ polymer solutions are ignored. These solutions also appear to have unusual values of the reduced viscosity at $\dot{\gamma}\,\eta_o\,J^o_e = 1$ as is discussed below. Without these three points the steady state shear compliance and the characteristic time of non-Newtonian flow have the same concentration-molecular weight dependence.

The Estimated Reduced Viscosity at $\dot{\gamma}\eta_o J^o_{eN} = 1$

The reduced viscosity at $\dot{\gamma}\eta_o J^o_e = 1$ of each of the concentrated solutions can be estimated from the master viscosity-shear rate curve using J^o_{eN} in Eq. 4. The narrow distribution samples, without the three solutions in question, give $\eta/\eta_o = 0.66 \pm 0.043$. Including these samples (whose

average reduced viscosity is 0.55) lowers the average η/η_o to 0.63 and increases the standard deviation by 50% to 0.065. Similar τ_o and τ_N data is available for concentrated solutions of samples with broad molecular weight distributions. The average reduced viscosity of four polystyrene experiments[14] is 0.66 ± 0.054. For 16 branched polyvinyl acetate systems[18] $\eta/\eta_o = 0.64 \pm 0.056$. This average includes three samples with exceptionally low reduced viscosities (0.54, 0.54, and 0.56). Without these samples $\eta/\eta_o = 0.66 \pm 0.035$.

These estimates of η/η_o and $J^o_{e\tau}$ assume that the viscosity shear-rate data fit the master curve at $\dot{\gamma}\eta_o J^o_{eN} = 1$ and that the limiting low shear value of J^o_{eN} is obtained. If this last requirement is not fulfilled the calculated reduced viscosity will be too low. This may account for the few estimates of η/η_o that are exceptionally low. The sensitivity of $J^o_{e\tau}$ to the type of data fit can be demonstrated by assuming that the Pressure Chemical polystyrene samples are monodisperse. The characteristic times τ_o, obtained by fitting the data to the differently shaped monodispersed master curve[13], are described by equation 2 with $A = 3.57$ and $\beta = 1.33 \times 10^{-5}$[12]. This change increases $J^o_{e\tau}$ by 27% at $cM = 10^5$ and 14% at $cM = 10^6$.

The average reduced viscosity obtained from melt data (0.67 ± 0.023) is above the averages estimated from concentrated solution measurements but within the standard deviation of these measurements. Considering the magnitude of the standard deviation and the assumptions involved in the estimates of η/η_o, no distinctions can be made between the solution and melt results.

Calculation of J_e^o from Capillary Measurements

Capillary measurements of the apparent viscosity have been found to agree with $\eta^*(\omega)$[8,9] for several polymer systems. For these cases the flow curves should define the compliance of the melt. Stratton's[19] flow data for the Dow series of narrow distribution polystyrenes was used to test the applicability of the $J_{e\tau}^o$ calculation for capillary measurements. These results, shown as the open points on Figure 6, agree well with the measured compliances of the Pressure Chemical melts and those calculated from Segal and Graessley's characteristic times.

It is concluded that the correlation between the steady state shear compliance and non-Newtonian flow, found for dynamic measurements of polymer melts, applies to apparent viscosity measurements of polymer melts and concentrated solutions.

ACKNOWLEDGEMENT

This work was supported through a fellowship granted by the Plastics Institute of America.

TABLE I

Characterization Parameters and the Reduced Complex Viscosity at $\omega\eta_o J_e^o = 1$ of Seven Polystyrene Samples

Polystyrene Sample	$M_w \times 10^{-3}$	M_w/M_n	η^*/η_o at $\omega\eta_o J_e^o = 1$
Pressure Chemical	411	1.06	0.68
Pressure Chemical	97.2	1.06	0.67
160 Blend[10]	98	1.3	0.68
411 Blend[10]	98	1.7	0.67
NBS 706	257.8	2.1	0.66
T - 666	230	2.2	0.66
QX4457	190	2.6	0.67

TABLE II

The Relationship Between Characteristic Times and J_e^o

Master Curve of:	Characteristic Time, τ	$\zeta \equiv \frac{\eta_o J_e^o}{\tau}$
Rouse[11]	τ_R	0.69
Bueche[4]	τ_B	1.44
Bueche-Harding[1]	τ_{BH}	1.44
Graessley[13]	$\tau_{z=\infty}$	0.54
	$\tau_{z=10}$	0.64
	$\tau_{z=0}$	1.85

REFERENCES

1. F. Bueche, S. W. Harding, J. Polym. Sci., 32, 177 (1958).
2. M. H. Birnboim, U.S. Patent No. 3,286,176, November 15, 1966.
3. J. M. O'Reilly and W. M. Prest, Jr., presented at the Society of Rheology Meeting, Atlantic City, New Jersey, Oct. 1966.
4. F. Bueche, J. Chem. Phys., 22, 1570 (1954).
5. W. P. Cox and E. H. Merz, J. Polym. Sci., 28, 619 (1958).
6. S. Onogi, H. Kato, S. Ueki and T. Itharagi, J. Polym. Sci., C15, 481 (1966).
7. S. J. Strella, J. Polym. Sci., 60, 59 (1962).
8. J. W. C. Adamse, H. Janeschite-Kriegl, J. L. den Otter, J. L. S. Wales, J. Polym. Sci., A-2, 6, 871 (1968).
9. R. A. Mendelson, W. A. Bowles and F. L. Finger, J. Polym. Sci., A-2, 8, 105 (1970).
10. W. M. Prest, Jr., ACS Polymer Preprints 10, 137 (1969).
11. P. E. Rouse, Jr., J. Chem. Phys. 21, 1272 (1953).
12. W. W. Graessley, R. L. Hazleton and L. R. Lindeman, Trans. Soc. Rheol. 1113, 267 (1967).
13. W. W. Graessley, J. Chem. Phys. 47, 1942 (1967).
14. W. W. Graessley and L. Segal, Macromolecules, 2, 49, (1969).
15. J. M. O'Reilly and W. M. Prest, Jr., presented at the Society of Rheology, Santa Barbara, Calif., Feb., 1967.
16. J. M. O'Reilly and W. M. Prest, Jr., presented at the American Physical Society Meeting, Berkeley, Calif., March, 1968.
17. B. D. Coleman and H. Markovitz, J. Appl. Phys., 35, 1 (1964).

18. W. W. Graessley and J. S. Prentice, J. Polym. Sci., A-2, 6, 1887 (1968).

19. R. A. Stratton, J. Colloid and Interface Sci., 22, 517, (1966).

CAPTIONS FOR FIGURES

Figure 1. The reduced complex viscosity of two polystyrene samples with different molecular weight distributions as a function of $\omega\eta_o J_e^o$.

Figure 2. The reduced viscosity curves of narrow distribution polystyrene samples showing the point at which $\omega\eta_o J_e^o = 1$. K is an arbitrary constant. The dashed line corresponds to $\eta^*/\eta_o = 0.67$.

Figure 3. The reduced viscosity curves of several polymer systems showing the point at which $\omega\eta_o J_e^o = 1$. From left to right are commercial samples of Silly Putty, poly-carbonate, polyisobutylene, poly-dimethylsiloxane, polystyrene, polypropylene and high density polyethylene. The dashed line corresponds to $\eta^*/\eta_o = 0.67$.

Figure 4. Distribution of η^*/η_o at $\omega\eta_o J_e^o = 1$ for 52 experiments on 32 different commercial polymer melts.

Figure 5. The calculated compliances (0, □, Δ) of binary blends of high molecular weight polydimethylsiloxanes as a function of their weight average molecular weight. Solid lines represent the measured values.[12]

Figure 6. Measured[16,17] and calculated compliances of narrow distribution polystyrene. The solid points represent the most probable value of J_e^o. The brackets on these points span the results of several experimental measurements.

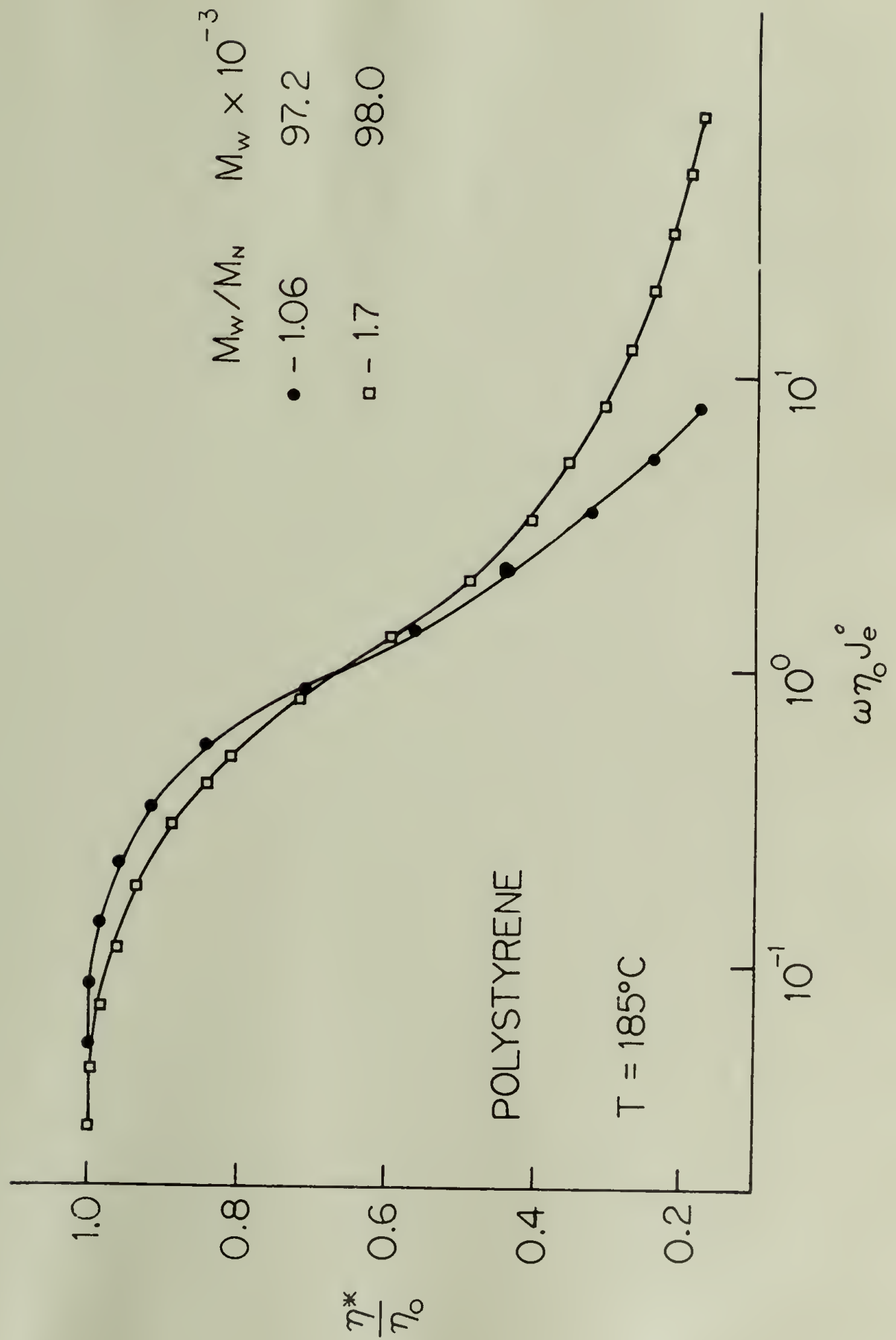
M_w/M_N $M_w \times 10^{-3}$
• - 1.06 97.2
▫ - 1.7 98.0
POLYSTYRENE
T = 185°C
$\frac{\eta^*}{\eta_o}$
1.0
0.8
0.6
0.4
0.2
10^{-1}
10^{0}
10^{1}
$\omega\eta_o J_e^\circ$

Figure 1

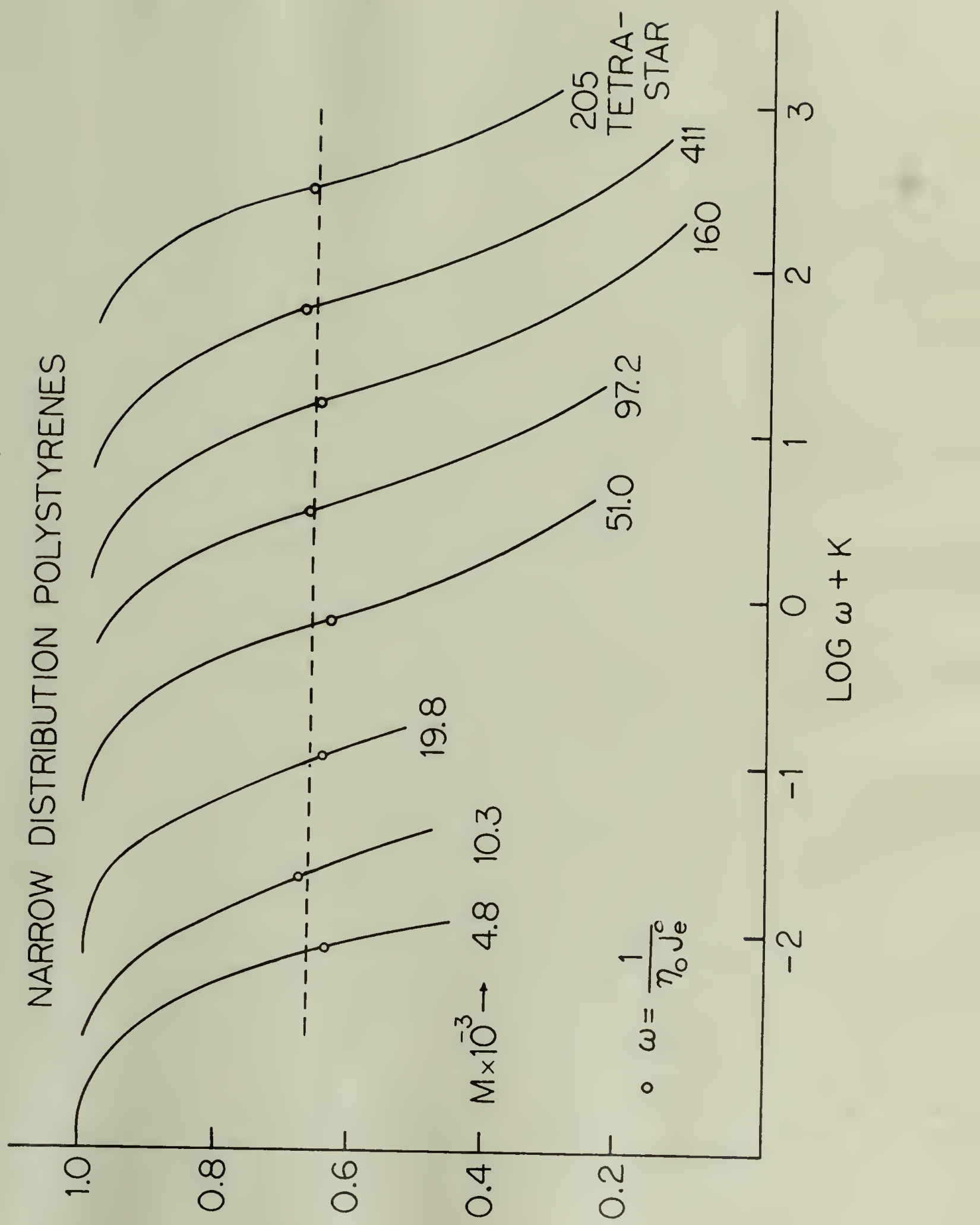
NARROW DISTRIBUTION POLYSTYRENES
205
TETRA-
STAR
411
160
97.2
51.0
19.8
10.3
4.8
M×10⁻³→
1.0
0.8
0.6
0.4
0.2
0
1
2
3
-1
-2
LOG ω + K
∘ ω = 1/(η₀ J_e^c)

Figure 2

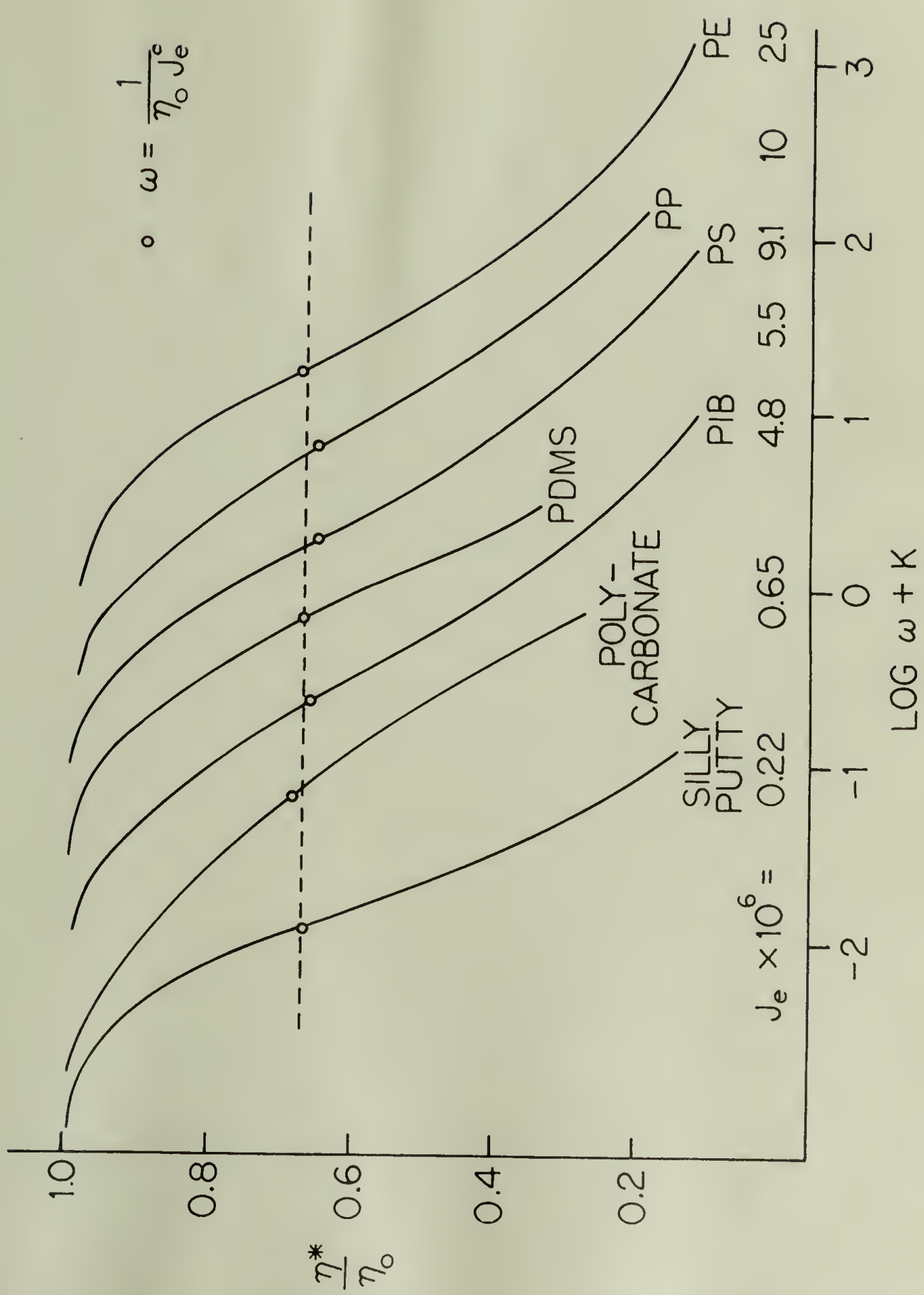
$\omega = \frac{1}{\eta_o J_e^o}$
PE
PP
PS
PIB
PDMS
POLY-
CARBONATE
SILLY
PUTTY
$J_e \times 10^6 =$
4.8
5.5
9.1
10
25
0.22
0.65
$\frac{\eta^*}{\eta_o}$
1.0
0.8
0.6
0.4
0.2
-2
-1
0
1
2
3
LOG $\omega + K$

Figure 3

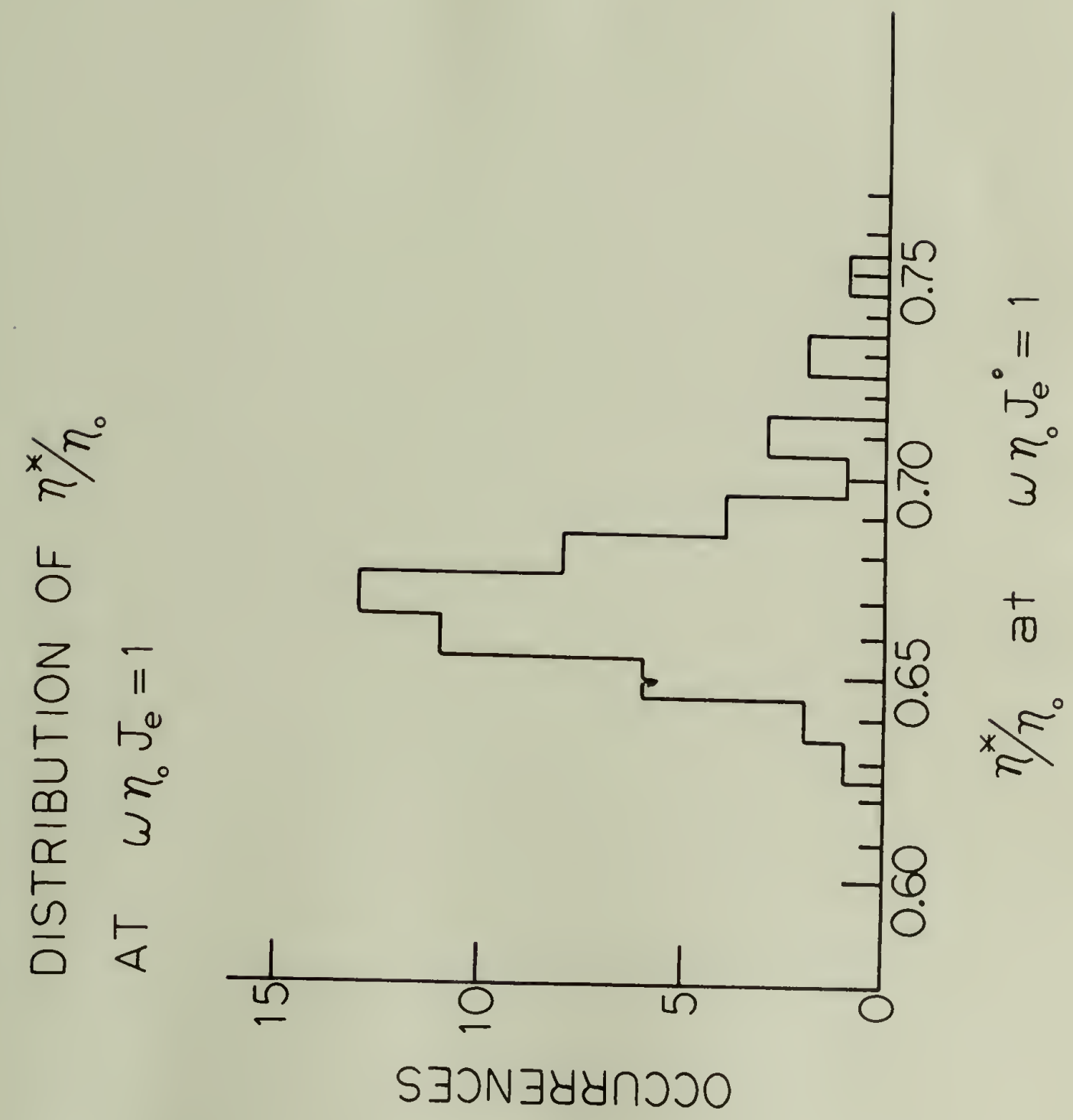
DISTRIBUTION OF $\eta^*/\eta_\circ$
AT $\omega\eta_\circ J_e^\circ = 1$
OCCURRENCES
15
10
5
0
0.60
0.65
0.70
0.75
$\eta^*/\eta_\circ$ at
$\omega\eta_\circ J_e^\circ = 1$

Figure 4

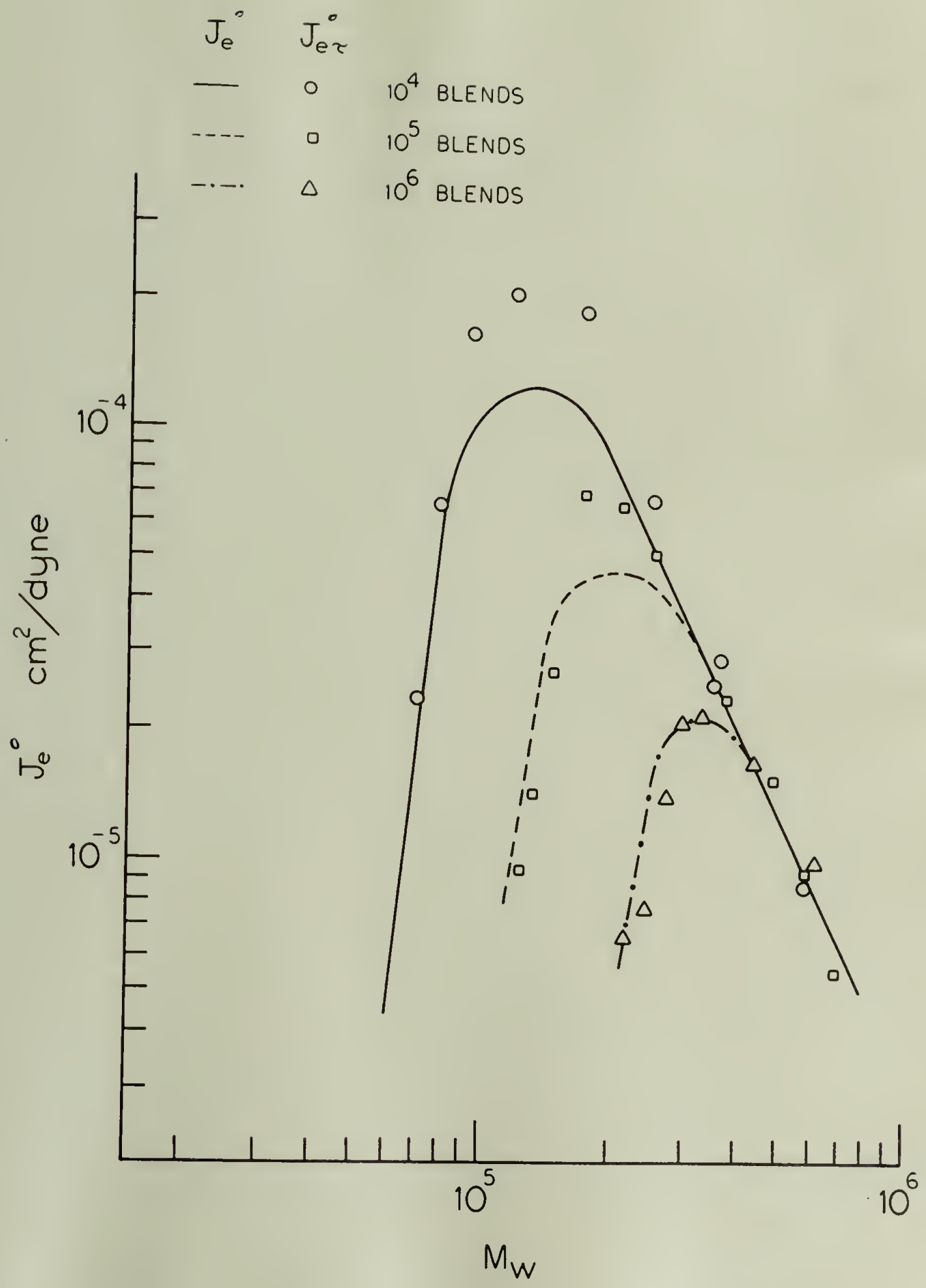
J_e° $J_{e\tau}^\circ$
10^4 BLENDS
10^5 BLENDS
10^6 BLENDS
J_e° cm^2/dyne
10^{-4}
10^{-5}
10^5
10^6
M_w

Figure 5

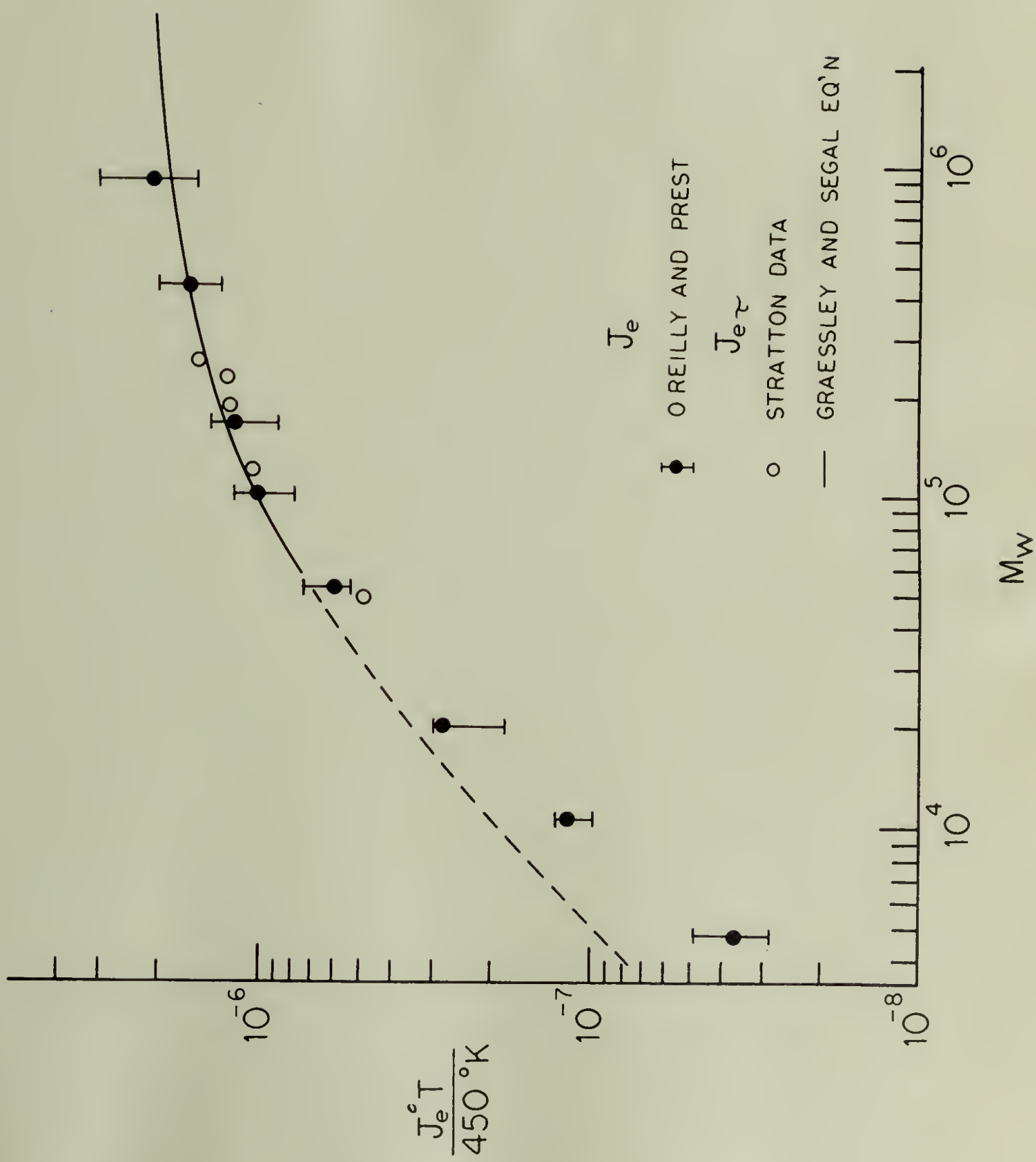
J_e
REILLY AND PREST
$J_{e\tau}$
STRATTON DATA
GRAESSLEY AND SEGAL EQ'N
10^{-6}
10^{-7}
10^{-8}
$\frac{J_e^\circ T}{450\,^\circ K}$
10^5
10^6
10^4
M_W

Figure 6

CHAPTER II

The Effects of High Molecular Weight Components on the Viscoelastic Properties of Polystyrene

W. M. Prest, Jr. and Roger S. Porter
Polymer Science and Engineering
University of Massachusetts
Amherst, Massachusetts 01002

SYNOPSIS

The effects of molecular weight distribution (MWD) on the steady state shear and the dynamic viscoelastic properties of high molecular weight (MW>97,000) polystyrene have been examined with a Weissenberg rheogoniometer. Synthetic MWDs were produced by blending polystyrene components of defined MWs and narrow MWDs. Experiments were designed to examine the effects of small amounts of a high MW component on the viscous and elastic properties of the melt.

The frequency response of the storage and loss moduli, G' and G", and the storage compliance J', are compared with the shear rate dependence of the shear stress τ_{12}, the primary normal stress difference $P_{11} - P_{22}$, and the shear modulus G, as a function of the composition of the blend. At low deformation rates the dynamic and the steady state shear properties are equal; $G'' = \tau_{12}$, $G' = (P_{11} - P_{22})/2$, and $G = 1/J'$. At higher deformation rates the steady state shear properties are primarily controlled by the high MW component while the dynamic

properties reflect the response of each component. The zero shear viscosities of the blends and the narrow MWD components exhibit the same dependence on the weight average MW. Four predictions for the MWD dependence of the steady state shear compliance J_e^o are compared with the experimental results. Although overestimating the magnitude in the maximum in J_e^o, only Graessley's theory accounts for the observed behavior on either side of the maximum.

The data is used to discuss the previously reported dependence of the characteristic relaxation time, $\tau = \eta_o J_e^o$, on the shape of the non-Newtonian flow response. The τ is found to be a measure of the time scale of the relaxation processes of the high MW component.

INTRODUCTION

The viscoelastic properties of polymer melts are strongly dependent on molecular weight, MW, and molecular weight distribution, MWD. Recently studies by different investigators[1,2,3] have been aimed at elucidating the molecular weight distribution dependence of the viscoelastic response of high MW polymer systems. These rheological experiments represent a form of mechanical spectroscopy for the examination of interactions between molecules of different sizes. Synthetic molecular weight distributions have been created by blending different components of defined MW. This technique allows the investigator to follow the response of each component in the changing environment created by different compositional ratios.

Two distinct blending regions have now been experimentally defined[1]. They are characterized by the MW dependence of the steady state shear

compliance, J_e^o, of samples with narrow MWDs, where J_e^o is defined as the low frequency limit of the storage compliance, J'. One region consists of blends of relatively low MW polymers in which the components have different values of J_e^o. Typically the compliance of these components is proportional to molecular weight, as predicted by the modified Rouse theory for polymer melts[4]. At high MWs, the steady state shear compliance of systems with similar MWDs is relatively independent of MW[1,3,5,6,7]. This second region involves strong interactions between molecules, i.e., "entanglements". Studies of blends in the entanglement region show that J_e^o is a strong function of MWD. The J_e^o of binary blends passes through a very high maximum at low values of w_2, the weight fraction of the high MW component. Beyond this maximum it has been previously shown that J_e^o is proportional to w_2^{-2} or M_w^{-2} of the blends[3,1]. To date, however, only one set of experiments have actually shown the shape of the maximum in J_e^o as well as the rapid fall off of J_e^o at lower values of w_2 [1]. These earlier experiments were performed with blends of polydisperse polydimethyl siloxane samples, where the MWD of the components obscured the interactions between the blended species. Other prior blending experiments with narrow MWD components have chiefly delt with the compositional range beyond the maximum in J_e^o.

The purpose of this study has been to examine the low end of the compositional range (i.e., the region of small w_2) in the entanglement region. The goal is to study the interactions responsible for the maximum in J_e^o as a function of MWD. In addition this study seeks to

test the various blending laws which have been proposed to explain the viscoelastic response of high MW polydisperse systems.

EXPERIMENTAL

The high MW, narrow MWD polystyrene samples used to create the synthetic MWDs in this study were obtained from the Pressure Chemical Company, Pittsburgh, Pa. Previous studies have shown that the steady state shear compliance of polystyrene samples with narrow MWDs is approximately independent of MW above a molecular weight of about 100,000[3,5,6,7]. The blended components were chosen to be in this range. The MW characteristics of the components are listed in Table I along with the MW averages of the blends, calculated by the Peticolas and Menefee technique[8]. The identification numbers of the blends represent the weight fraction of the high MW component/ the MW in thousands of the high MW component/ and the MW in thousands of the low MW component. Samples were prepared by dissolving weighed amounts of the components in benzene at a concentration of 1-2% by volume. The solutions were gently agitated for 24 hours and then freeze-dryed. This technique was chosen to avoid possible sample fractionation which might result from extraction methods such as solvent evaporation or non-solvent precipitation. The resultant blends and components were compacted into disks and molded at 170°C at 10,000 PSI for two minutes.

The viscoelastic properties of the samples were measured with a

model R-17 Weissenberg Rheogoniometer used in the cone and plate configuration. A 4° cone, 2.5 cm in diameter was chosen to minimize sample size and to optimize the normal stress measurements. The dynamic properties of the samples were measured with an improved version of the Birnboim Ultra Low Frequency Phase Meter[9]. The modifications incorporate variable trigger levels which allow the operator to examine different portions of the input signals. In this manner the purity and balance of the wave forms may be checked and any perturbation or distortion in the signals may be detected and avoided. The modified phase meter defined phase angles to less than ± 0.2 degrees and determined the amplitude of the sinosoidal signals to within $\pm 2\%$.

Different strain amplitudes were used to insure that all measurements were conducted in the region of linear viscoelastic response. Generally measurements were made at maximum strains of 5-9%.

RESULTS

Viscoelastic Response

Figure 1 shows the viscoelastic response of the narrow MWD polystyrene component with a MW of 97,200. All data was reduced to a reference temperature, $T_o = 192°C$, by multiplying the measured stresses by $\rho_o T_o / \rho T$. The densities, ρ, were calculated from the relationship given by Fox and Loshack[10]. The reference temperature was chosen to correspond to a convenient value of the zero shear viscosity.

The master curve was constructed from measurements made at five different temperatures. The reduced data was superimposed by multiplying the frequency axis by a factor a_T. At low frequencies the loss modulus,

G'', is proportional to ω and the storage modulus, G' is proportional to ω^2. At the reference temperature of 192°C, the low frequency limit of the dynamic viscosity $\eta' = G''/\omega$ is 10^4 poise and the elastic coefficient, $A_G \equiv G'/\omega^2$, is 110 dyne sec^2/cm^2. The storage compliance J', can be calculated from G' and G'' by Eq. 1.

$$J' = \frac{G'}{G'^2 + G''^2} \tag{1}$$

The reciprocal of J' is shown in Figure 1 to be a constant, with a value of 9×10^5 dynes/cm^2, over the two lowest decades of frequency. This value is the reciprocal of J_e^o.

The measurements of the storage modulus extend down to 32 dynes/cm^2 which, in this instance, corresponds to a phase angle of 89.7 degrees between the stress and the strain. The lack of scatter in $1/J'$ at low frequencies is an indication of the precision of the measurements of the phase angle, ϕ. In this region $1/J'$ is proportional to the secant of ϕ which approaches infinity as ϕ approaches 90 degrees. A tenth of a degree error in the measurement of ϕ at 89.7 degrees would change $1/J'$ by 33%, a variation which would be very noticeable in Figure 1.

The data points in Figure 2 give the steady state shear measurements of the shear stress τ_{12}, half the primary normal stress difference $(P_{11} - P_{22})/2$, and the shear modulus $G = 2\tau_{12}/(P_{11} - P_{22})$ as a function of the reduced shear rate $\dot{\gamma}\, a_T$. These are compared with lines which represent the dynamic measurements of G', G'', and $1/J'$ as a function of ωa_T, (see Fig. 1). The superposition of the steady state shear data by

the shift factor a_T, indicates that τ_{12}, and $P_{11} - P_{22}$ have the same temperature dependence as the viscoelastic properties. The data shows that for this system G' equals half the primary normal stress difference. At low shear rates τ_{12} is equal to G". At higher shear stresses the samples extrude from the test region making the calculated τ_{12} appear to fall below G". This figure shows that the shear modulus determined in steady state flow G, is equal to the low frequency limit of 1/J', in accordance with the predictions of the Theory of Second Order Fluids[11].

Figure 3 presents the viscoelastic response of a blend of two narrow MWD samples which was formed by adding a high MW component to the 97,200 sample described above. The identification number indicates that the blend consists of 20.9 weight percent of a sample with a molecular weight of 411,000 mixed with the 97,200 MW component. At low frequencies G' and G" are shown to be proportional to ω^2 and ω respectively, as was found for the base 97,200 MW sample. The time dependence of this response is shifted to lower frequencies relative to the response of the base component (see Fig. 1), reflecting the increased viscosity and the changes in the elastic properties caused by blending. The zero shear viscosity η_o, of this blend is 5.43×10^4 poise and the elastic coefficient is 3.1×10^4 dyne-cm^2/sec^2 at 192°C. At intermediate frequencies the effects of blending become apparent when both G' and G" deviate from the low ω dependencies. At this point both the position and the shape of the frequency response differs from that seen in Figure 1 for the low MW component. At high frequencies all functions have the same shaped response as the properties of the 97,200 MW sample. The entire response can be

viewed as a weighted combination of the viscoelastic properties of each component. At low frequencies the 411,000 MW component controls the magnitude of the viscous and elastic response. At high frequencies the properties of the blend are those of the 97,200 MW, shifted towards longer times by the interactions with the high MW component. Figure 3 shows that as ω decreases, 1/J' first approaches the limiting value of 9×10^5 dynes/cm^2 which is the value of $1/J_e^o$ found for the 97,200 MW sample. The effects of blending then appear as a sudden decrease in the magnitude of 1/J' with decreasing ω, ultimately reaching a limiting value of 9.5×10^4 dynes/cm^2, the characteristic $1/J_e^o$ of the blend. For this blending MW ratio the compliance changes by almost a decade with a 20.9% change in composition while the viscosity increases by a factor of 5.43.

The steady state shear response of the 0.209/411/97.2 blend is compared, in Figure 4, with lines which represent the dynamic properties G', G", and 1/J'. At low shear rates $(P_{11} - P_{22})/2$ equals G' and is proportional to $\dot{\gamma}^2$. At higher shear rates G' deviates from the square dependence sooner and more rapidly than $P_{11} - P_{22}$. This reflects the differences between the linear response of the dynamic measurements and the non-linear response of the steady state shear experiment. The modulus calculated from the primary normal stress difference is independent of $\dot{\gamma}$ over most of the experimentally accessible range. At low ω, G equals $1/J_e^o$, again in agreement with the Theory of Second Order Fluids. This fact was confirmed for all of the blending experiments described in this paper. Note that 1/J' departs from the limiting value

of $1/J_e^o$ at lower shear stresses than does G. Thus a good estimate of $1/J_e^o$ can even be made from measurements of a constant value of G in the non-linear region of τ_{12}.

The changes in the response of G', caused by the blending of different molecular weight species, are shown in Figure 5. As more of the 411,000 MW component is added to the 97,200 MW base sample, the response of the system shifts to lower frequencies and an inflection point appears in G'. The magnitude of the stress at the inflection point increases with w_2 and the initial formation of a plateau becomes apparent. In this region the response of the blend can be visually decomposed into the contributions of each component.

The blending induced changes in 1/J' are given by the family of curves presented in Figure 6. Two distinct concentration regions are observed. For blends with small amounts of high MW material, the low ω limit of 1/J' decreases rapidly with increasing w_2, while the high frequency response remains essentially unchanged. The location of the transition between the two extremes shifts to higher frequencies as w_2 increases. At higher concentrations the magnitude of both the low and high frequency responses increase with w_2 and the position of the transition region shifts toward lower ω.

The shear rate dependencies of $P_{11} - P_{22}$ and G for the 411/97.2 blend series are shown in Figure 7. As the concentration of the high MW material is decreased the deviation of $P_{11} - P_{22}$ from the $\dot{\gamma}^2$ dependence occurs at progressively lower stress levels. However, these deviations are minor when compared with the associated rapid change in G' (see Figs. 4 and 5). In addition, the shear rate dependence of

$P_{11} - P_{22}$ does not indicate the presence of the two MW species as clearly as does G'. Therefore the high shear rate dependence of the primary normal stress difference is controlled primarily by the high MW component.

For the narrow MWD components, the shear modulus is independent of $\dot{\gamma}$ over the experimentally accessible range. The measured G remains relatively insensitive to $\dot{\gamma}$ for the blends in which $w_2 > 0.2$. The shear moduli of blends containing small amounts of high MW material is constant at low $\dot{\gamma}$ but increases rapidly at higher shear rates. This curvature is the result of the more rapid deviation of $P_{11} - P_{22}$ from $\dot{\gamma}^2$ than τ_{12} from $\dot{\gamma}$. For large concentrations of the high MW component, the deviation of $P_{11} - P_{22}$ is balanced by pronounced non-Newtonian flow (see Fig. 4), resulting in a relatively constant value of G. The less pronounced non-Newtonian flow in the low w_2 blends makes G more sensitive to the shear rate dependence of $P_{11} - P_{22}$. Presumably, if higher normal stresses could be measured, the shear modulus of the low w_2 blends would become less dependent on $\dot{\gamma}$ in the region of substantial non-Newtonian flow. As in Figure 4, the shear moduli of all the blends are less dependent on $\dot{\gamma}$ than J' is on ω. This reflects the difference between the time dependencies of $P_{11} - P_{22}$ and G' and reinforces the previously stated observation that $1/J_e^o$ can be estimated from the nonlinear region of steady state flow.

Zero Shear Viscosity

This study provides an important test of the MW averages which control the long time properties of high MW polymer melts because it deals primarily

with the low w_2 range, the region in which the ratios of the higher MW averages, M_z/M_w, M_{z+1}/M_z, reach a maximum. Berry and Fox[12] have shown that the zero shear viscosity η_o, is a unique function of the chain length of the molecule when the systems are reduced to a constant free volume. This condition is automatically satisfied in this study by the high MWs of the blended components. For all of the samples studied, the steady state shear measurement of η_o equaled the low frequency limit of η'. Figure 8 presents the zero shear viscosities of the blends and the components at 192°C, plotted against the weight average molecular weight M_w. The solid line, determined by the viscosities of the narrow MWD samples, is given by the relationship

$$\log \eta_o = -12.7 + 3.35 \log M_w \qquad (2)$$

Within experimental error, the viscosities of all the blends obey this relationship. The least squares line determined by all the data is:

$$\log \eta_o = -13.0 + 3.41 \log M_w \qquad (3)$$

These equations are in agreement with the findings of a recent survey[13] which compared several investigators' measurements of the viscosity of these and other standard polystyrene samples. Bueche[14] has predicted that the MW averages which control η_o shift from M_w to M_z as the higher moments of the MWD become significantly different from M_w. If this were true the viscosities of the blends would show a systematic deviation from the $M_w^{3.4}$ dependence as the ratio of M_z/M_w passes through a maximum. This is not observed experimentally.

Steady State Shear Compliance

Several different predictions for the MWD dependence of J_e^o have been proposed[3,15,20,22]. Two of these define blending laws which describe the viscoelastic response of the blend in terms of $H(\tau)$, the relaxation spectrum of the system. This quantity is particularly useful because it can be used to calculate the entire response of all the viscoelastic functions. Ninomiya[15] has proposed a blending law, Eq. 4, in which the relaxation spectrum of the blend is described as a weighted sum of the relaxation spectra of the individual components, each shifted in time by an amount λ_i.

$$H_B(\tau) = \sum v_i H_i(\tau/\lambda_i) \qquad (4)$$

These shift factors take into account the different environment that a molecule encounters when immersed in different MW surroundings. In a mono-disperse sample, a molecule "sees" certain viscous drag forces which determine the time constants of its relaxation mechanisms. In a blend each molecule experiences a new set of viscous drag forces which establish a new set of relaxation times. The relaxation spectrum of the molecule is then shifted in time by an amount determined by these new interactions. This shift in time scale can be represented by the parameters λ_i.

Ninomiya and Ferry's[15,16,17,18] work primarily involved blends of components with different moduli. For these systems, it was found that the weighting factors, v_i, were equal to the weight fractions of the components. Coupling this result with the observation that η_{oB} depends only on M_w leads to the prediction that the compliance of the blend J_{eB}^o,

is proportional to $(M_{z+1}\ M_z/M_w)$ for systems in which $J^o_{ei}\ \alpha M$. This relationship is generally observed. When J^o_{ei} is independent of M, the blending law predicts $J^o_{eB}\ \alpha M_z/M_w$ or in another modification[19], $J^o_{eB}\ \alpha(M_{z+1}\ M_z)/M_w{}^2$. Previous studies by these[1] and other authors[2,3] have shown that these MW averages grossly underestimate the magnitude of the changes in J^o_{eB} and the dependence of J^o_{eB} on w_2. Experimentally J^o_{eB} is found to be approximately proportional to w_2^{-2} for large values of w_2 [1,12]. In addition Masuda et al.[2] found a spread in the relaxation spectrum of the blends. They postulated that this spread was the result of contributions of $H_B(\tau)$ from relaxation mechanisms involving couplings between the high and low MW components.

Based on these observations, Bogue and coworkers[20] suggested the quadratic blending law given in Eq. 5.

$$H_B = w_1{}^2 H_{11} + 2w_1 w_2 H_{12} + w_2{}^2 H_{22} \tag{5}$$

where H_{ii} is the relaxation spectrum caused by interactions between molecules of MW i and j. The shift factors λ_{ij}, do not appear in this formalism, but are indirectly incorporated in terms of a predefined MW dependence of the relaxation times, $\tau_{ij}\ \alpha\ M_i M_j M_w{}^{1.5}$. This approach predicts that

$$J^o_{eB} = (M_z/M_w)^2 J^o_{ei} \tag{6}$$

In work unrelated to the specific form of the blending laws, Mills[3,21] has found a correlation between J^o_{eB} and $(M_z/M_w)^{3.7}$.

A theoretical attempt to explain the MW and MWD dependence of J^o_{eB} has recently been proposed by Graessley. The theory introduces inter-

molecular interactions into the Rouse model by considering both the elastic contributions of entanglements and the viscous drag forces at these points. The drag forces depend on the lengths of the interacting chains. This results in a non-uniform drag coefficient for polydisperse systems. The sum of the relaxation times caused by these interactions is in the form of the quadratic blending law. Averages of τ over each type of relaxation process automatically include the shift factors.

Figure 9 compares the measured compliances of the 411/97.2 series of blends with the predictions described above. The lines represent the results of: 1-The quadratic blending law, $(M_z/M_w)^2$; 2-The modified Rouse theory, $(M_{z+1}M_z/M_w^2)$; 3-Mills' correlation, $(M_z/M_w)^{3.7}$; and 4-Graessley's theory.

The quadratic blending law predicts the least pronounced dependence of J^o_{eB} on MWD. This is particularly surprising because this law was designed to explain the experimentally observed dependence of J^o_{eB} on w_2^{-2}. However larger compliances may be predicted by the quadratic blending law if the shift factors, i.e. the relaxation times of the individual molecular species, are more sensitive to the MWD of the melt than the proposed $M_iM_jM_w^{1.5}$ dependence. This is illustrated by the predictions of Graessley's theory which incorporates calculated λ_{ij} with a form of the quadratic blending law. While Graessley's theory overestimates the maximum change in J^o_{eB}, it is the only representation which approximates the shape and the magnitude of the observed response on either side of the maximum.

Non-Newtonian Response

The authors have previously reported that the non-Newtonian response of many polymer melts is related to the characteristic relaxation time of the system, $\tau = \eta_o J_e^o$ [23]. A correlation was found between τ and the reduced complex viscosity, $\eta^*/\eta_o = (G'^2 + G''^2)^{1/2}/\omega\eta_o$. In particular, at $\omega = 1/\tau$, $\eta^*/\eta_o = 0.67 \pm 0.03$. It was noted that this relationship did not apply to systems containing small amounts of high MW material. The data presented in this paper can be used to examine this behavior in more detail. The reduced complex viscosities of the PS blends are plotted as a function of ωa_T in Figure 10. The point (o) on each response corresponds to $\omega a_T = 1/\eta_o J_e^o$. The values of η^*/η_o at this point are listed in Table II.

As the 97,200 MW PS is added to the higher MW sample, the Newtonian response extends to progressively higher values of ωa_T. In addition, the presence of the low MW material initially changes the shape of the non-Newtonian response at low values of η^*/η_o. This contribution becomes more significant as w_2 decreases. The shape of the response in the neighborhood of $\eta^*/\eta_o = 0.67$ becomes a function of the low MW component when $w_2 < 0.2$. As shown in Figure 9, this is the concentration range where J_{eB}^o is a maximum, and thus the region in which the elastic properties of the 97,200 MW sample first begin to influence the properties of the blend. At small w_2 the correlation fails when the properties of the low MW component dominate the response of the blend. However, in this region $\omega = 1/\eta_o J_e^o$ predicts the approximate position where the contribution of the high MW component to η^*/η_o equals 0.67. This may be seen by shifting the response of the high MW component so that it corresponds with the initial

non-Newtonian flow region of the low w_2 blends. Therefore the characteristic time, $\eta_o J_e^o$, can be considered to be a measure of the time scale of the relaxation processes of the high MW component.

TABLE I

Molecular Weight Distribution of the Blends

Sample	$M_w/10^3$	M_w/M_n	M_z/M_w
97.2	97.2	1.04	1.04
0.023/411/97.2	104.4	1.10	1.25
0.033/411/97.2	107.6	1.12	1.32
0.049/411/97.2	112.5	1.16	1.42
0.089/411/97.2	125.1	1.25	1.57
0.209/411/97.2	162.7	1.46	1.68
0.399/411/97.2	222.3	1.66	1.54
411	411.	1.04	1.05

TABLE II

Properties of the Blends at 192°C

w_2	$\eta_{oB}/10^4$ poise	$J^o_{eB}/10^{-6}$ $cm^2/dyne$	η^*/η_{oB} @ $\omega\eta_{oB}J^o_{eB}=1$
0.000	1.00	1.1	0.67
0.023	1.15	4.5	0.85
0.033	1.27	7.0	0.85
0.049	1.51	9.0	0.83
0.089	1.97	11.	0.76
0.209	5.43	10.5	0.67
0.399	16.0	6.7	0.66
1.000	125.	1.4	0.68

REFERENCES

1. W. M. Prest, Jr., J. Polymer Sci., A-2, 8, 1897 (1970).
2. T. Masuda, K. Kitagawa, T. Inoue, and S. Onogi, Macromolecules, 3, 116 (1970).
3. N. J. Mills and A. Nevin, J. Polymer Sci., A-2, 9, 267 (1971).
4. J. D. Ferry, M. L. Williams, and D. M. Sterns, J. Phys. Chem., 58, 987 (1954).
5. J. M. O'Reilly and W. M. Prest, Jr., Trans. Soc. Rheol., 10:2 (1967).
6. S. Onogi, T. Masuda, and K. Kitagawa, Macromolecules, 3, 109 (1970).
7. H. J. M. H. Mieras and C. F. H. van Rijn, Nature, 218, 865 (1968).
8. W. L. Peticolas and E. Menefee, J. Chem. Phys., 35, 957 (1961).
9. M. H. Birnboim, U.S. Pat. 3,286,176 (Nov. 15, 1966).
10. T. G. Fox and S. Loshaek, J. Polymer Sci., 15, 371 (1955).
11. B. D. Coleman and H. Markovitz, J. Appl. Phys., 35, 1 (1964).
12. G. C. Berry and T. G. Fox, Adv. Polymer Sci., 5, 261 (1968).
13. A. Casale, R. S. Porter, and J. F. Johnson, J. Macromol. Sci - Revs. Macromol. Chem., C5(2), 387 (1971).
14. F. Bueche, J. Polym. Sci., 43, 527 (1960).
15. K. Ninomiya, J. Colloid Sci., 14, 49 (1959).
16. K. Ninomiya, J. Colloid Sci., 17, 759 (1967).
17. K. Ninomiya and J. D. Ferry, J. Colloid Sci., 18, 421 (1963).
18. K. Ninomiya, J. D. Ferry, and Y. Oyanagi, J. Phys. Chem., 67, 2297 (1963).
19. W. W. Graessley and L. Segal, Macromolecules, 2, 49 (1969).
20. D. C. Bogue, T. Masuda, Y. Einaga, and S. Onogi, Polym. J., 1, 563 (1970).

21. N. J. Mills, Europ. Polym. J., 5, 675 (1969).

22. W. W. Graessley, J. Chem. Phys., 54, 5143 (1971).

23. W. M. Prest, Jr., R. S. Porter, and J. M. O'Reilly, J. Appl. Sci., 14, 2697 (1970).

FIGURE CAPTIONS

Fig. 1 Frequency dependence of G', G", and 1/J' for sample 97.2 reduced to 192°C.

Fig. 2 Shear rate dependence of τ_{12}, $(P_{11} - P_{22})/2$ and G compared with the frequency dependence of G', G", and 1/J' for sample 97.2 reduced to 192°C.

Fig. 3 Frequency dependence of G', G", and 1/J' for sample 0.209/411/97.2 reduced to 192°C.

Fig. 4 Shear rate dependence of τ_{12}, $(P_{11} - P_{22})/2$ and G compared with the frequency dependence of G', G", and 1/J' for sample 0.209/411/97.2 reduced to 192°C.

Fig. 5 Frequency dependence of G' for the 411/97.2 blend series reduced to 192°C.

Fig. 6 Frequency dependence of 1/J' for the 411/97.2 blend series reduced to 192°C.

Fig. 7 Shear rate dependence of G and $P_{11} - P_{22}$ for the 411/97.2 blend series reduced to 192°C.

Fig. 8 The weight average molecular weight dependence of the zero shear viscosity for the 411/97.2 blend series.

Fig. 9 The dependence of the steady state shear compliance on the weight fraction of the high MW component of the 411/97.2 blend series. Solid lines are the predictions of 1) Bogue et al. quadratic blending law; 2) Modified Rouse Theory; 3) Mills' Correlation; 4) Graessley's Theory.

Fig. 10 The reduced complex viscosities of the 411/97.2 blend series as a function of ωa_T. The point o represents $\omega a_T = 1/\eta_o J_e^o$.

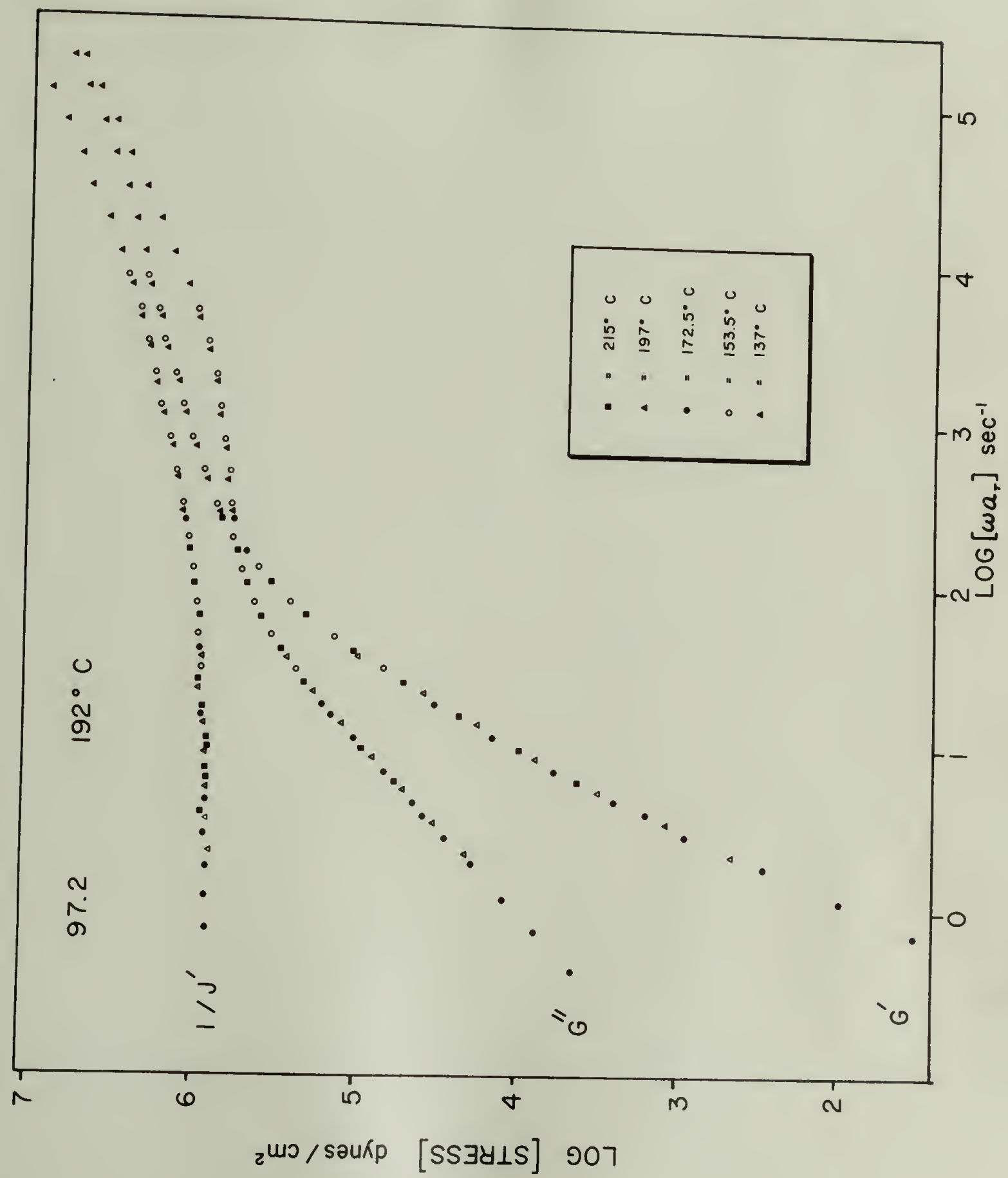
LOG [STRESS] dynes / cm²
7
6
5
4
3
2
0
1
2
3
4
5
LOG [ωa_T] sec⁻¹
97.2
192° C
1 / J′
G″
G′
■ = 215° C
▲ = 197° C
● = 172.5° C
○ = 153.5° C
△ = 137° C

Figure 1

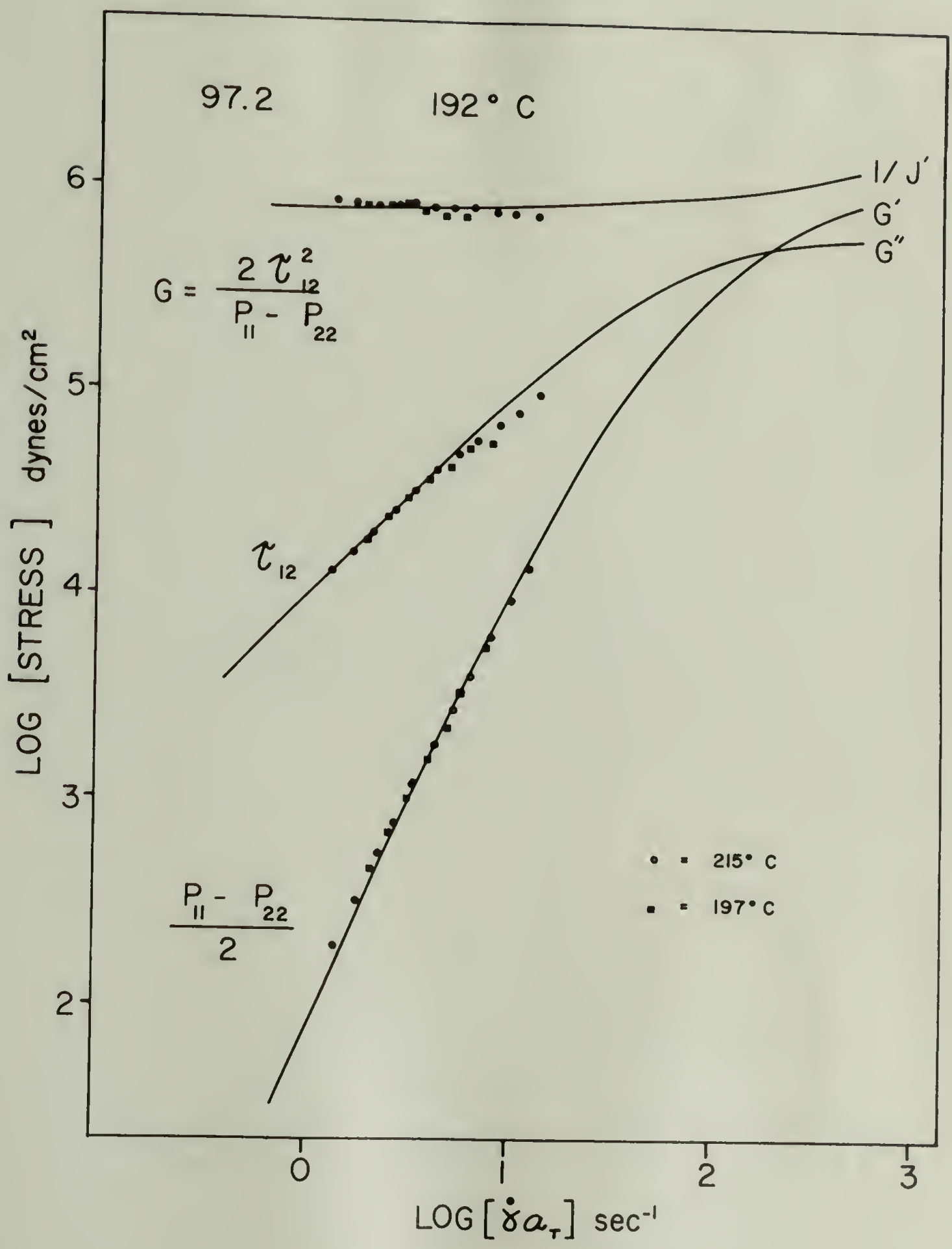
97.2
192° C
1/ J'
G'
G''
$G = \frac{2\tau_{12}^2}{P_{11} - P_{22}}$
τ_{12}
$\frac{P_{11} - P_{22}}{2}$
• = 215° C
▪ = 197° C
LOG [STRESS] dynes/cm²
LOG [$\dot{\gamma} a_T$] sec⁻¹
6
5
4
3
2
0
1
2
3

Figure 2

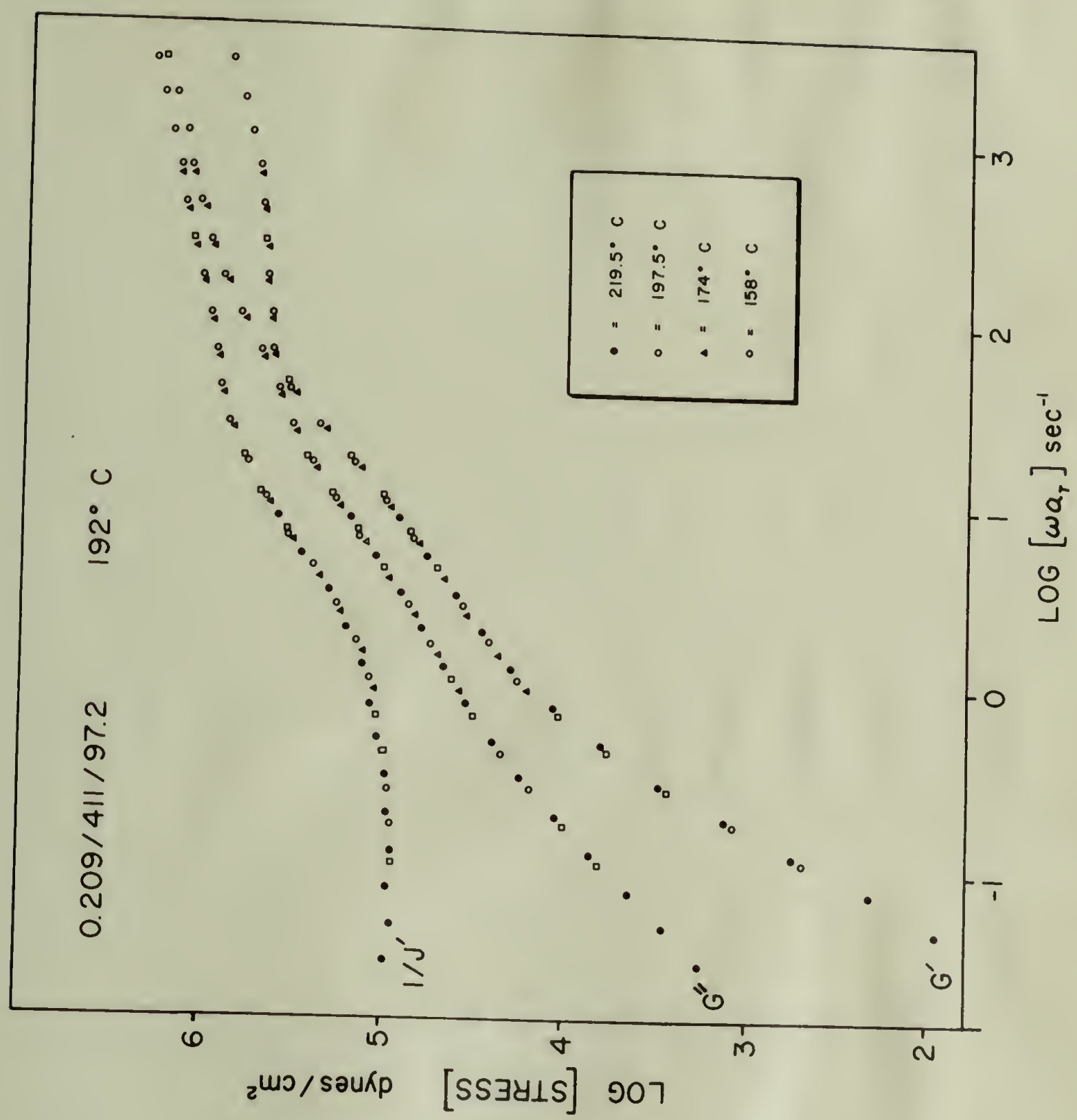
192° C
0.209/411/97.2
• = 219.5° C
○ = 197.5° C
▲ = 174° C
△ = 158° C
1/J′
G″
G′
LOG [STRESS] dynes/cm²
LOG [ωa_T] sec⁻¹
2
3
4
5
6
-1
0
1
2
3

Figure 3

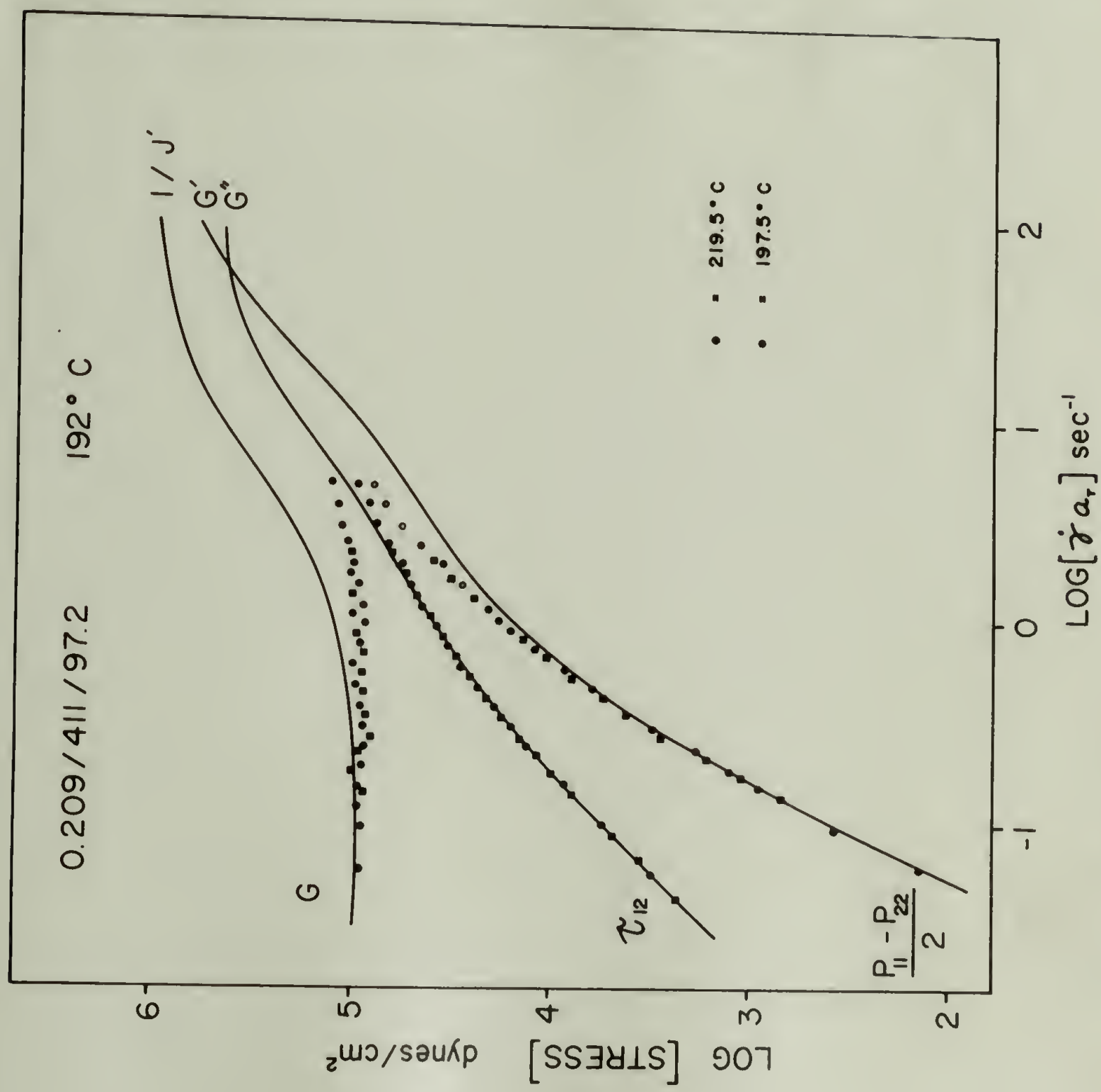
192° C
0.209/411/97.2
1/J'
G'
G"
G
τ_{12}
$\frac{P_{11}-P_{22}}{2}$
• = 219.5° C
• = 197.5° C
LOG [STRESS] dynes/cm²
LOG [$\dot{\gamma}a_T$] sec⁻¹
2
3
4
5
6
-1
0
1
2

Figure 4

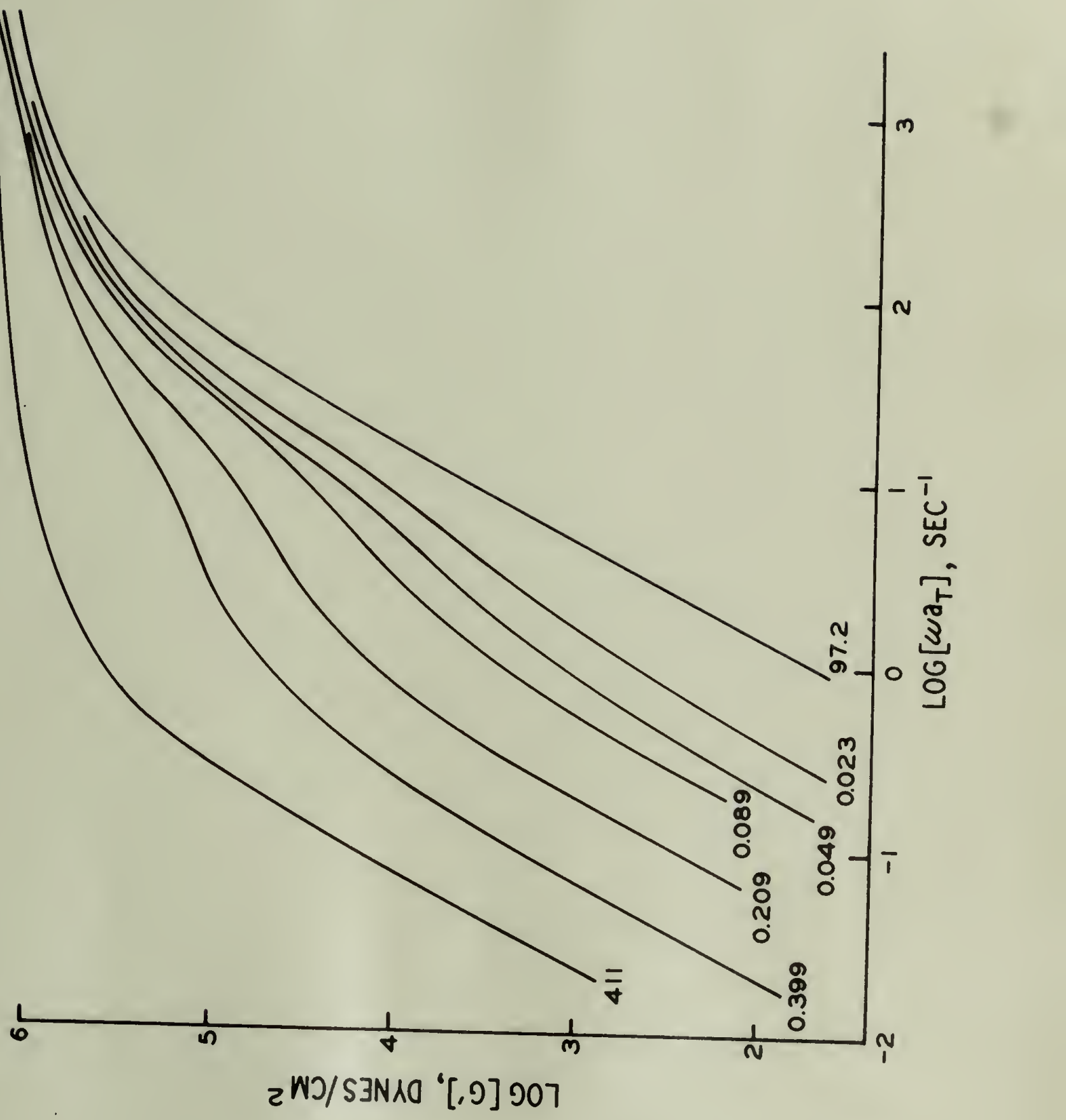
LOG [G'], DYNES/CM²
6
5
4
3
2
-2
-1
0
1
2
3
LOG [ωa_T], SEC⁻¹
411
0.399
0.209
0.089
0.049
0.023
97.2

Figure 5

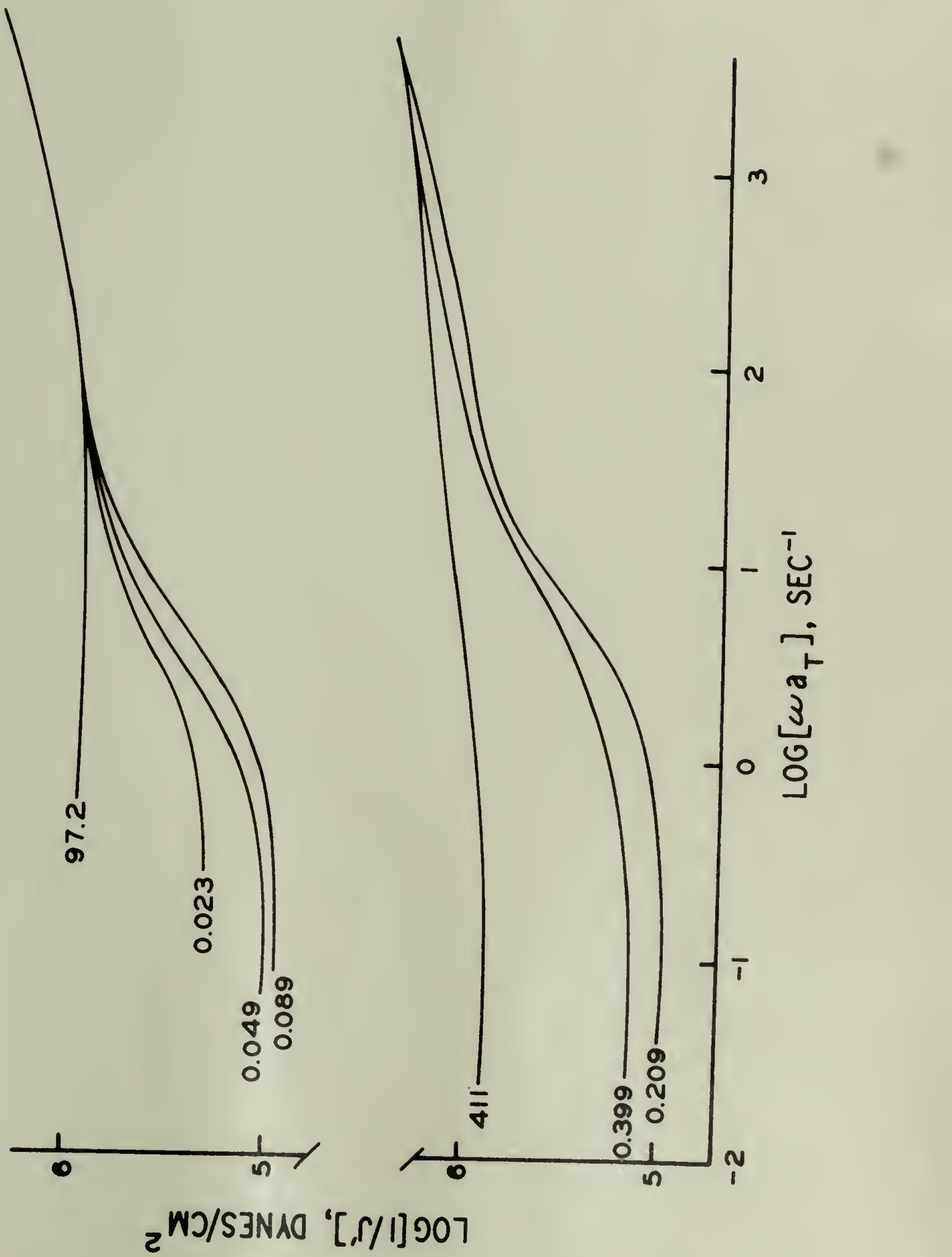
LOG[I/J'], DYNES/CM²
6
5
97.2
0.023
0.049
0.089
411
0.399
0.209
-2
-1
0
1
2
3
LOG[ωa_T], SEC⁻¹

Figure 6

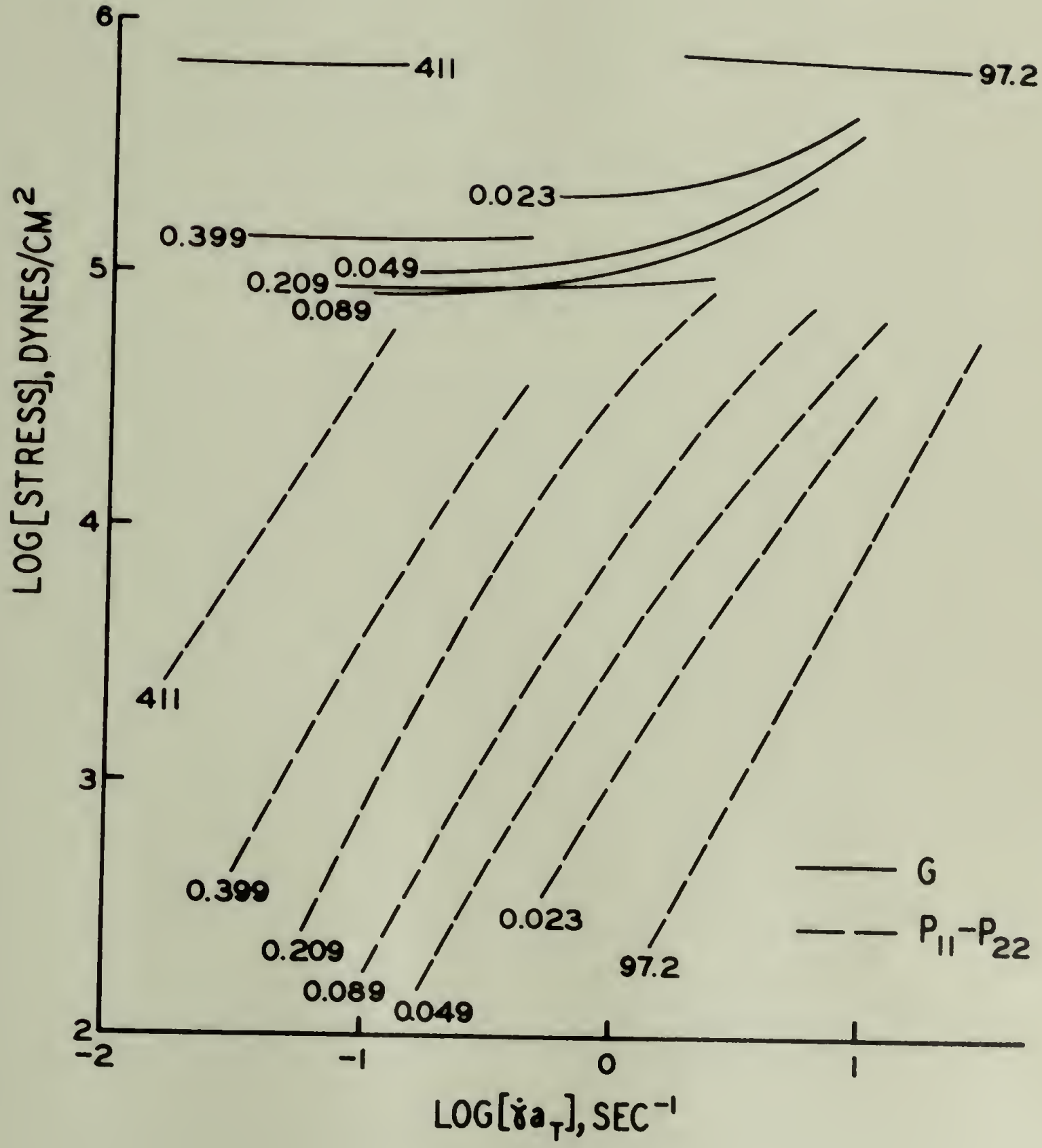
6
5
4
3
2
LOG[STRESS], DYNES/CM²
411
97.2
0.023
0.399
0.049
0.209
0.089
411
0.399
0.209
0.089
0.049
0.023
97.2
G
P11-P22
-2
-1
0
1
LOG[γa_T], SEC⁻¹

Figure 7

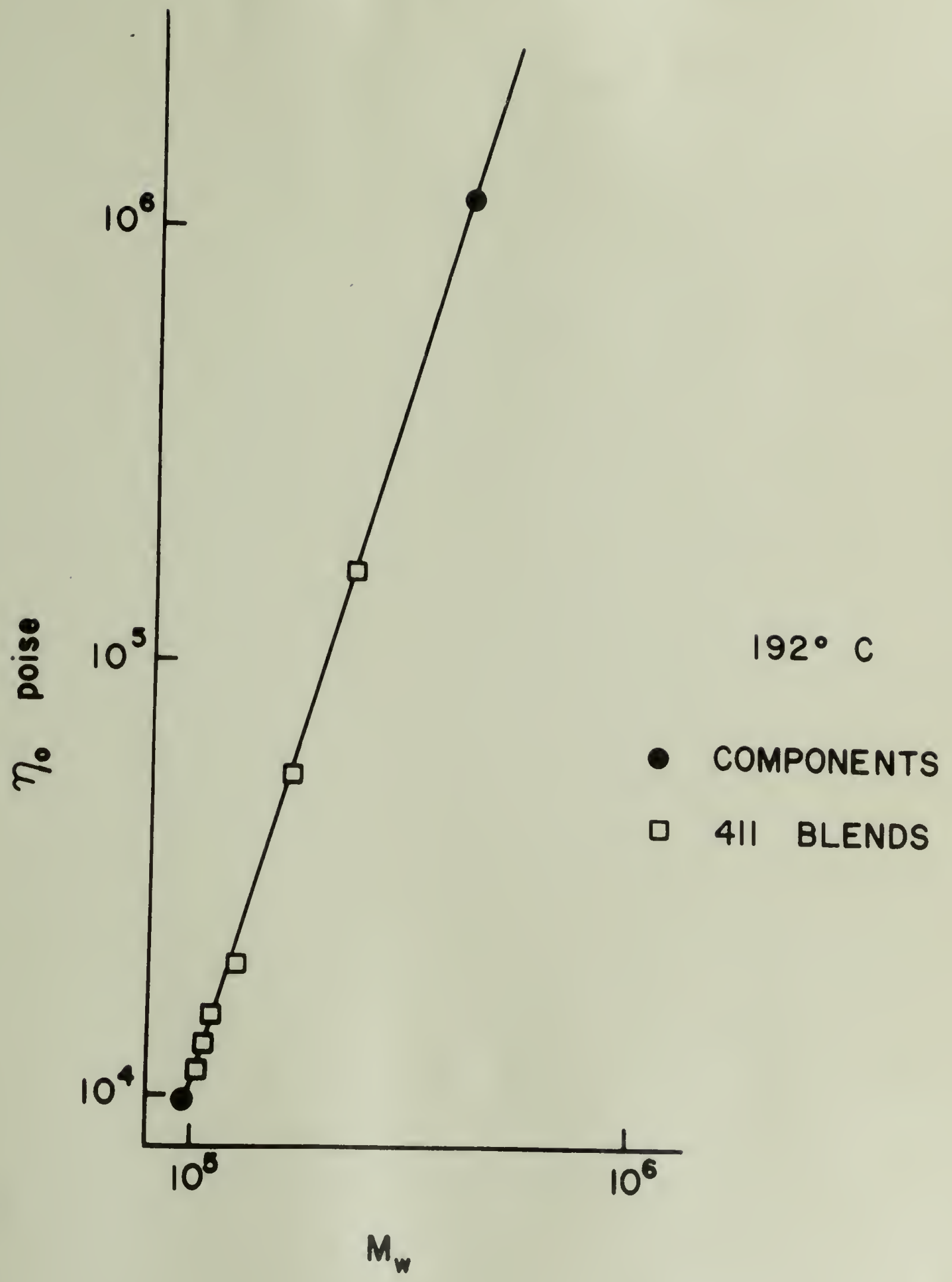

Figure 8

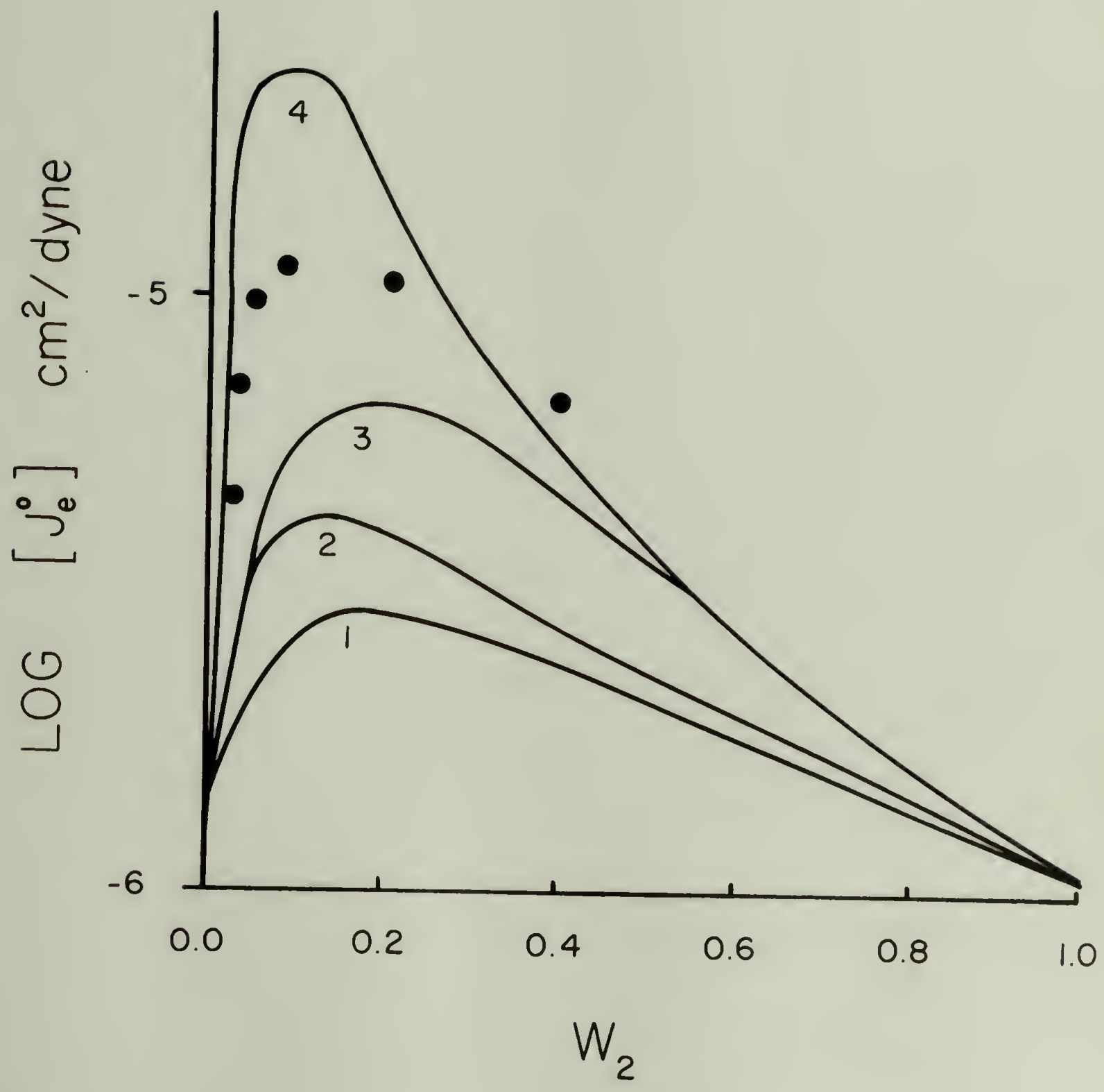

Figure 9

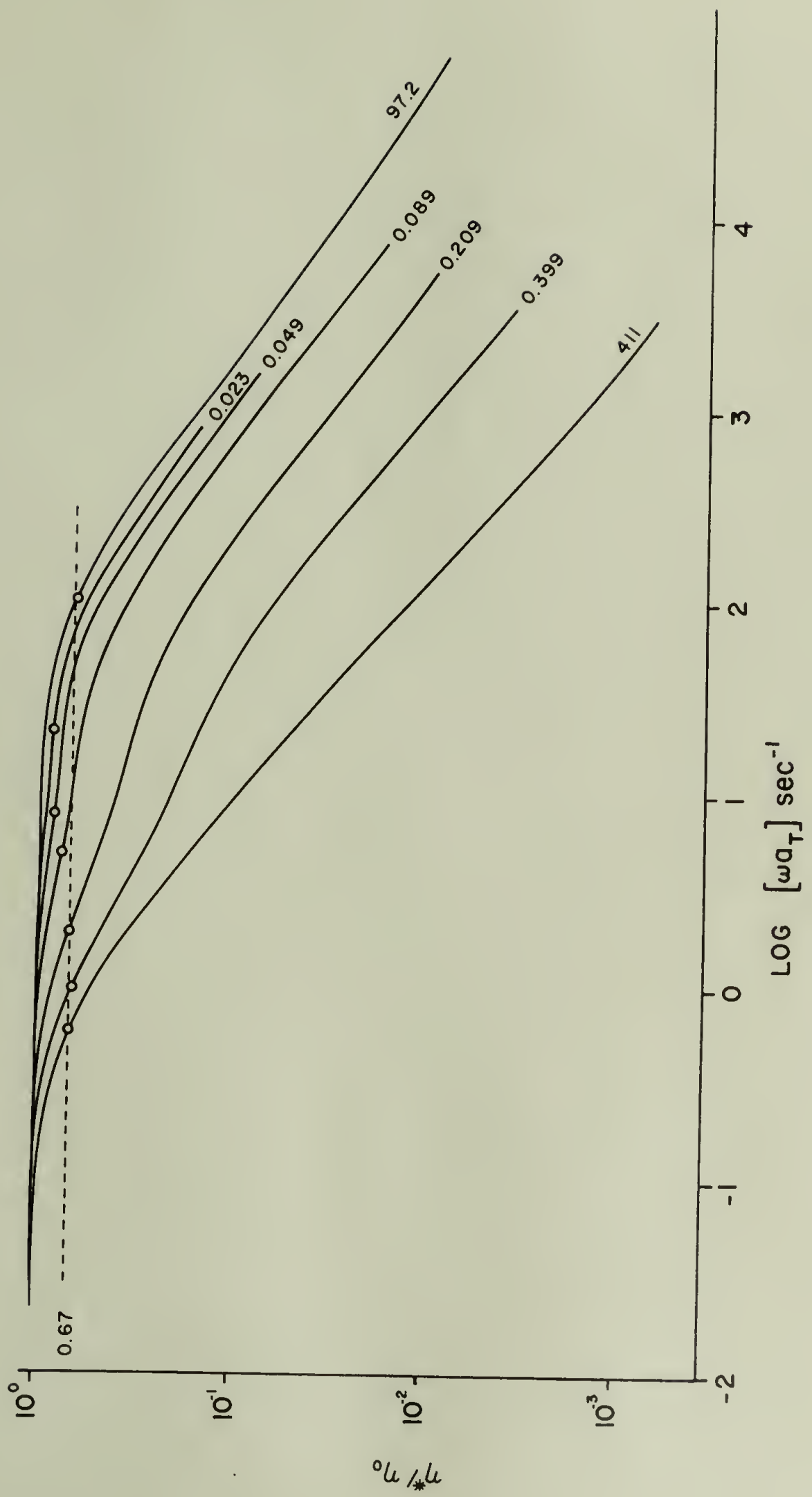
97.2
0.089
0.209
0.399
411
0.023
0.049
0.67
10^{0}
10^{-1}
10^{-2}
10^{-3}
η^*/η_0
-2
-1
0
1
2
3
4
LOG $[\omega a_T]$ sec^{-1}

Figure 10

CHAPTER III

Blending Laws for High Molecular Weight Polymer Melts

W. M. Prest, Jr.*
Polymer Science and Engineering
University of Massachusetts
Amherst, Massachusetts 01002

ABSTRACT

Blending laws have been previously proposed to describe the effects of molecular weight distribution (MWD) on the viscoelastic properties of polymer melts. The blending laws represent the relaxation spectrum of a blend $H_B(\tau)$ as a weighted sum of the relaxation spectra of the individual components, each shifted in time by an amount characteristic of the interactions between the molecular species. In general, the binary blending law is

$$H_B(\tau) = \sum_{i,j=1}^{2} V_{ij} H_{ij}(\tau/\lambda_{ij})$$

The weighting factors V_{ij}, and shift factors λ_{ij} may be obtained directly from the calculated relaxation spectra of blends of narrow MWD fractions. These parameters are used to test the applicability of two types of blending laws: 1) The quadratic blending law, $V_{ij} = w_i w_j$, where w_k is the weight fraction of the k^{th} component; and 2) The simple blending law, $V_{ij} = v_i \delta_{ij}$. The experimental results give qualified support to the quadratic blending law but place strong restrictions on the magnitude and shape of the cross relaxation spectra term H_{ij}.

---

* Present address, Xerox Corporation, Rochester, N.Y. 14604

These require that $H_{ij} \neq H_{ji}$, H_{ij}/H_{ii} = constant, and $\lambda_{ij} = \lambda_{ii}$. In addition, the restrictions imply that the simple and the quadratic blending laws are equivalent representations of $H_B(\tau)$.

INTRODUCTION

Blending laws have been previously proposed (1,2,3) to describe the effects of molecular weight distribution (MWD) on the viscoelastic properties of polymer melts. The blending laws represent the relaxation spectrum of a blend $H_B(\tau)$, as a weighted sum of the relaxation spectra of the individual components, each shifted in time by an amount characteristic of the interactions between the molecular species.

Ninomiya (1) originally suggested the simple blending law given by equation 1.

$$H_B(\tau) = \sum_i v_i H_i(\tau/\lambda_i) \qquad (1)$$

where v_i is the volume fraction of the i^{th} component and $H_i(\tau/\lambda_i)$ is the relaxation spectrum of that component shifted in time by a factor λ_i. This blending law has been examined in detail by Ninomiya, Ferry and coworkers (4-8) and has been used to predict the viscoelastic response, the zero shear viscosity η_{oB}, and the steady state shear compliance J^o_{eB} of several homopolymer blends and polymer solvent systems.

Recently, it has been shown (9-12) that eq. 1 does not explain the MWD dependence of J^o_{eB} and the viscoelastic response of high MW polymer blends. Prest (9) has reported that the properties and response of high MW poly dimethyl siloxane blends may be described by eq. 1 with effective

weighting factors v_i, which are in general, less than the volume fractions of the components. Masuda and coworkers (10) suggested that, in high molecular weight blends, entanglement couplings between the different MW species give rise to a set of relaxation mechanisms with time constants between the shifted relaxation times of the individual components. Bogue et al. (2) formalized this proposal by suggesting a quadratic blending law of the form

$$H_B(\tau) = w_1^2 H_{11}(\tau/\lambda_{11}) + 2w_1w_2H_{12}(\tau/\lambda_{12}) + w_2^2 H_{22}(\tau/\lambda_{22}) \qquad (2)$$

where w_i is the weight fraction of the i^{th} component and $H_{12}(\tau)$ is a cross relaxation spectrum term. Recently Graessley (3) has proposed a theory to explain the effects of MWD in high MW systems. This approach to binary blends considers the relaxation processes of molecule A interacting with molecule B, to be different from those of B interacting with A. This leads to a quadratic blending law in which the cross term consists of the separate components $w_1w_2\ H_{12}(\tau/\lambda_{12})$ and $w_2w_1\ H_{21}(\tau/\lambda_{21})$, where in general $H_{12}(\tau) \neq H_{21}(\tau)$ and $\lambda_{12} \neq \lambda_{21}$.

A general binary blending law encompassing all of the above can be written as

$$H_B(\tau) = \sum_{ij=1,2} V_{ij}H_{ij}(\tau/\lambda_{ij}) \qquad (3)$$

For the simple blending law $V_{ij} = v_i\ \delta_{ij}$ where $\delta_{ij} = 1$ if $i = j$ and is zero otherwise and v_i is the effective weighting factor, which is equal to the volume fraction for the Ninomiya blending law. The quadratic blending law is given by $V_{ij} = w_iw_j$ where w_k is the weight fraction of each component.

The viscoelastic properties of a blend described by eq. 3 may be calculated from the phenomenological relations of linear viscoelasticity (13,14). The loss modulus of the blend $G''_B(\omega)$, is

$$G''_B(\omega) = \sum_{i,j} V_{ij} G''_{ij}(\omega\lambda_{ij}) \tag{4}$$

A similar equation applies to the storage modulus, $G'_{ij}(\omega\lambda_{ij})$. The properties of the blend in the terminal region, J^o_{eB} and η_{oB} are related to the properties of the components by

$$\eta_{oB} = \sum_{i,j} V_{ij} \lambda_{ij} \eta_{oij} \tag{5}$$

and

$$J^o_{eB} = \sum_{i,j} V_{ij} (\lambda_{ij} \eta_{oij} / \eta_{oB})^2 J^o_{eij} \tag{6}$$

The experimental viscoelastic response of blends of different molecular weight polymers can be used to evaluate the parameters V_{ij} and λ_{ij}. Previously these parameters were obtained by an intercomparison of the measured viscoelastic properties, G'and G", from eq. 4 and related equations. However, this technique depends primarily on the choice of the poorly defined quantity V_{22}. A more direct test of the successes and deficiencies of the proposed blending laws can be obtained through a comparison of the calculated relaxation spectra of blends, $H_B(\tau)$. This study determines the blending law parameters from relaxation spectra calculated from the previously reported (12) viscoelastic response of blends of high MW, narrow MWD polystyrene samples. The experimentally defined parameters are used to analyze the proposed blending laws.

Relaxation Spectra

Several approximations (14) have been used to calculate $H(\tau)$ from the experimentally measured viscoelastic response. These techniques, involving various combinations of the derivatives of a viscoelastic function, are very sensitive to small variations in the data. In a companion study (15), a comparison was made between the relaxation spectra calculated by five different approximations. The method proposed by Tschoegl (16) was found to produce the least fluctuations in the terminal region of the calculated $H(\tau)$. However, small fluctuations were apparent when the slope of $H(\tau)$ changed rapidly. Previous studies (12) have shown that changes in MWD primarily effect the long time region of the viscoelastic response. The relaxation spectra presented in this paper were calculated by Tschoegl's approximation in order to examine the effects of MWD in the terminal region. The calculation of $H(\tau)$ is based on values of G' and G" defined by the master curves of the samples viscoelastic response. The spectra determined from G' and G" were in close agreement, indicating that both sets of data were consistent with each other.

The relaxation spectra at T = 192°C, of blends formed by mixing samples with MWs of 97,200 and 411,000, are shown in Figure 1. The numbers indicate the weight fraction of the high molecular weight component. The relaxation spectrum of the 411,000 MW, narrow MWD component shows a long plateau at short and intermediate times. This is associated with the relaxation processes involving the interactions or "entanglements" between molecules. Others report a minimum in $H(\tau)$ in this region for high MW systems with narrow MWD's (10). The data

presented here indicates a slight decrease in $H(\tau)$. This difference may be the result of the particular MWD of the samples. However it should be noted that the subsequent analysis of the data is insensitive to the specific shape of this intermediate response region of $H(\tau)$. At long times there is a very rapid decrease in $H(\tau)$. The slope of the log $H(\tau)$ vs log τ plot in the terminal region is initially equal to -2 and then becomes less than -3. This end result, which is expected to be different from the -1/2 predicted by the Rouse theory (17) for non-interacting molecules, is still much less than the -1 dependence predicted by the Chompff and Duiser theory (18) for a network with moble cross-links. The relaxation spectrum of the 97,200 MW, narrow MWD component also shows the same rapid decrease in $H(\tau)$ at long times and a short rubbery plateau, 50% higher than that observed for the 411,000 sample.

The addition of a small amount of the 411,000 MW sample to the 97,200 MW sample shifts the relaxation spectrum of the latter toward longer times and produces a distinct shoulder on $H(\tau)$. This shoulder becomes more prominant and greater in magnitude as the concentration of the high MW component increases. Little significance can be attached to the small maxima which appear on the shoulders of the calculated $H_B(\tau)$. These occur in a region where the numerical approximations for the second derivatives of the VE function used in the Tschoegl approximation are very sensitive to the experimental data (15). Thus the calculated $H_B(\tau)$ is expected to be subject to fluctuations. Typical oscillations in the experimental data are given in Figure 2 for the $w_2 = 0.049$ blend. The additional contribution to $H(\tau)$, represented by the shoulders, is responsible for the very high compliances of the blends. As w_2 increases, the initial fall off in $H_B(\tau)$ moves gradually to longer times while,

beyond the shoulder, the final decrease in $H_B(\tau)$ shifts rapidly towards much longer times.

Parameters of the Simple Blending Law

The general properties of the simple blending laws may be seen by considering the addition of idealized box shaped relaxation spectra. This is demonstrated in Fig. 3 where H_{ij} is the magnitude of the relaxation spectrum and τ_{ij} is the maximum relaxation time of component i in blend j. By definition the weighting factors and shift parameters for blend k are

$$V_{11} = \frac{H_{1k} - H_{2k}}{H_{11}} \quad \tau < \tau_{1k};\ \lambda_{11} = \tau_{1k}/\tau_{11} \tag{7}$$

$$V_{22} = H_{2k}/H_{22} \quad \tau > \tau_{1k};\ \lambda_{22} = \tau_{2k}/\tau_{22} \tag{8}$$

Note that V_{11} is determined by subtracting the contribution of H_{2k} from the relaxation spectrum of the blend, H_{1k}.

The calculated relaxation spectra shown in Figure 1 allow the direct measurement of the weighting factors V_{ii} and the shift factors λ_{ii} of the simple blending law. The contribution of the high MW component to the relaxation spectrum of the blend V_{22}, is the ratio of the height of the shoulder of $H_B(\tau)$ to the height of the plateau of the relaxation spectrum of the high MW component, $H_{22}(\tau)$. The shift factor λ_{22} is the constant needed to superimpose the long time portion of $V_{22}H_{22}(\tau)$ on $H_B(\tau)$. The quantity V_{11} is obtained from the low τ plateau response of the components by equation 7. The shift factor λ_{11} is determined by matching the initial decrease in the response of $H_{11}(\tau)$ and $H_B(\tau)$. These values are listed in Table I.

In Figure 1, it appears that the shape of the long time response changes with composition. This would make superposition an arbitrary procedure. However, close inspection of Figure 1 reveals that the apparent differences reflect the change in the shape of the terminal region of the high MW components $H(\tau)$ from the initial τ^{-2} dependence to the final τ^{-3} response.

The terminal properties of the blends, η_{o1B} and J^o_{eB}, may be calculated from the blending law parameters with equations 5 and 6 or by the direct intergration of $H_B(\tau)$ according to the phenomenological relations of linear viscoelasticity (13,14). Table II demonstrates the agreement that is found between the calculated values of these properties and the experimental results.

Weighting Factors

The dependence of the weighting factors V_{ii}, on the respective weight fractions w_k are shown in Figure 4. The brackets on the data are determined by the maximum and minimum values of the height of the shoulders and represent the possible uncertainties in the calculated weighting factors. The dot-dash-dot line is the behavior that would be expected if $V_{ii} = w_i$, the condition of the simple blending law proposed by Ninomiya (1). The dashed line corresponds to $V_{ii} = w_i^2$. The observed V_{22} are proportional to w_2^2 at large w_2. However, significant deviations from this quadratic behavior are observed at small w_2. Note that unlike V_{22}, the weighting factors for the low MW component V_{11}, are approximately equal to the weight fractions of the low MW component, w_1. Thus even though there is a great deal of

uncertainty in the determination of V_{11}, the sum of V_{11} and V_{22} is not one. This observation is confirmed by calculating V_{11} from equation 5 and the measured values of V_{22}, λ_{22}, λ_{11} and the experimental η_{oB}. The calculated V_{11}, listed in Table III, are consistent with the measured values. Thus, if the simple blending law is to describe the interactions of high MW polymers, the resulting blending law is not symmetric in the weighting factors of the components.

Shift Factors

Implicit in the determination of V_{ii} is the necessity of shifting the components spectra by an amount λ_{ii}. The shift factors represent the ratios of a molecular species relaxation time in a blend to that time in the pure component. Relaxation times in polymers are controlled by the elastic properties and the viscous drag forces in the melt. In blends of components with similar elastic properties the shift factors are expected to be related to the same MW averages which control the viscosity of the melt, M_w. This is also implied by the simple blending law. If $V_{ii} = w_i$ and all the viscosities are simply related to M_w, then eq. 5 implies that λ_{ii} is a function of M_w. This restriction is relaxed as V_{ii} becomes a more complicated function of w_i, i.e., as the elastic effects of entanglements become more important. The experimental shift factors are listed in Table I along with $\lambda_{22}/\lambda_{11}$. This ratio is seen to increase with w_2. Examination of the data shows that while λ_{11} can be represented by a power of M_w, λ_{22} depends on a higher moment of the MWD. A correlation of λ_{11} with M_w and λ_{22} with M_z is presented in Figure 5. The asymmetry of this dependence reflects the differences

between the functional forms of V_{11} and V_{22}.

If the blending law is to apply to the entire relaxation spectrum of the components, that is to the relaxation mechanisms of short molecular segments as well as those associated with entanglements, then the experimental parameters must be consistent with the response of $H(\tau)$ in the transition region. The Rouse theory (17) predicts that $H(\tau)$ is proportional to $\tau^{-1/2}$ in the transition region. For a given polymer, the iso-free volume transition region response is independent of MW and MWD. (14). This has been demonstrated for polystyrene (10). The simple blending law reduces each component's $\tau^{-1/2}$ region response by V_{ii}. In addition, the shift factors effectively change the contribution to $H_B(\tau)$ at a given τ by $\lambda_{ii}^{1/2}$. Therefore, if the transition region response is to be independent of MWD,

$$\sum_{i=1}^{2} V_{ii} \lambda_{ii}^{1/2} = 1 \qquad (9)$$

The experimental values of this sum, listed in Table I, prove that the simple blending law may be applied to the entire VE spectrum of high MW polystyrene blends. Equation 9 also explains why the sum of the experimental weighting factors is not equal to one.

Relationships between the shift factors may be obtained from Figure 3. Define the ratio of the maximum relaxation times of the components and the ratio of the blend shifted τ as

$$L_{21} = \tau_{22}/\tau_{11} \; ; \quad l_{21k} = \tau_{2k}/\tau_{1k} \qquad (10)$$

Then from equations 7 and 8

$$\lambda_{2k}/\lambda_{1k} = l_{21k}/L_{21} \qquad (11)$$

The choice of the components defines L_{21}, which is a constant for any blend series. For the box shaped relaxation spectra in Fig. 3, $\eta_{oii} = H_{ii}\lambda_{ii}$. Then L_{21} is proportional to the ratio of the viscosities of the components and thus to a power of the ratio of the molecular weights of the blended species. The width of the secondary plateau is proportional to l_{12k}. Thus the ratio of the shift factors is a measure of the width of the secondary plateau relative to the difference between the components terminal response. Figure 1 shows that the width of the shoulder on $H_B(\tau)$ decreases with the concentration of the high MW component, in accordance with the observed dependence of $\lambda_{22}/\lambda_{11}$. (See Table I). This conflicts with Ninomiya and Ferry's (6) observation that $\lambda_{22}/\lambda_{11}$ is a constant for high MW polystyrene blends. However, in that study, the V_{ii} were assumed to be the weight fractions of the components and the λ_{ii} were determined from the experimental relaxation moduli. This definition of V_{ii} would decrease the apparent compositional dependence of the ratio of the shift factors.

The observed compositional dependence of $\lambda_{22}/\lambda_{11}$ limits the general application of the blending laws. Ninomiya and Ferry (16) have shown that the blending laws may be applied to blends of blends, if and only is the ratio of the shift factors is independent of w_2 for a given ratio of MWs. This is demonstrated by the relaxation spectrum of blend j in Figure 3. Sample j may be considered to be either a blend of components 1 and 2 or an appropriate mixture of component 1 and blend k. If the blending laws apply to the latter case, the maximum relaxation time of blend k is shifted by an amount

$\lambda_{kj} = \tau_{2k}/\tau_{2j}$. But all parts of the spectrum must be shifted by the same amount, $\tau_{1k}/\tau_{1j} = \tau_{2k}/\tau_{2j}$, which is equivalent to $l_{21j} = l_{21k}$. This states that the width of the secondary plateau must be a constant if the blending law is to apply to blends of blends, a condition which is not observed in the experimental data presented in Figure 1.

Parameters of the Quadratic Blending Law

Long Time Response

The initial dependence of V_{22} on w_2^2 shown in Figure 4 supports the idea of a quadratic blending law. In addition, it may be argued that the deviation of V_{22} from the quadratic behavior is the result of the contribution of the cross relaxation spectrum. To test this proposition it is necessary to calculate $H_{12}(\tau/\lambda_{12})$.

If the cross term is to account for the observed deviations, the response of the shoulder of the relaxation spectrum of a blend must be composed of the sum of the quadratic term $w_2^2 H_{22}(\tau/\lambda_{22})$ and $2w_1w_2H_{12}(\tau/\lambda_{12})$. Then, since w_1, w_2 and $H_{22}(\tau)$ are defined, and $w_1^2 H_{11}(\tau/\lambda_{11})$ is negligible, the experimental $H_B(\tau)$ can be used to obtain the response of $H_{12}(\tau/\lambda_{12})$ and the shift factor λ_{22}.

In the analysis of the simple blending law it was found that the shoulder in $H_B(\tau)$ could be described by $V_{22}\ H_{22}\ (\tau/\lambda_{22})$. Then for τ corresponding to relaxation processes represented by the shoulder in $H_B(\tau)$, the experimental data is related to the quadratic blending law by

$$V_{22}\ \frac{H_{22}(\tau/\lambda^*_{22})}{H_{22}(\tau/\lambda_{22})} = w_2^2 + 2w_1w_2\ \frac{H_{12}(\tau/\lambda_{12})}{H_{22}(\tau/\lambda_{22})} \qquad (12)$$

where the experimentally measured shift factor is denoted by λ_{22}^*. The cross term $H_{12}(\tau/\lambda_{12})$ can be calculated from the experimental data once λ_{22} is chosen. In general the shape of $H_{12}(\tau)$ will be different than the shape of $H_{22}(\tau)$ unless $\lambda_{22} = \lambda_{22}^*$. However, if λ_{22} does not equal λ_{22}^* the shape of $H_{12}(\tau)$ is a function of the composition of the blend (see equation 12). But the form of the blending law states that $H_{12}(\tau)$ is independent of w_2. Therefore $\lambda_{22} = \lambda_{22}^*$ and $H_{12}(\tau/\lambda_{12})/H_{22}(\tau/\lambda_{22})$ is a constant. Then, if the quadratic blending law describes the blends long time response, a plot of log $(V_{22}-w_2^2)$ versus log $(2w_1w_2)$ will produce a line with a slope of one. From this graph the quantity H_{12}/H_{22} can be evaluated. The data presented in Figure 6 give qualified support to the cross term proposal. The line drawn with unity slope indicates that the magnitude of H_{12} in the long time region is approximately one-tenth that of H_{22}.

Short Time Response

While the cross term, $H_{12}(\tau/\lambda_{12})$ can be used to account for the difference between V_{22} and w_2^2; it does not explain the observed dependence of V_{11} on w_1. The shape of the blends short time rubbery plateau response is experimentally independent of the compositional ratio (see Figure 1). Therefore by the arguments developed above, the responses of $H_{11}(\tau/\lambda_{11})$ and $H_{12}(\tau/\lambda_{12})$ have similar shapes and, at short times, $\lambda_{12} = \lambda_{11}$. The ratio of the magnitude of these spectra may be calculated in a manner similar to equation 12. The widely scattered results shown in Figure 6 imply that $H_{12}/H_{11} \approx 0.6$. Thus, since

$H_{12}/H_{22} \simeq 0.1$, the cross term H_{12} must be a two step function of τ (i.e., - exhibit two plateaus). However, the experimentally observed compositional dependence of $\lambda_{22}/\lambda_{11}$ (Table I) states that the cross term can not remain independent of w_2 and simultaneously be subject to the conditions that $\lambda_{12} = \lambda_{11}$ at low τ and $\lambda_{12} = \lambda_{22}$ at high τ. Therefore the quadratic blending law with a single cross term (equation 2) does not describe the observed relaxation spectra.

It is important to note that Graessley's quadratic blending law is not subject to the above condition because it contains two cross terms, $H_{12}(\tau/\lambda_{12})$ and $H_{21}(\tau/\lambda_{21})$, which in general are not equal. In addition, the required similarity between the shapes of the cross terms and the component's spectra make Graessley's quadratic blending law equivalent to the simple blending law with

$$V_{11} = w_1^2 + w_1 w_2 \, H_{12}/H_{11} , \qquad \lambda_{12} = \lambda_{11}$$

$$V_{22} = w_2^2 + w_1 w_2 \, H_{21}/H_{22} , \qquad \lambda_{21} = \lambda_{22}$$

Thus, by definition, the two term quadratic blending law describes the experimental long and short time response of $H_B(\tau)$.

The experimental conclusion that the simple and the quadratic blending laws are equivalent representations of $H_B(\tau)$ is particularly surprising because the cross terms were originally introduced to account for the appearance of a set of relaxation times intermediate to the shifted spectra of the components (10). This set of τ appears in the spectra of the $w_2 = 0.209$ and $w_2 = 0.399$ blends shown in Figure 1 as the broad transition between the main body and the shoulder of $H_B(\tau)$.

Note that this transition is more gradual than the rapid fall off in the terminal response of the 97,200 MW component.

While this broad intermediate response seems to represent a new set of relaxation times, it can be shown that this region is just the sum of the relaxation spectra of the components. This is demonstrated in Figure 7 for the $w_2 = 0.209$ blend. The solid line is the measured $H_B(\tau)$. The broken lines are the spectra of the two components, weighted and shifted by V_{ii} and λ_{ii}. The solid points are the sum of these contributions. The shape of this intermediate region is controlled by the terminal response of $V_{11} H_{11} (\tau/\lambda_{11})$ over the range of τ where it intersects $V_{22} H_{22} (\tau/\lambda_{22})$. As $H_{11}(\tau)$ decreases, the slope of $H_{11}(\tau)$ decreases. Thus the contribution of $H_{11}(\tau/\lambda_{11})$ to the intermediate time response decreases with the concentration of the higher MW component. This accounts for the broad transition observed at large w_2 and the apparent lack of this response at small w_2.

Discussion

The choice of a particular blending law depends on a proposed theoretical models ability to calculate either the set of parameters, V_{11} and V_{22} or H_{12}/H_{22} and H_{12}/H_{22}. At first it appears that the V_{ii} are useful only in the calculation of H_{21}/H_{22} and H_{12}/H_{22} from experimental data. However the V_{ii} have particular significance by themselves. This may be seen from eq. 4. At low frequencies G" is the stress on the sample. Then the V_{ii} represent the contribution of molecular species i, to the total stress supported by the sample.

As an example, the simple blending law may be applied to the formalism developed by Fixman (19) concerning the behavior of molecules in solution. According to Fixman (19), the stress tensor of a flexible molecule in solution is

$$\sigma = \langle\sigma_o\rangle + c \sum_i R_i \nabla_i U + 1/2\ c^2 \langle R_{12} \nabla_2 V(R_{12})\rangle \qquad (14)$$

where $\sum_i R_i \nabla_i U$ is an average over the interactions between each segment and all other segments in the solution and c is the concentration of the molecules in solution. The coefficient of the c^2 term takes into account interactions between separate molecules other than entanglements (i.e., excluded volume) through the potential $V(R_{12})$ where R_{12} is the vector distance between the molecules center of mass. Applications of Fixman's equation assume that the interaction potential U is a pair wise additive function of the potential energy between segments. Williams (20) points out that this assumption fails in concentrated solutions where it is necessary to take into account three body cooperative interactions. Such a treatment would add a c^3 term to the stress tensor, physically corresponding to entanglement interactions. If individual molecules in a melt can be considered to be molecules in a very concentrated solution and if the stress contributions can be treated in this manner the experimental V_{ii} should be representable by a cubic equation in the individual weight fractions, w_i. The coefficients of the c, c^2, and c^3 terms would then represent the intramolecular, the intermolecular and the entanglement interaction contributions to the total stress. As the size (i.e., MW) and concentration of the individual components is increased the major contribution to the stress would shift from a primary dependence on c,

to c^2, and c^3. The weighting factors of the low MW species in a blend would then have a different functional dependence than the V_{ii} of the high MW components.

The systematic deviation of the data in Figure 5 from the first power dependence on $w_1 w_2$ suggests that the V_{ii} may be better represented by a cubic equation in w_2 than by the quadratic blending law. The results of a least squares regressional analysis are given by equation 15.

$$V_{22} = 0.21\ w_2 + 0.42\ w_2^{\ 2} + 0.37\ w_2^{\ 3} \qquad (15)$$

In the context of the previous discussion this suggests that, for M = 411,000, the entanglement contribution to the stress is of the same order as that supported by the intermolecular interactions and about twice that of the intramolecular term.

Table I

Blending Law Parameters

w_2	V_{11}	V_{22}	λ_{11}	λ_{22}	$\lambda_{22}/\lambda_{11}$	$\sum_{i=1}^{2} V_{ii}\lambda_{ii}^{1/2}$
0.000	1.00		1.00			
0.023	0.95	0.007	1.06	0.17	0.16	0.98
0.049	0.90	0.0125	1.25	0.23	0.184	1.01
0.089	0.85	0.024	1.35	0.27	0.20	1.00
0.209	0.80	0.067	1.80	0.45	0.25	1.12
0.399	0.60	0.175	2.40	0.70	0.29	1.08
1.000		1.000		1.00		

Table II

Terminal Properties of Blends at 192°C

w_2	$\eta_{oB} / 10^4$, poise			$J^o_{eB} / 10^{-6}$, cm^2 / dyne		
	Measured	Calculated from eq. 5	$H_B(\tau)$	Measured	Calculated eq. 6	$H_B(\tau)$
0.000	1.00		1.08	1.1		1.08
0.023	1.15	1.16	1.26	4.5	4.2	5.15
0.049	1.51	1.48	1.59	9.0	7.3	9.65
0.089	1.97	1.96	1.97	11.	10.4	9.00
0.209	5.43	5.21	5.53	10.5	11.	9.85
0.399	16.0	16.9	17.0	6.7	6.6	6.95
1.000	125.		140.	1.4		1.88

Table III

Experimental and Calculated V_{11}

w_2	Measured	V_{11} from eq. 5
0.023	0.95	0.94
0.049	0.90	0.92
0.089	0.85	0.83
0.209	0.80	0.83
0.399	0.60	0.67

REFERENCES

1. K. Ninomiya, J. Colloid Sci., 14, 527 (1959).
2. D. C. Bogue, T. Masuda, Y. Einaga, and S. Onogi, Polym. J., 1, 563 (1970).
3. W. W. Graessley, J. Chem. Phys., 54, 5143 (1971).
4. K. Ninomiya, J. Colloid Sci., 17, 759 (1967).
5. K. Ninomiya, J. D. Ferry, and Y. Oyanagi, J. Phys. Chem., 67, 2297 (1963).
6. K. Ninomiya and J. D. Ferry, J. Colloid Sci., 18, 421 (1963).
7. K. Ninomiya and G. Yasuda, Rubber Chem. Technol., 40, 493 (1967).
8. K. Ninomiya and J. D. Ferry, J. Macromol. Sci. - Phys., B3(2), 237 (1969).
9. W. M. Prest, Jr., J. Polymer Sci., A-2, 8, 1897 (1970).
10. T. Masuda, K. Kitagawa, T. Inoue and S. Onogi, Macromolecules, 3, 116 (1970).
11. N. J. Mills and A. Nevin, J. Polymer Sci., A-2, 9, 267 (1971).
12. W. M. Prest, Jr. and R. S. Porter, submitted to Polymer Journal.
13. B. Gross, Mathematical Structure of the Theories of Viscoelasticity, Hermann et Cie., Paris, 1953.
14. J. D. Ferry, Viscoelastic Properties of Polymers, John Wiley & Sons, Inc., New York, N.Y., 1961, 1970.
15. W. M. Prest, Jr. and R. S. Porter, in preparation. (Appendix A).
16. N. W. Tschoegl, submitted to Trans. Soc. Rheology. - (ref. 14 pps. 92,94).
17. P. E. Rouse, J. Chem. Phys., 21, 1272 (1953).

18. A. J. Chompff and J. A. Duiser, J. Chem. Phys., 45, 1505 (1966).

19. M. J. Fixman, J. Chem. Phys., 42, 3831 (1965).

20. M. C. Williams, A.I.Ch.E. J., 12, 1064 (1966).

FIGURE CAPTIONS

Figure 1 The relaxation spectra of blends of 97,200 MW and 411,000 MW polystyrene at 192°C. The numbers indicate the weight fractions of the 411,000 MW sample.

Figure 2 Relaxation spectrum of the $w_2 = 0.049$ blend.

Figure 3 Addition of box shaped relaxation spectra.

Figure 4 The dependence of the effective weighting factors V_{ii} on the weight fractions w_i of the high (i = 2) and low (i = 1) MW components of the 411,000/97,200 blend series. --- = w_i^2, - · - = w_i^1.

Figure 5 The dependence of the shift factors λ_{11} and λ_{22} on the weight and Z average molecular weights of the blends.

Figure 6 Calculation of the magnitude of the cross relaxation spectrum.

Figure 7 The simple blending law construction of the relaxation spectrum of the $w_2 = 0.209$ blend from the sum (...) of the relaxation spectra (---) of the components.

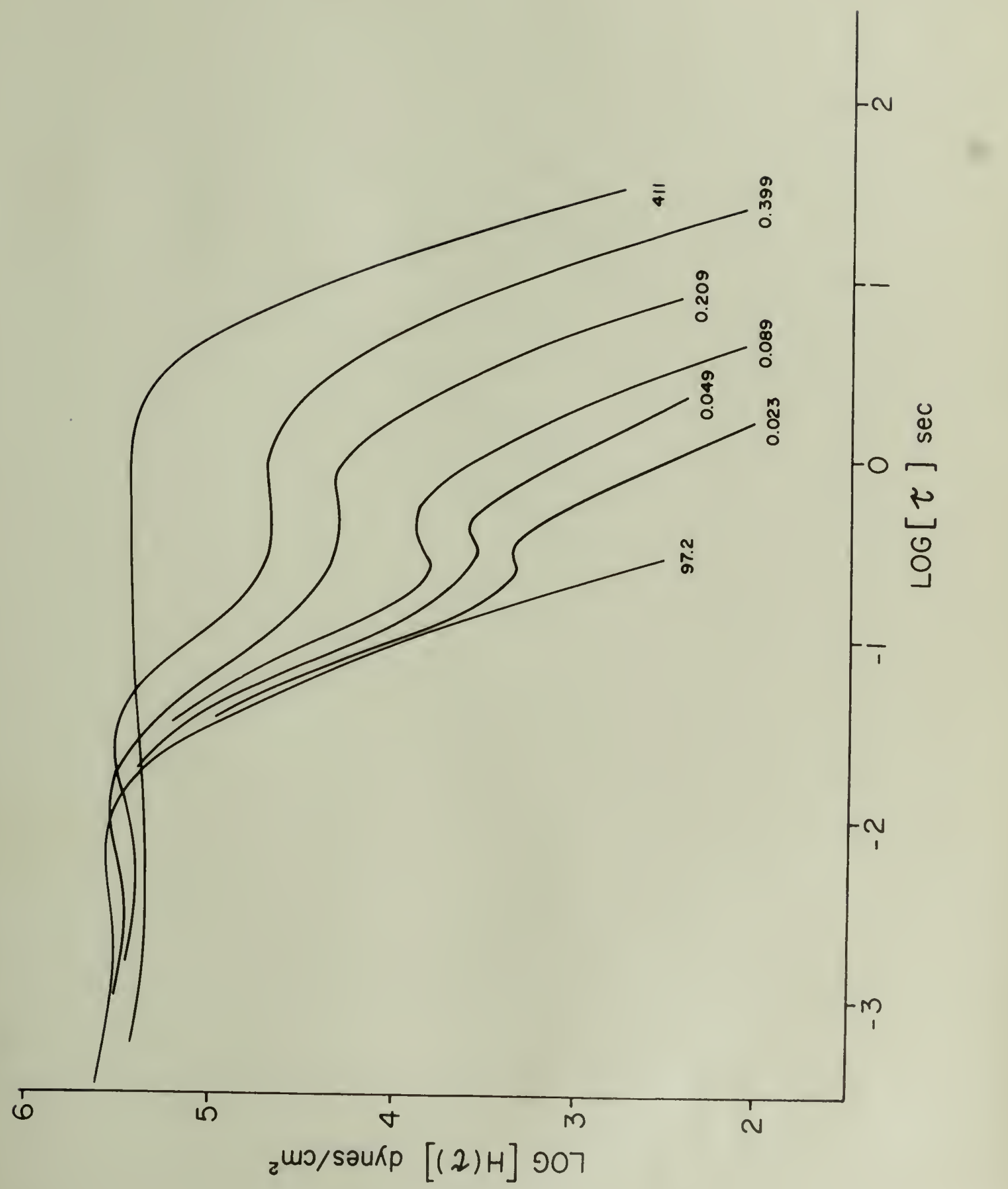
411
0.399
0.209
0.089
0.049
0.023
97.2
LOG [H(τ)] dynes/cm²
LOG[τ] sec
6
5
4
3
2
2
1
0
-1
-2
-3

Figure 1

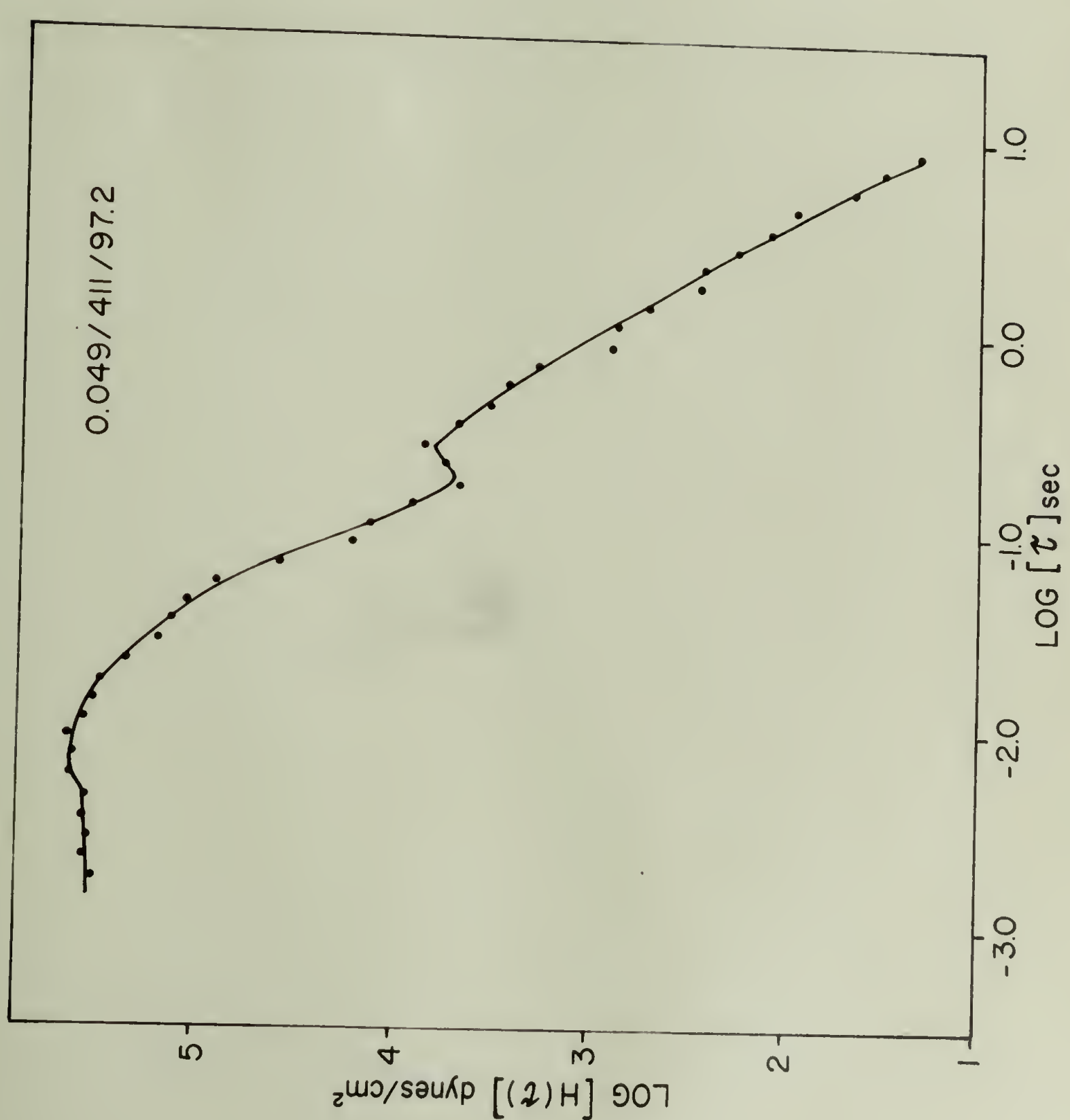

Figure 2

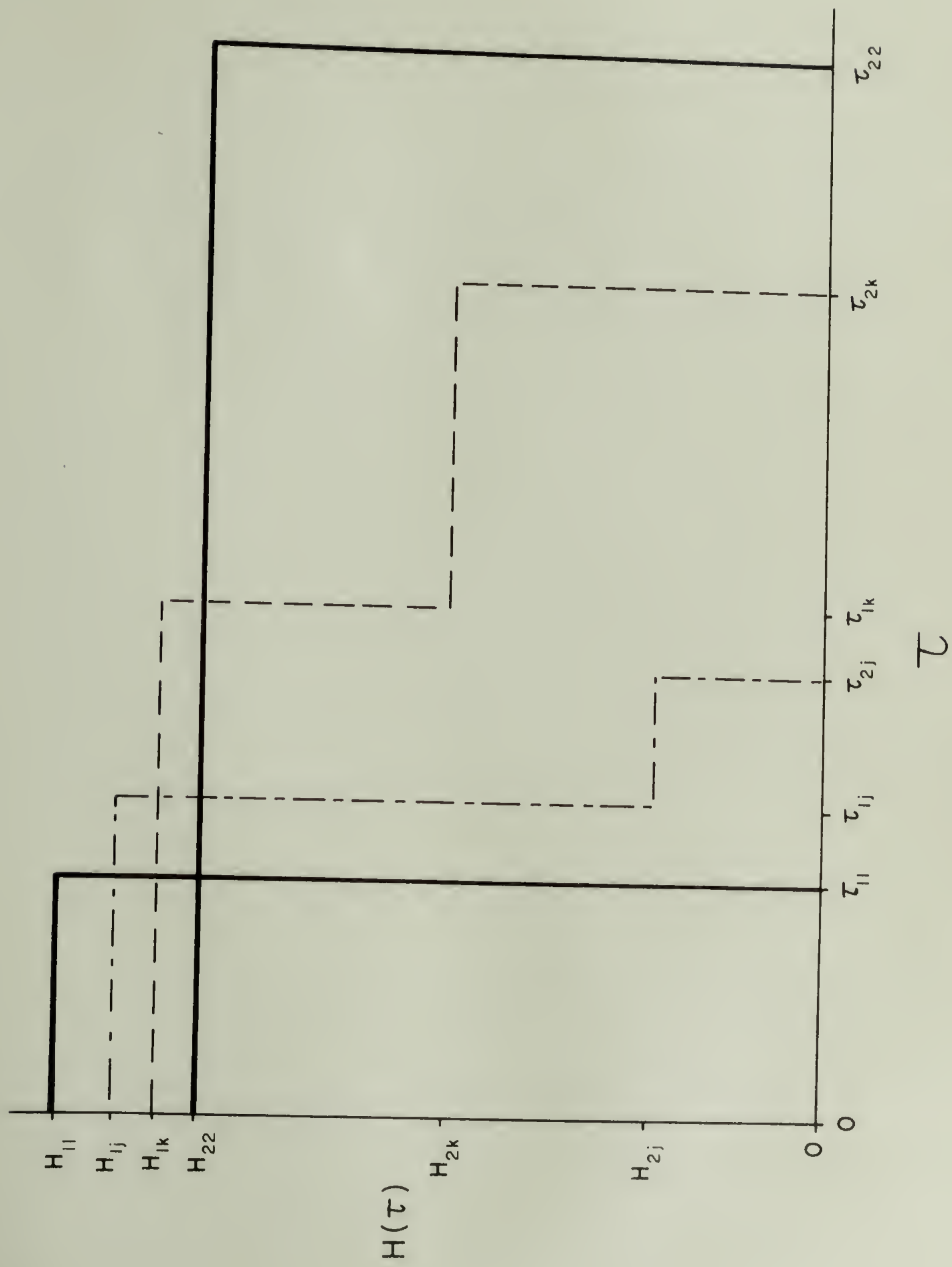
τ_{22}
τ_{2k}
τ_{1k}
τ_{2j}
τ_{1j}
τ_{11}
0
H_{11}
H_{1j}
H_{1k}
H_{22}
H_{2k}
H_{2j}
0
$H(\tau)$
τ

Figure 3

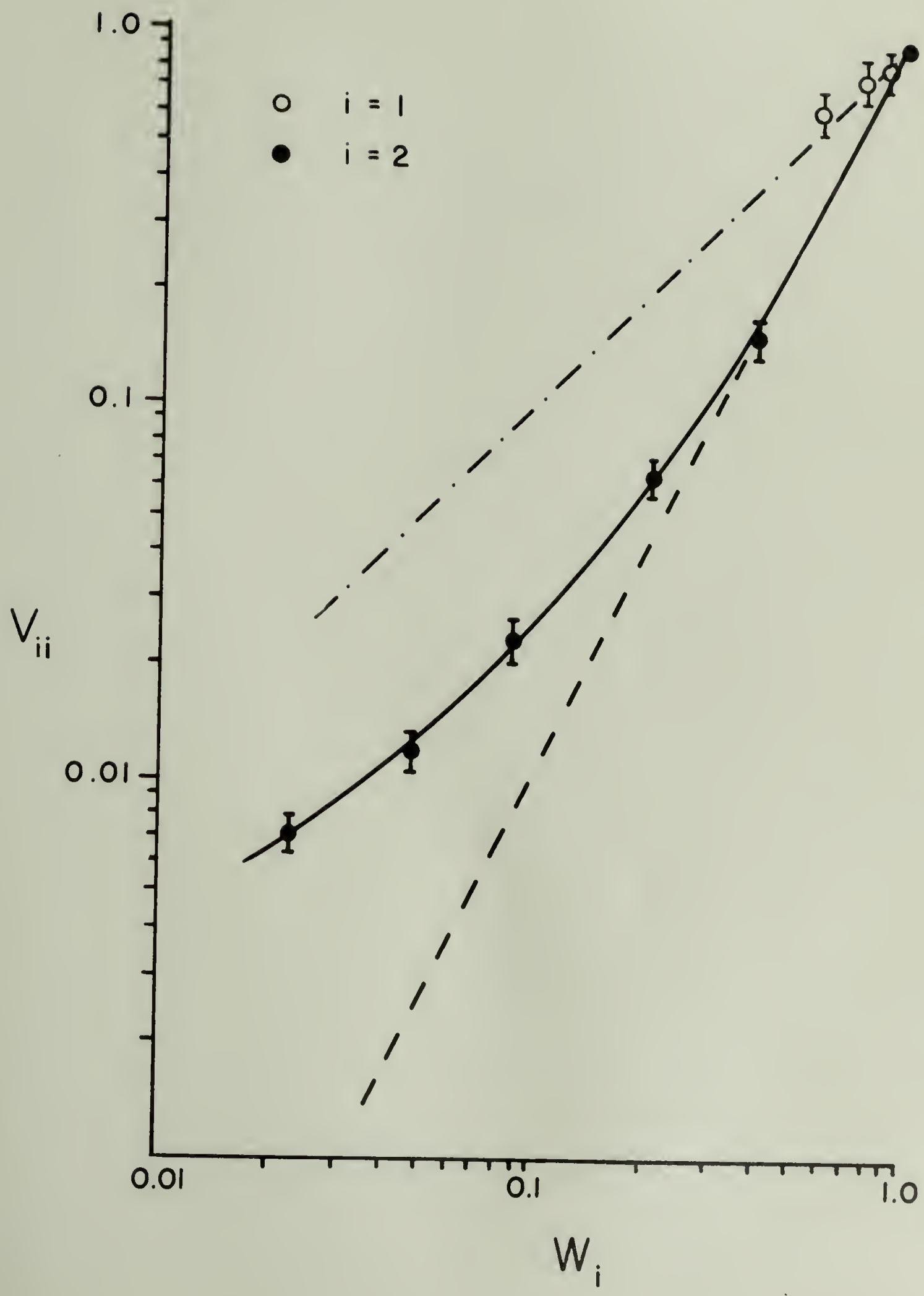

Figure 4

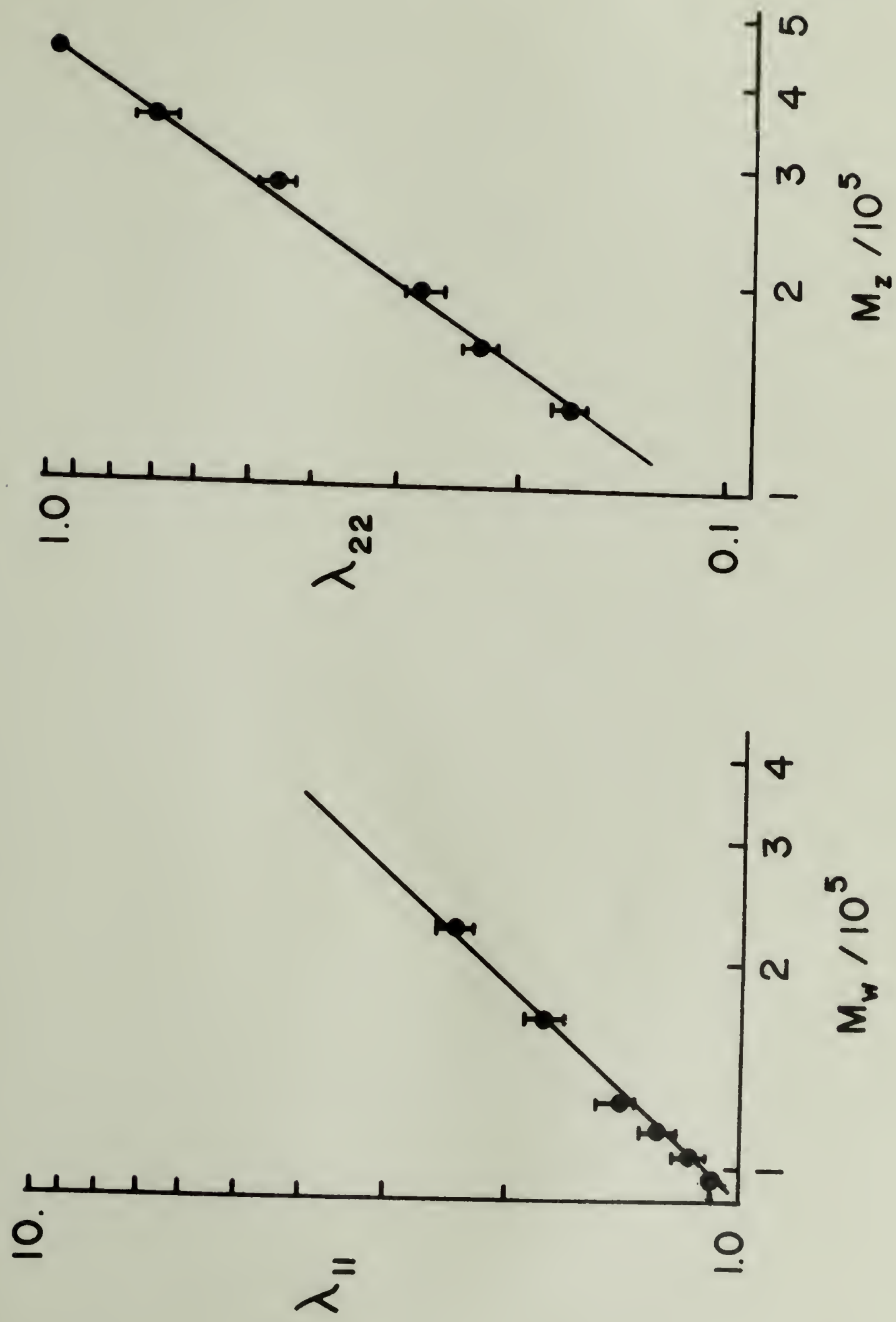

Figure 5

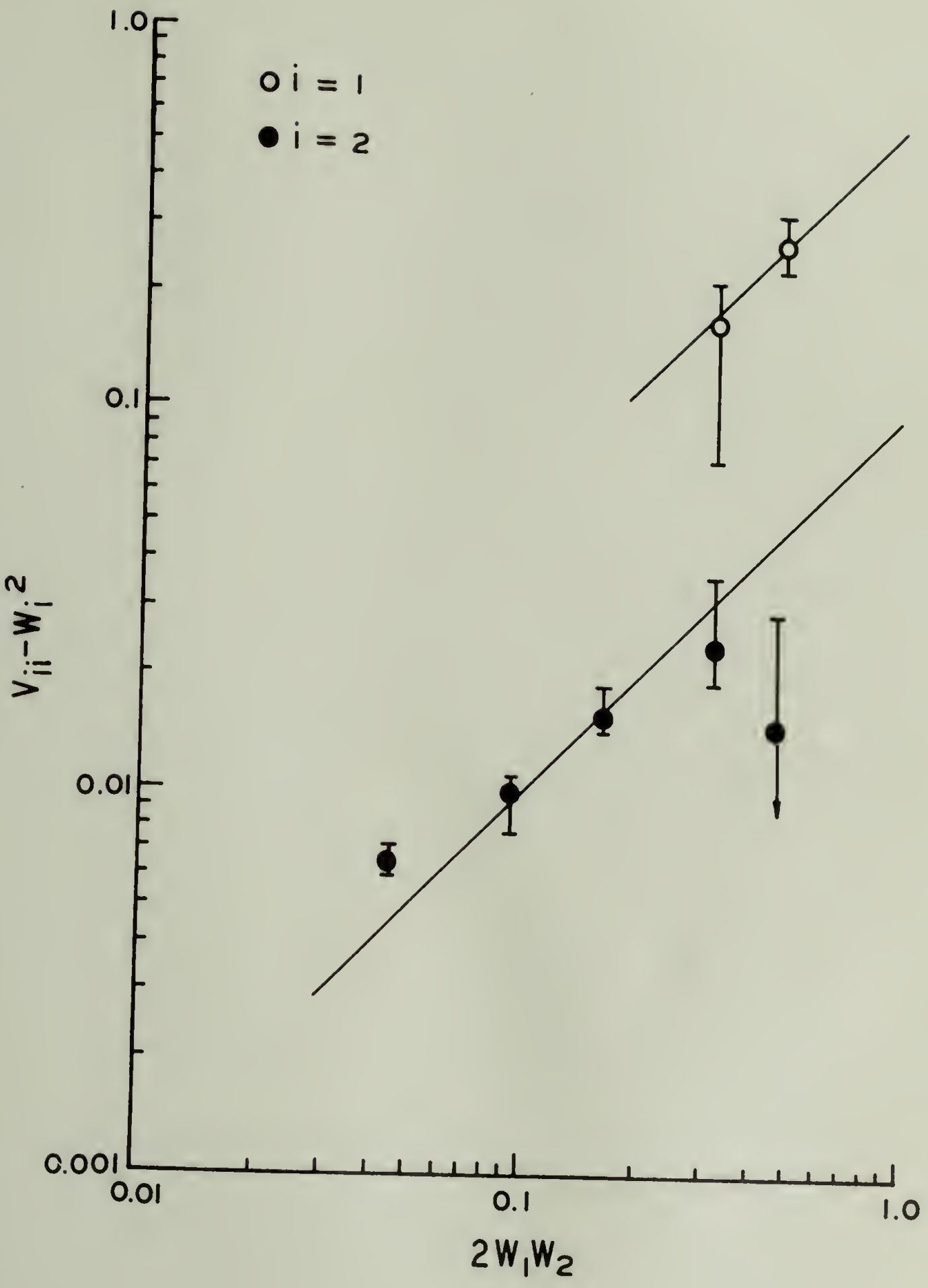

Figure 6

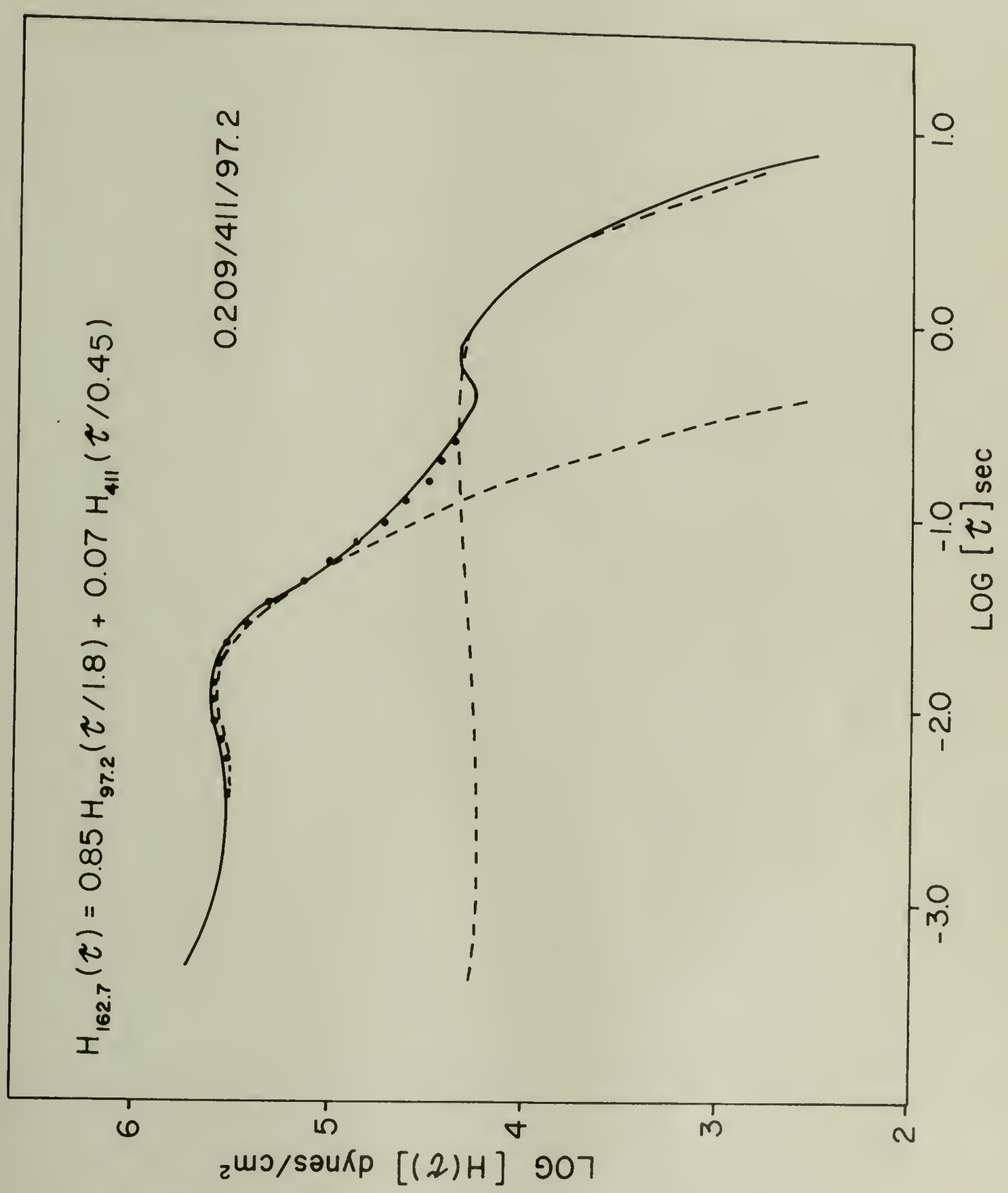
$H_{162.7}(\tau) = 0.85\, H_{97.2}(\tau/1.8) + 0.07\, H_{411}(\tau/0.45)$
0.209/411/97.2
LOG [H(τ)] dynes/cm²
LOG [τ] sec
6
5
4
3
2
1.0
0.0
-1.0
-2.0
-3.0

Figure 7

CHAPTER IV

Rheological Properties Of Poly (2,6 Dimethyl pheneylene Oxide) - Polystyrene Blends

W. M. Prest, Jr. and Roger S. Porter
Polymer Science and Engineering
University of Massachusetts
Amherst, Massachusetts 01002

ABSTRACT

The viscoelastic (VE) response of freeze dried blends of polystyrene (PS) and poly (2,6-dimethyl pheneylene oxide) (PPO), has been studied as a function of composition, frequency, and temperature to examine the degree of rheological compatability. When blended together, the relaxation processes of both molecular species exhibit the same temperature dependence. However, the temperature dependence of the VE response is a function of composition. It is shown that this behavior can be predicted from the measured glass transition temperatures by assuming the additivity of the free volumes of the components.

The properties of the blends are compared at equal free volumes. The effective segmental friction factor is found to be independent of composition while the modulus of the rubbery plateau increases with PPO concentration. This result is interpreted as a change in the entanglement molecular weight, M_e, of the blends. When the changes in M_e are considered the relationship between the zero shear

viscosity, η_o, and the 3.4 power of the weight average molecular weight, commonly found for high molecular weight homopolymers, predicts the compositional dependence of η_o for the PPO-PS blends. It is concluded that the PPO-PS system forms a rheologically compatible blend.

INTRODUCTION

The viscoelastic (VE) properties of polymer melts are controlled by the monomeric friction coefficient ζ_o, the molecular weight (MW), and the molecular weight distribution (MWD) of the system. At high MW's, intermolecular interactions, characterized by an entanglement MW, M_e, become important. The ζ_o is a measure of the local resistance that restricts the motion of a segment of a polymer chain. The magnitude of the modulus for the rubbery plateau is controlled by M_e. The properties ζ_o and M_e are constant for a given polymer type. However, if two different polymeric species can be found which mix together on a segmental scale, it should be possible to vary ζ_o and the effective M_e of the melt. Thermodynamically, segmental miscibility can only be achieved if the free energy of mixing ΔF_m, is negative.

$$\Delta F_m = \Delta H_m - T\Delta S_m \qquad (1)$$

There is a negligible change in the entropy of mixing, ΔS_m, for blends of high MW polymers. Therefore, for segmental miscibility to occur, the heat of mixing, ΔH_m, must be very small and thus the segment-segment interactions must be nearly the same. These conditions are rarely, if ever achieved. However the thermodynamic requirements for compatibility

may be met over some scale larger than the extent of the individual segments.

The experimental determination of compatibility depends upon the effective size of the volume that is perturbed by the measurement technique. For a given experiment, a blend can be considered to be a compatible mixture if the properties of the blend do not show the individual transitions of the components (1,2). High frequency and or low temperature experiments examine the degrees of freedom for motion in the molecular backbone and in the side chains of polymer systems. These would be expected to provide information on the segmental miscibility of polymer-polymer blends. On the other hand, long time melt rheology experiments, which measure the relaxation processes of the entire molecule, should test molecular compatibility.

Several polymer systems have been reported to be compatible (1-3). However, most of these blends exhibit compatibility over only a portion of the composition scale. This implies that the polymer-polymer interactions are not similar enough to keep $\Delta F_m \leq 0$ at all concentrations and therefore the degree of mixing is limited. Recently it has been reported that poly (2,6 dimethyl phenylene oxide) (PPO) is compatible with polystyrene (PS) over the entire compositional range (3). Mixtures of PPO and PS produce clear, single phase solutions in a variety of solvents. High shear rate co-extrusion at 290°C (3) or compression molding above 290°C (4,5) of mechanically mixed components produce a uniform and optically clear system whose physical properties are intermediate to thoses of the components. Most significantly, dif-

ferential scanning calorimetry (DSC) has shown that the blends have a single glass transition temperature T_g, intermediate between those of PPO and PS with no evidence of the caloritimetric transition of either pure component (3,4). However, further investigations of the PPO-PS system have shown that the DSC T_g is different from that found by dynamic-mechanical measurements (4) which in turn is different from that determined by dielectric measurements (5). These results can be interpreted in terms of the degree of compatibility in the effective volume size averaged over by each of the measurements. The dependence of the observed T_g's on the measurement technique imply that the PPO-PS system is not compatible on the segmental level. However the existance of a single, although broad T_g implies that the degree of mixing extends to very small volumes.

In view of the above, rheological measurements on the melt properties of the PPO-PS blends may be expected to reflect changes in the effective M_e of the entanglement network and possibly in ζ_o. This work examines the degree of rheological compatibility of the PPO-PS blends in light of previous studies on the effects of MWD on the VE properties of entangled polymer melts (6,7).

EXPERIMENTAL

Materials:

High MW PPO was obtained through the courtesy of R. A. Kluge of the General Electric Company, Selkirk, N.Y. The weight to number average MW, was found to be 2.1 by Gel Permeation Chromotography.

This information coupled with intrinsic viscosity measurements in chloroform at 25°C indicates that the sample has a weight average MW of 69,000 (8).

Anionically polymerized, atactic PS was chosen for the blending experiments to minimize the effects of MWD on the VE response. The PS sample used in this study, #4a manufactured by the Pressure Chemical Co., Pittsburgh, Pa., had a M_w of 97,200 and an $M_w/M_n = 1.04$.

Sample Preparation

Polystyrene is unstable at the elevated temperatures ($\geq$ 290°C) previously used to prepare "compatible" PPO-PS blends (3,4). Any thermal and/or shear degradation which might occur when the samples are mixed in this manner would change the MWD of the components and thus the rheological properties of the blends. Freeze drying techniques were used to prevent this type of degradation from occuring in the samples studied in this work. The blends were prepared by dissolving weighted amounts of the components in benzene at 40°C. The solutions, containing 1-2 weight percent polymer, were allowed to stand overnight. The solutions were frozen in a dry ice isoproponal bath and the solvent was removed under 10^{-3} mm-Hg. The samples were kept under vacuum at 85°C for 24 hours to remove any residual solvent. The resulting powder was compressed at room temperature and then molded into sample disks for two minutes under 10,000 PSI at a temperature approximately 75°C above the T_g of the blend. The disks were optically clear and homogeneous.

Measurements

The VE properties of the low PPO concentration blends were determined with the Model R-17 Weissenberg Rheogoniometer equipped with the modified Birnboin phase meter used in previous studies (6). The cone and plate geometry with $\alpha = 4°$, d = 2.5 cm, was used for both the steady state shear and the dynamic oscillatory measurements. These measurements were limited to samples containing less than 50 weight percent PPO by the high viscosity of PPO and by the thermal instability of each component. Measurements at higher concentrations, which required higher temperatures because of the increased viscosity, were considered to be unreliable. For these conditions decomposition was indicated by bubble formation.

Additional rheological measurements were conducted with the Perkin Elmer Thermomechanical analyzer TMS-1 used as a penetrometer. The glass transitions of the samples were obtained with a Perkin Elmer DSC-1B Differential Scanning Calorimeter. The penetration and DSC measurements were conducted at a heating rate of 10°/minute. All samples were initially heated at 10°/minute to 250°C to insure equal thermal histories and to allow the relaxation of surface irregularities.

RESULTS

The viscoelastic response from 0.19 to 75.0 radians/sec of each PPO-PS blend was measured for at least six different temperatures over a range of 70°C. In general, two phase systems (such as filled polymer melts) exhibit a non-linear VE response (9). In contrast the

VE properties of the PPO-PS blends were independent of the applied strain over the measured range of strain amplitudes (5-9%). Therefore, the blends exhibit the linear VE response that is characteristic of compatible polymer solutions and melts.

The experimental responses of each blend could be superimposed by shifting the time scale of each measurement by a factor a_T. Figure 1 presents the master curves of the shear loss modulus G", as a function of the reduced frequency ωa_T and the weight fraction of the PPO component w_2. All data is reduced to a reference temperature of 220°C. At low frequencies each samples response extends into the region where G" is proportional to ωa_T, i.e., the region of Newtonian flow where the dynamic viscosity $\eta' = G''/\omega$, is independent of frequency.

The steady state shear rate response of each sample was measured on completion of the dynamic tests. The X symbols in Figure 1 represent the dependence of the shear stress τ_{12} on the reduced shear rate $\dot{\gamma} a_T$. Over the experimentally accessible range τ_{12} at $\dot{\gamma} a_T$ is equal to G" at ωa_T. Therefore, the samples exhibit the same zero shear viscosity η_o and the same temperature dependence of the shift factors when subject to either an oscillatory or a steady state shear deformation.

At high frequencies G" becomes proportional to $\omega^{1/2}$. This is the response predicted for the transition region by the modified Rouse theory (10). A plateau appears in G" at intermediate frequencies. This reflects the intermolecular or entanglement interactions in the blends.

As the PPO concentration is increased, the time scale of the relaxation processes and the height of the intermediate τ plateau increases. Thus the PPO component increases both the viscosity and the apparent modulus of the PS. The solid line in Figure 1 shows the extent of the Newtonian behavior. Increasing the PPO content of the sample causes the initial deviation from Newtonian response to occur at lower shear stresses. As G'' and τ_{12} increase, the blends response becomes slightly non-Newtonian. Pronounced non-Newtonian flow occurs only at much higher shear stresses. This response is typical of the behavior of systems with broad MWD's.

A broad response is also observed in the ω dependence of the storage modulus G'. The master curves representing the dependence of G' on ωa_T reduced to 220°C are given in Figure 2. At low ω, the G' of the narrow MWD PS component is proportional to ω^2. However, the addition of the PPO sample to this PS component decreases the exponent from the expected value of 2 to 1.6$\underline{5}$, 1.5 and 1.2$\underline{5}$ for the blends containing 4.9%, 19.2% and 40.3% PPO respectively. Thus, even though the measurements extend into the Newtonian region of G'', the experimental data to not give a constant limiting value of the steady state shear compliance, $J_e^o \equiv \lim_{\omega \to 0} G'/(G'^2 + G''^2)$. This result is also typical of the response of systems with broad MWDs. The X symbol in Fig. 2 represent half the measured primary normal stress difference, $(P_{11} - P_{22})/2$, plotted as a function of $\dot{\gamma} a_T$. Within experimental error, the shift factors for both the dynamic and the steady state shear measurements are equal and $[P_{11} - P_{22}](\dot{\gamma} a_T) \approx 2G'(\omega a_T)$.

A second set of rheological measurements were made with the Perkin-Elmer thermomechanical analyzer to obtain information about the rubbery plateau of the blends. This instrument measures the penetration of a probe into a sample as a function of applied stress, temperature and heating rate. A load of 4700 dynes/cm^2 was placed on the sample and the position of the probe was monitored as a function of temperature as the system was heated at a rate of 10°C/minute. At low temperatures the sample expands as the temperature increases. Above the glass transition temperature the probe sinks into the sample at a rate determined by the VE properties and thermal expansion of the melt.

The penetration measurements are roughly analogous to a creep experiment in which the time scale of the relaxation processes is contracted by constantly increasing the sample temperature. This allows the measurement of the VE response in only a few minutes. A quantitative analysis of this technique is being developed. However, the results of the thermomechanical measurements do allow the qualitative comparison of the VE response of different systems. To illustrate this technique consider the thermomechanical response of the 97,200 (w_2 = 0.00) and 411,000 MW PS samples shown in Figure 3. The response indicates that the samples have the same T_g. Above T_g the load rapidly sinks into the sample. This initial deformation reflects the transition region of the VE response, corresponding to rearrangements of short segments of the molecular chain backbone. At higher temperatures, and longer times, the relaxation processes involve relaxations of larger molecular segments. For sufficiently

long molecules, intermolecular interactions hinder the relaxation processes and decrease the observed penetration rate of the probe. The shape of this region is determined by the sum of the thermal expansion of the melt and the VE response of the rubbery plateau. The height of the plateau is related to the modulus of the entanglement network formed in the melt. By analogy with the classical theory of rubber elasticity (11), this modulus is inversely proportional to the MW between entanglements M_e. The width of the plateau is a function of the number of intermolecular interactions and thus the MW of the sample. The higher the MW; the greater the number of entanglements per molecule; the wider the rubbery plateau. The sample flows at the combination of times and temperatures where relaxation processes involving the entire length of the molecules can take place. The location of this terminal region, where the penetration rate increases, is a function of the melt viscosity. The response of the PS samples in Figure 3 illustrate the MW dependence of the width of the rubbery plateau.

The thermomechanical response of the PPO-PS blends are also shown in Figure 3. The PPO sample (w_2 = 1.00) has a pronounced rubbery plateau which is significantly higher and wider than the rubbery plateau of the PS component. This demonstrates that PPO is a highly entangled polymer melt at a MW of 69,000. A quantitative comparison of the heights of the plateaus can not be made at this time but Figure 3 does show that the modulus of the rubbery plateau of PPO is significantly greater than that of PS. Thus the entanglement MW

of PPO is less than the M_e of PS.

The thermomechanical response of the PPO-PS blends exhibits a single T_g and a single step rubbery plateau that falls between the response of the individual components. There is no evidence of the residual properties of either component. As the PPO concentration increases the height of the rubbery plateau increases. This is in agreement with the change in the magnitude of the G" plateau, see Figure 1. These changes indicate that the effective MW between entanglements decreases with increasing PPO concentration. The question of whether this is the result of the moduli of two separate phases or the properties of an entanglement network composed of both species will be discussed below.

An independent determination of T_g can be made with a Differential Scanning Calorimeter (DSC). These measurements show the single thermal transition that has been previously cited as evidence for the compatibility of the two components (3,4). The general agreement between the compositional dependence of the thermomechanical and DSC determined T_g is shown in Figure 4. The thermomechanical T_g were defined as the temperature of the initial deviation of the penetration response from the low temperature thermal expansion behavior. The DSC T_g was defined as the temperature at the midpoint of the transition in the heat capacity of the sample. As has been previously reported the T_g of the blends fall below the linear weight fraction addition of the T_g's of the components, denoted by the dashed line in Figure 4 (4).

DISCUSSION

The ability to superimpose data taken over a wide range of temperatures indicates that when blended, the relaxation mechanisms of the PPO and PS components have the same temperature dependence. For each of the blends, the shift factors determined in the construction of the G' curves are the same as those required for the superposition of the G" response. Therefore relaxation processes associated with the loss mechanisms measured by G" and τ_{12} have the same temperature dependence as those associated with the energy storage mechanisms determined by G' and $P_{11} - P_{22}$. In general this would not be true if two separate phases were present in the melt unless each phase had the same temperature dependence or unless one phase completely dominated the response over the experimental time scale. These possibilities would require that the relaxation processes of the blends have the same temperature dependence as the response of the dominate component and thus that there exist no more than two temperature dependencies for the blend series. However, it is shown in Figure 5 that the experimental dependence of the shift factors is a function of the composition of the blend. Therefore the PPO-PS blends act like a one phase system for rheological measurements above T_g.

The dramatic compositional change in the temperature dependence of the shift factors shown in Figure 5, can be explained in terms of the free volume concept by combining the WLF equation (12) with Kelley and Bueche's model (13) for the change in the glass transition temperature

of the blend, T_{gB}. The free volume that exists in a blend, f_B, at a temperature T is

$$f_B = f_{gB} + \alpha_B(T - T_{gB}) \tag{1}$$

where f_{gB} is the free volume at T_{gB} and α_B is the thermal expansion coefficient of that free volume. If it is assumed that the free volume of a binary blend is equal to the volume fraction sum of the free volumes of the components (13) then

$$f_B = v_1 f_{g1} + v_2 f_{g2} + v_1\alpha_1(T - T_{g1}) + v_2\alpha_2(T - T_{g2}) \tag{2}$$

It has been predicted (14) and observed (15) that the free volume at T_g is approximately a constant for many polymer systems. If it is assumed that this is also true for the PPO-PS blends, that is that f_{gB} is independent of composition, then from equations 1 and 2

$$T_{gB} = \frac{v_1\alpha_1 T_{g1} + v_2\alpha_2 T_{g2}}{v_1\alpha_1 + v_2\alpha_2} \tag{3}$$

The compositional dependence of the expansion coefficient of the blend can be obtained by combining eqs. 1-3.

$$\alpha_B = v_1\alpha_1 + v_2\alpha_2 \tag{4}$$

While the free volume expansion coefficient of PS has often been reported in the literature (15) this coefficient is not available for PPO. However, this quantity may be calculated, within the experimental limitations of the model, from the measured T_g of the PPO-PS blends. The ratio of the expansion coefficients is given by the inversion of equation 3,

$$\alpha_2/\alpha_1 = \frac{v_1(T_{gB} - T_{g1})}{v_2(T_{g2} - T_{gB})} \qquad (5)$$

The calculated values of this ratio defined by the DSC measured T_{gB} are listed in Table I. Importantly, this ratio is approximately constant over the compositional range, and thus is consistent with the concept of the additivity of free volumes.

It has been widely shown (15,16) that the WLF equation for the temperature dependence of the viscoelastic response can be obtained from the Doolittle equation (17) which describes the relationship between the viscosity of a system and the temperature dependence of free volume. In terms of the free volume parameters the shift factors relative to a reference temperature T_o are

$$\log (a_T) = -c_1^{\,o} (T - T_o)/(c_2^{\,o} + T - T_o) \qquad (6)$$

where $c_1^{\,o} = B/2.303\ f_o$, $c_2^{\,o} = f_o/\alpha$ and B is a constant of order one.

Plazek (18) has reported that the free volume expansion coefficient of high MW PS, determined by eq. 5, is $6.9 \times 10^{-4}/°C$. The new results presented in Table I then indicate that $\alpha_{PPO}/B \approx 4.8 \times 10^{-4}$. This result is in general agreement with the value of 4.5×10^{-4} which was obtained for the related polymer, poly (1-methyl 6-phenyl phenylene oxide), whose temperature dependence was reported by Eisenberg to be "exceedingly similar" to the response of PPO (19). Thus the compositional dependence of T_g for the PPO-PS blends can be explained by the additivity of free volume where the expansion coefficient of PPO is approximately $0.69\ \alpha_{PS}$. The solid line in

Figure 4 represents the results of this prediction.

The above results (equations 4-6) can be used to predict the temperature dependence of the shift factors as a function of composition. The results of these calculations are given by the lines in Figure 5. Extremely good agreement is found between the predicted and experimental values of log (a_T) except for the w_2 = 0.049 blend. This anomaly also appears in the experimentally determined WLF parameters. These parameters can be determined from the least squares slope and intercept of the data plotted as $(T - T_o)/\log (a_T)$ vs $T - T_o$ (12). Figure 6 presents this data for the reference temperature of 220°C. The parameters obtained in this manner are very sensitive to experimental errors. The WLF parameters for the blends were obtained by repeating the least squares calculations using each experimental temperature in turn as the reference temperature, and then reducing the parameters to T_g by

$$c_1^g = c_1^o c_2^o/(c_2^o - (T_o - T_g))$$

and

$$c_2^g = c_2^o - (T_o - T_g) \qquad (7)$$

The mean values of $\alpha/B = 1/2.303\ c_1^g c_2^g$, $f_g/B = 1/2.303\ c_1^g$ and $T_\infty = T_{gB} - c_2^g$ are compared in Table II with the predictions of the assumption of the additivity of free volume based on Plazek's PS data and the DSC determined T_g's. Note that the assumption of equal free volumes at T_g is upheld by these calculations. Again, with the exception of the w_2 = 0.049 blend, the agreement is within the experimental

uncertainties of the measurements. The origin of this one exception is unknown. The DSC and the thermomechanical T_g's and the calculated values of α_{PPO}/α_{PS} are consistent with the known weight fraction of PPO. However, the rheological shift factors act as if the sample had a T_g 5°C higher than observed and thus a $w_2 \approx 0.10$. This may indicate imperfect mixing at low concentrations but, in view of previous work (4,5), is it unlikely that the large scale volume averaged over by the rheological measurements would yield a higher value of T_g than the calorimetric technique.

COMPOSITIONAL DEPENDENCE

To determine the compositional dependence of the viscoelastic properties it is necessary to compare the response of the blends when the volumes available for the relaxation processes are equal. The free volume of the PS component at 220°C is 0.115. The temperatures corresponding to this free volume are 226, 244 and 276°C for the $w_2 = 0.049$, 0.192 and 0.403 blends respectively. The WLF equation was used to determine the shift factors for the appropriate blend at each of these temperatures.

When the loss moduli of the PPO-PS blends are compared at equal free volumes, the transition region for the blends response ($G'' \alpha \omega^{1/2}$) is, within experimental error, independent of composition. The segmental friction coefficient ζ_o can be calculated from the predictions of the Modified Rouse theory (10). In the transition region,

$$G'' = a\, N_o/4M_o\, (\zeta_o kT/3)^{1/2}\, \omega^{1/2} \qquad (8)$$

where ρ is the density, M_o is the monomer MW and a is the characteristic length of the molecule. The quantity $a^2\zeta_o/M_o^2$ is a measure of the effective friction coefficient of the blend (20). The direct calculation of ζ_o would require an arbitrary definition of M_o and a. Table III lists $\log(a^2\zeta_o/M_o^2)$ for the PPO-PS blends at equal temperatures (T = 220°C) and at equal free volumes (f = 0.115). The latter values are approximately equal demonstrating that reducing the VE response of the blends to an iso-free volume state is approximately equivalent to comparing the properties at a constant effective friction factor.

Data representing the dependence of the storage modulus of the blends at f = 0.115 are shown in Figure 7. The solid lines were defined by the data given in Figure 2. Note that the G' curves are parallel at high frequencies. Thus in addition to broadening the low frequency VE response, the PPO component increases the modulus of the blends even in the iso-free volume state. If this iso-free volume response is also the behavior at constant friction factor, as suggested above, then the differences in the heights of G' reflect the change in the elastic properties of the entanglement network and thus the effective entanglement MW of the melt. The quantity $G'(w_2)/G'(w_2 = 0)$ and the ratio of the heights of the loss modulus plateau $G''(w_2)/G''(w_2 = 0)$ are plotted as a function of composition in Figure 8. The ratio of the moduli are approximately equal to $(1 + 3.2\ w_2)$. For a high MW, narrow MWD polymer melt, the storage modulus in the entanglement plateau is proportional to $\rho\ RT/M_e$ (11). In addition the maximum in the loss

modulus is related to the reciprical of M_e (21). Then, neglecting the possible effects in the plateau region of the MWD of the blends, Figure 8 states that $M_e(w_2 = 0)/M_e(w_2) \approx (1 + 3.2\ w_2)$. If this relation holds for large w_2, $M_e(PPO) \approx M_e(PS)/4.2 \approx 4300$.

The relaxation spectra $H(\tau)$ of the blends were calculated using Tschoegl's second order approximation (15). The $H(\tau)$ calculated from the G' data were essentially equivalent to the spectra determined by G". The results of these calculations, reduced to the iso-free volume state of f = 0.115, are shown in Figure 9. As expected from the low frequency response shown in Figures 1, 2, and 7, the MWD of the PPO component introduces a broad distribution of long time relaxation processes. This contribution increases with the PPO concentration and dominates the response of the w_2 = 0.403 blend.

At low PPO concentrations, the intensity of the PS contribution to $H(\tau)$ appears to increase with w_2. This is opposite to the effects noted in earlier studies of the MWD dependence of $H(\tau)$ for PS-PS blends (7). In that case the decrease in $H(\tau)$ was attributed to the reduction in the amount of the low MW material and thus in the number of relaxation processes contributed by that component. The observed increase in the spectra in Figure 9 may be caused by the PPO relaxation mechanisms. However it is unlikely that the broad MWD PPO concentration would contribute evenly enough to the intermediate time response for $H(\tau)$ to retain the shape of the initial fall off in the PS response observed for the w_2 = 0.049 and 0.192 blends. In addition the magnitude of the PPO contribution to the long time response is not great enough to be responsible for the observed increase in the modulus of these

low concentration blends. Assuming compatability of the components on an entanglement scale, the increase in the spectra may be explained by the effective decrease in M_e and thus the increase in the average number of entanglements per molecule. As M_e decreases, the number of entanglements per PS molecule increases and therefore the total number of relaxation processes involving X entanglements increases while the distribution of the relaxation processes remains the same. At higher concentrations the number of relaxation processes due to the PPO component becomes significant and the initial portion of the terminal region of $H_B(\tau)$ begins to reflect the MWD of PPO.

THE ZERO SHEAR VISCOSITY

Berry and Fox have shown (22) that at equal free volumes the zero shear viscosity of homo-polymer melts is given by

$$\eta_o = \frac{N_o a^2}{36 M_o^2} \zeta_o M_w \left(\frac{M_w}{M_c}\right)^a \qquad \begin{array}{l} a = 1 \quad M < M_c \\ a = 2.4 \quad M > M_c \end{array} \qquad (9)$$

The critical MW, M_c is closely related to M_e, the MW between entanglements. In Bueche's model (23) for the behavior of polymer melts, $M_c \simeq 2M_e$. This is generally confirmed empirically (24).

If PPO and PS are compatible on the molecular level, it should be possible to describe the compositional dependence of the blend viscosity by equation 9. It was shown above that, at equal free volumes the effective segmental friction coefficient, $a^2\zeta_o/M_o^2$, is approximately independent of composition. The viscosity of a blend, in terms of the viscosity of the PS component is then

$$\eta_o(w_2) = \eta_o(PS) \frac{\rho(w_2)}{\rho(PS)} \left[\frac{M_w(w_2)}{M_w(PS)}\right]^{3.4} \left[\frac{M_c(PS)}{M_c(w_2)}\right]^{2.4} \quad (10)$$

If the ratio of the critical MW's is assumed to be equal to the ratio of the entanglement MW's, equation 10 can be used with the relation found in Figure 8 and the measured M_w's of the components to predict the iso-free volume viscosities of the blends. The results of this analysis are compared with the experimental results in Figure 10. There is extremely good agreement between the predicted and the experimental iso-free volume zero shear viscosities in view of the uncertainties involved in the estimation of $M_e(w_2)$. However, it should be noted that the η_o predicted for $w_2 > 0.4$ depend upon the validity of the extrapolation of $M_e(w_2)$ in the high concentration region. Note that the viscosity of the blends increases with w_2 even though the weight average MW of the blend is decreasing. This unusual behavior occurs only because the effective M_e changes more rapidly with w_2 than does M_w.

REFERENCES

1. L. Bohn, Kolloid Z., 213, 55 (1966).
2. B. D. Gesner, Encyclopedia of Polymer Science and Technology, Interscience, New York, N.Y., (1969) Vol. 10, p. 695.
3. E. P. Cizek, U.S. Patent 3,383,435 (May 14, 1968).
4. J. Stoelting, F. E. Karasz and W. J. MacKnight, Polym. Eng. Sci., 10, 133 (1970).
5. W. J. MacKnight, J. Stoelting and F. E. Karasz, Adv. Chem., Number 99, 29 (1971).
6. W. M. Prest, Jr. and R. S. Porter, submitted for publication in Polym. J.
7. W. M. Prest, Jr. and R. S. Porter, submitted for publication in Polym. J.
8. J. M. Barrales-Rienda and D. C. Pepper, Europ. Polym. J., 3, 595 (1967).
9. S. Onogi, T. Masuda and T. Matsumoto, Trans. Soc. Rheol., 14, 275 (1970).
10. J. D. Ferry, R. F. Landel and M. L. Williams, J. Appl. Phys., 26, 359 (1955).
11. A. J. Staverman, Handbuch Der Physik (edited by S. Flugge, 1962) Vol. 13, p. 432.
12. M. L. Williams, R. F. Landel and J. D. Ferry, J. Amer. Chem. Soc., 77, 3701 (1955).
13. F. N. Kelley and F. Bueche, J. Polym. Sci., 50, 549 (1961).
14. T. G. Fox and P. J. Flory, J. Appl. Phys., 21, 581 (1950).

15. J. D. Ferry, "Viscoelastic Properties of Polymers", 2nd ed. John Wiley, New York, N.Y., (1970).

16. D. J. Plazek and V. M. O'Rourke, J. Polym. Sci. A-2, 9, 209 (1971)

17. A. K. Doolittle, J. Appl. Phys., 22, 1471 (1951).

18. D. J. Plazek, J. Phys. Chem., 69, 3480 (1965).

19. A. Eisenberg and B. Cayrol, Advances in Chemistry, in press.

20. R. G. Mancke and J. D. Ferry, Trans. Soc. Rheol., 12, 335 (1968).

21. H. Oser and R. S. Marvin, J. Res. Nat. Bur. Standards, 67B, 87 (1963).

22. G. C. Berry and T. G. Fox, Adv. Polym. Sci., 5, 261 (1968).

23. F. Bueche, "Physical Properties of Polymers", Interscience, New York, (1962).

24. R. S. Porter and J. F. Johnson, Rheol. Acta. 7, 332 (1968).

Table I

Ratio of the thermal expansion coefficients of the components calculated from the compositional dependence of T_g for the PPO-PS blends

w_2	T_g(DSC), °C	α_{PPO}/α_{PS}
0.00	101	
0.049	105	0.69
0.192	118	0.71
0.403	139	0.70
0.500	148	0.66
0.604	161	0.68
0.833	192	0.67
1.00	219	

Table II

Measured and predicted free volume parameters

w_2	$\alpha/B \times 10^4$		$f_g/B \times 10^2$		T_∞, °C	
	EXP.	PREDICTION	EXP.	PREDICTION	EXP.	PREDICTION
0.00	7.0	6.9	3.2	3.3	55	53
0.049	5.9	6.8	3.3	3.3	49	58.6
0.192	6.6	6.5	3.3	3.3	67	67.3
0.403	6.4	6.1	3.2	3.3	90	86.1
1.00	(4.5)*	4.8	(3.3)*	3.3	(144)*	151.6

*Calculated from ref. 19.

Table III

Effective friction factors of the PPO-PS blends at equal temperatures and equal free volume $\log \left[\frac{a^2\zeta_o}{M_o^2}\right]$

w_2	T = 220°C	f = 0.115
0.00	-25.11	-25.11
0.049	-24.95	-25.08
0.192	-24.60	-25.18
0.403	-23.78	-25.24

FIGURE CAPTIONS

Figure 1 Master curve of $G''(\omega a_T)$ and $\tau_{12}(\dot{\gamma} a_T)$ reduced to 220°C for the PPO-PS blends as a function of the weight fraction of PPO. The solid lines represent the extent of the Newtonian region.

Figure 2 Master curve of $G'(\omega a_T)$ and $(P_{11} - P_{22})/2\ (\omega a_T)$ reduced to 220°C for the PPO-PS blends as a function of the weight fraction of PPO.

Figure 3 Thermomechanical response of the PPO-PS blends as a function of the weight fraction of PPO. The dashed line is the response of a PS sample with M_w = 411,000.

Figure 4 Compositional dependence of the glass transition temperatures of the PPO-PS blends. Dashed line is the weight fraction addition of the components T_g. Solid line is the equation 3 with $\alpha_{PPO} = 4.8 \times 10^{-4}$.

Figure 5 Temperature dependence of the shift factors for the PPO-PS blends. Lines are the predictions of the combination of equations 2, 4, and 6.

Figure 6 The determination of the WLF parameters at T = 220° for the PPO-PS blends.

Figure 7 Compositional dependence of $G'(\omega a_T)$ of the PPO-PS blends reduced to the iso-free volume state, f = 0.115.

Figure 8 The ratio of $G'(w_2)/G'(w_2 = 0)$ and $G''(w_2)/G''(w_2 = 0)$ in the rubbery plateau as a function of PPO concentration. The line is given by $(1 + 3.2\ w_2)$.

Figure 9 The Relaxation Spectra of the PPO-PS blends reduced to the iso-free volume state, f = 0.115.

Figure 10 The compositional dependence of the zero shear viscosity of the blends as a function of PPO concentration. Solid line is the prediction of equation 10 with $M_c(PS)/M_c(w_2) = (1 + 3.2\ w_2)$.

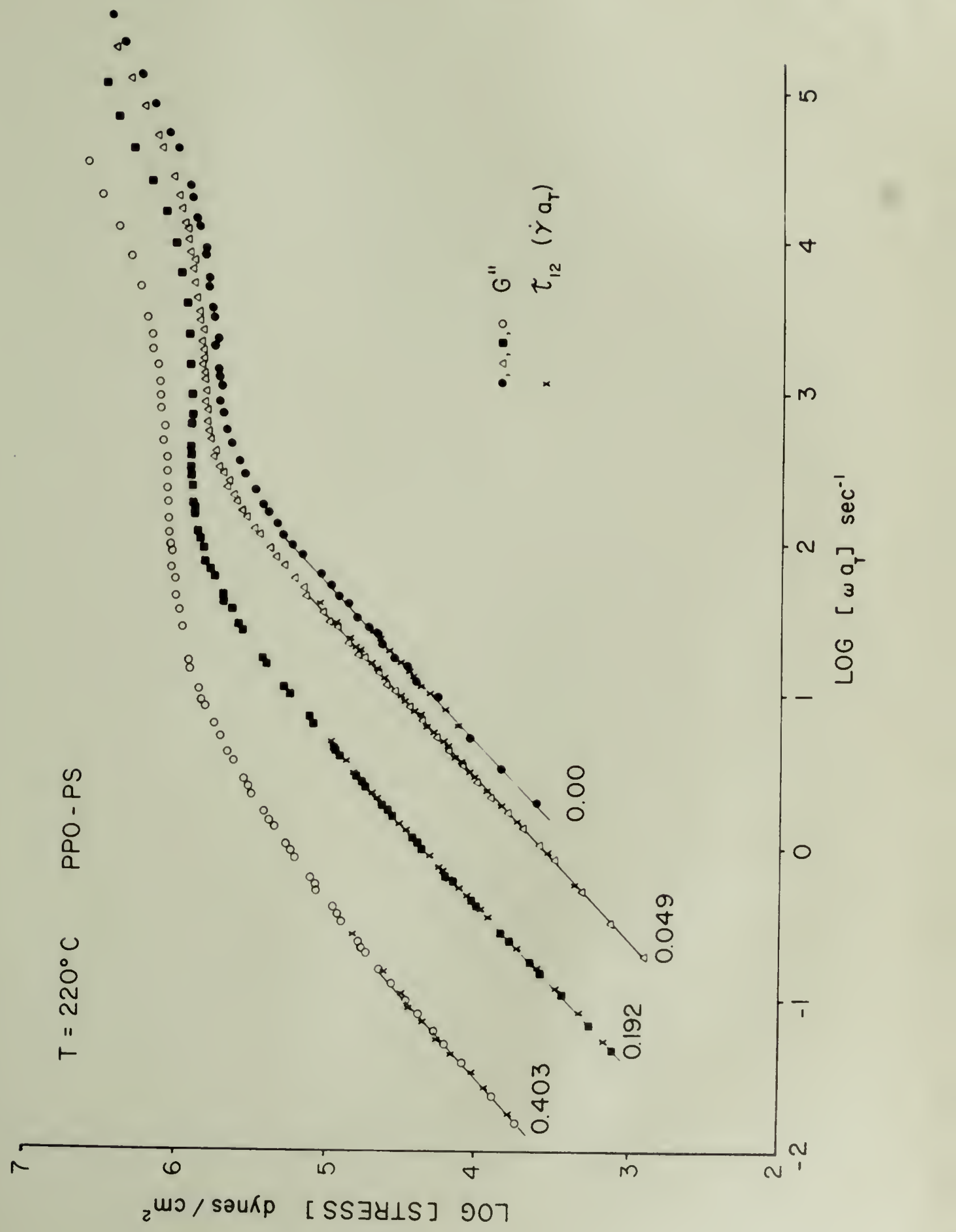
T = 220° C PPO-PS
•, △, ■, ○ G''
× τ_{12} ($\dot{\gamma} a_T$)
0.00
0.049
0.192
0.403
LOG [STRESS] dynes / cm²
LOG [ω a_T] sec⁻¹
7
6
5
4
3
2
-2
-1
0
1
2
3
4
5

Figure 1

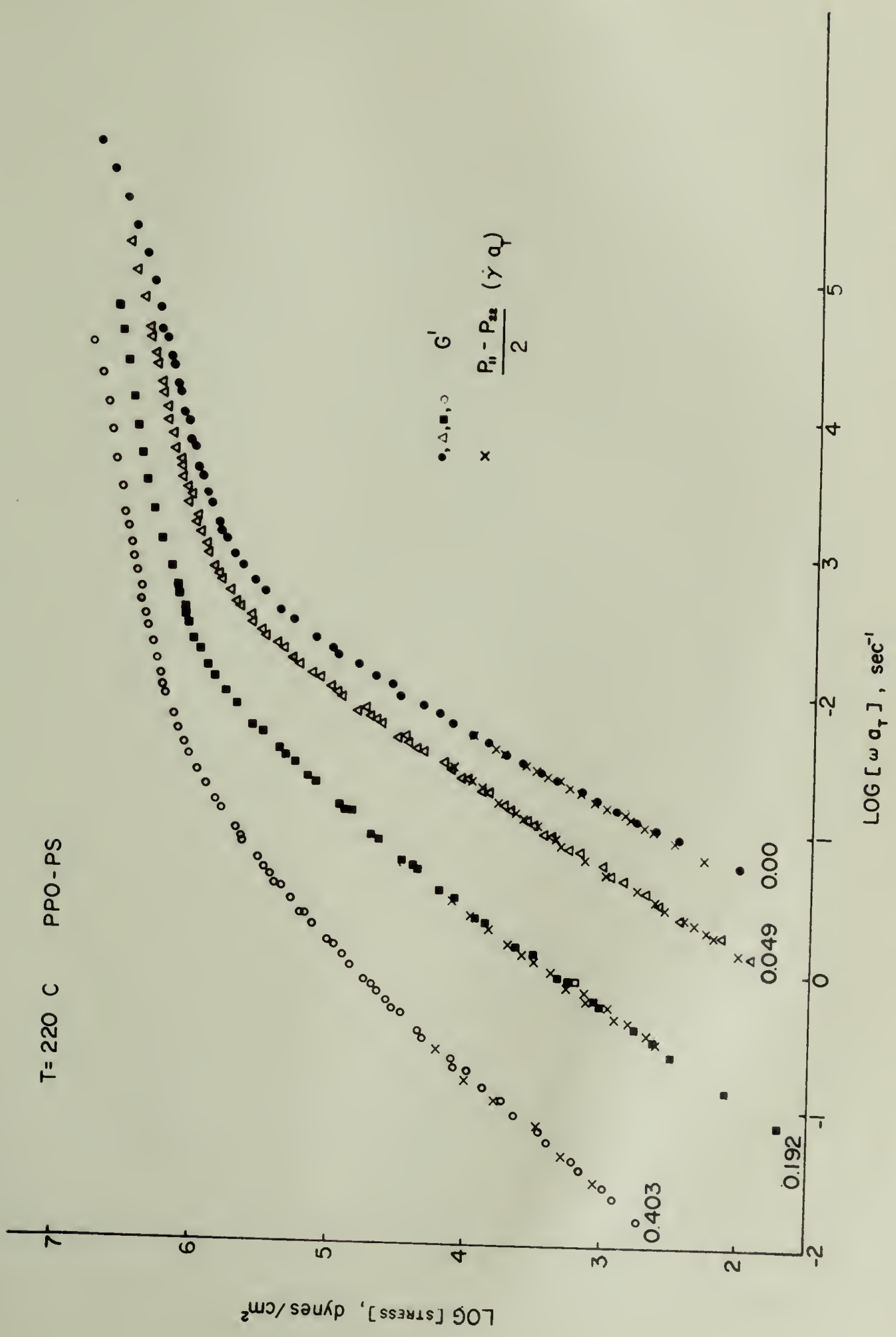
T= 220 C PPO-PS
•,△,■,○ G'
× $\frac{P_{11} - P_{22}}{2}$ $(\dot{\gamma} a_T)$
LOG [stress], dynes/cm²
LOG [ω a_T], sec⁻¹
0.403
0.192
0.049
0.00

Figure 2

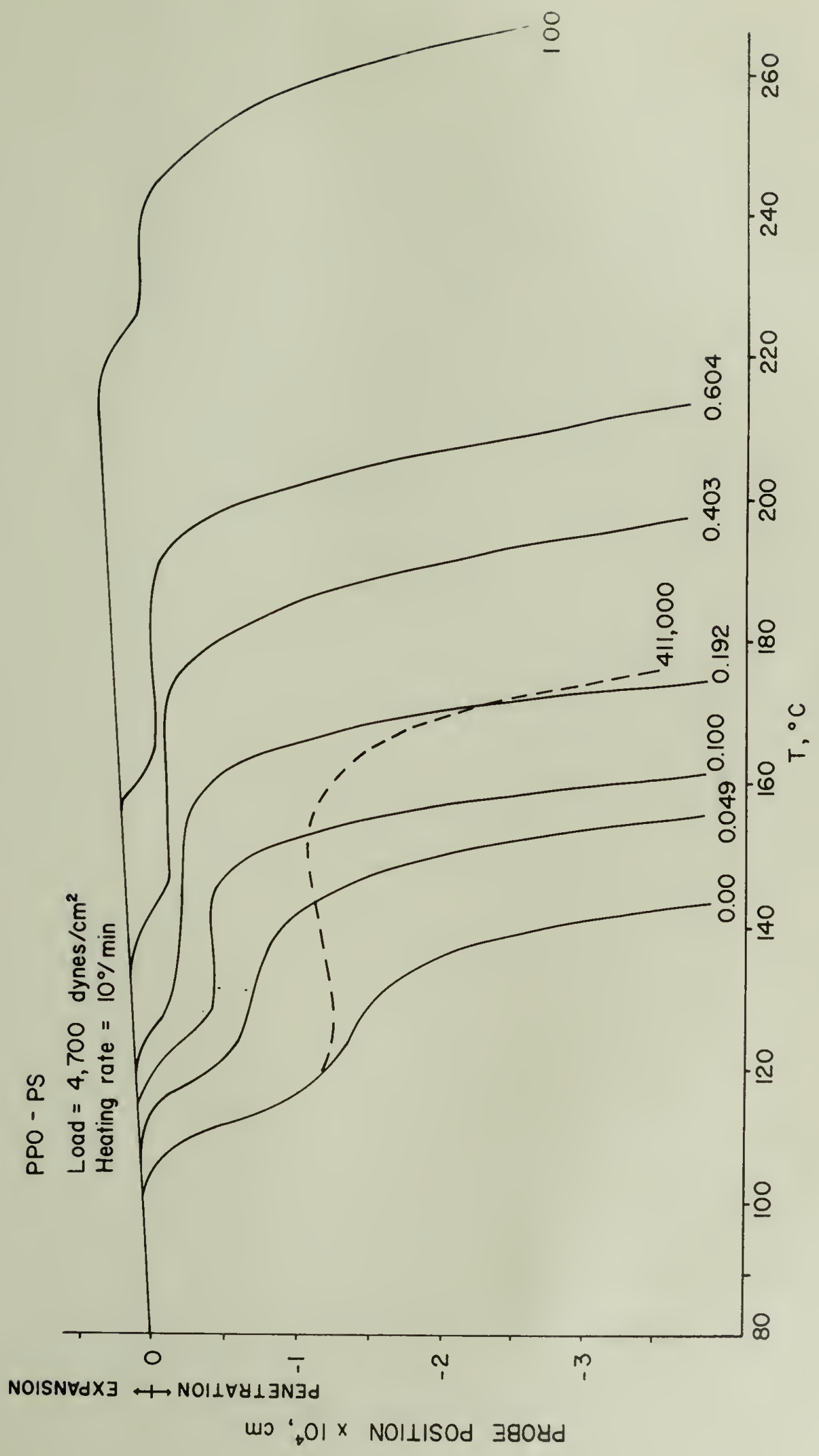
PPO - PS
Load = 4,700 dynes/cm²
Heating rate = 10°/min
PENETRATION ⟷ EXPANSION
PROBE POSITION x 10⁴, cm
T, °C
100
0.604
0.403
411,000
0.192
0.100
0.049
0.00
0
-1
-2
-3
80
100
120
140
160
180
200
220
240
260

Figure 3

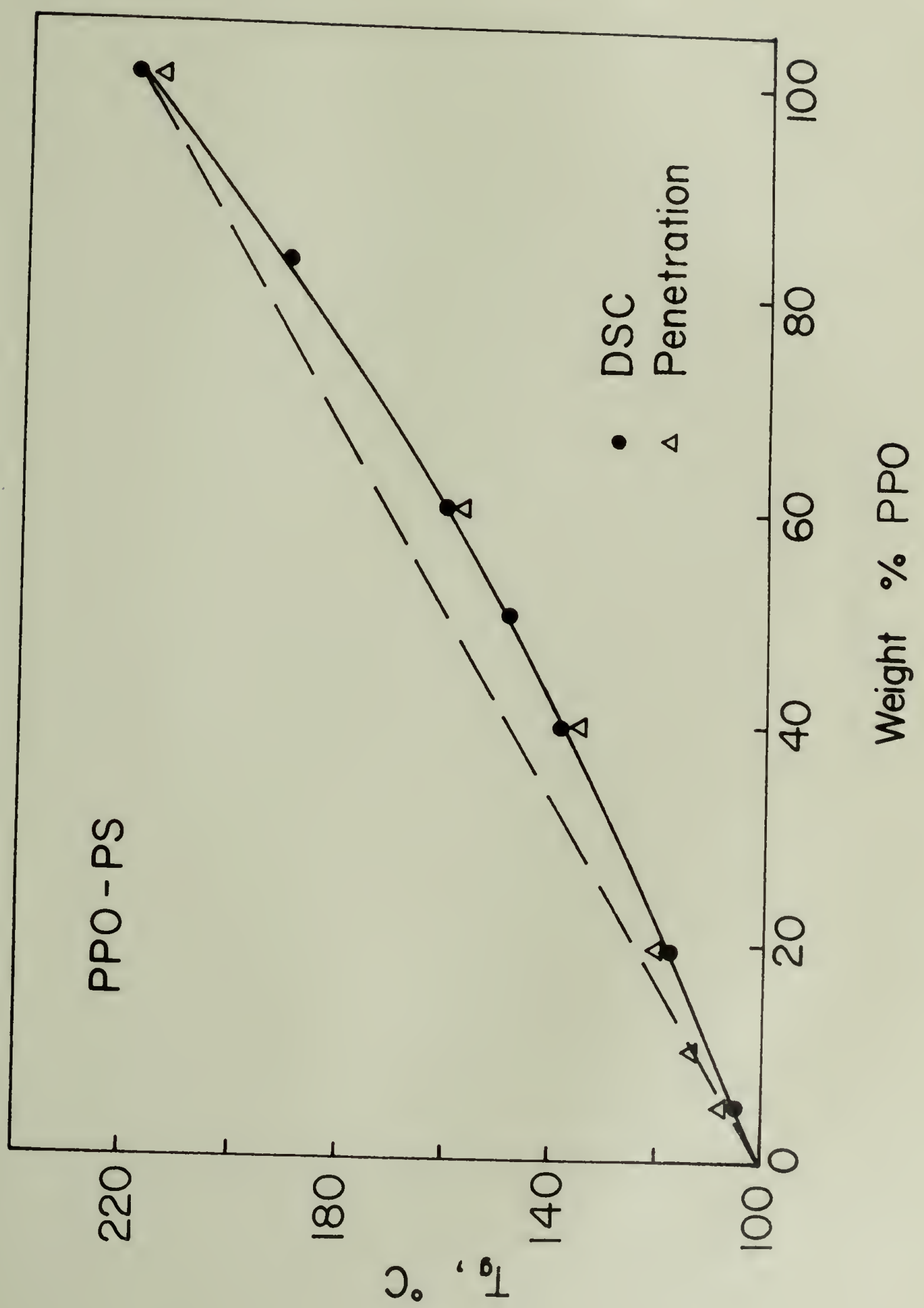
PPO-PS
T_g, °C
220
180
140
100
0
20
40
60
80
100
Weight % PPO
DSC
Penetration

Figure 4

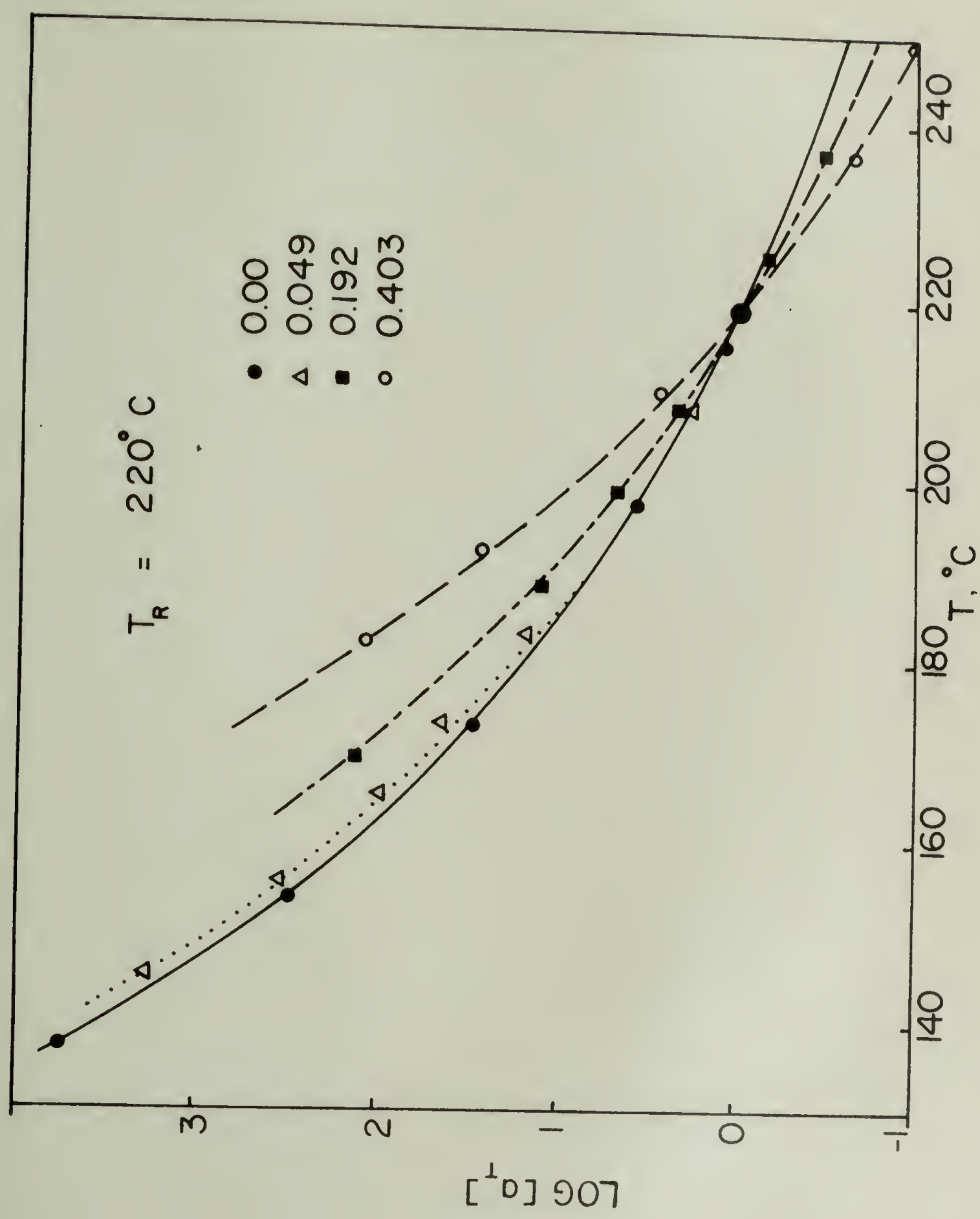
T_R = 220°C
● 0.00
△ 0.049
■ 0.192
○ 0.403
LOG [Q_T]
3
2
1
0
-1
140
160
180
200
220
240
T, °C

Figure 5

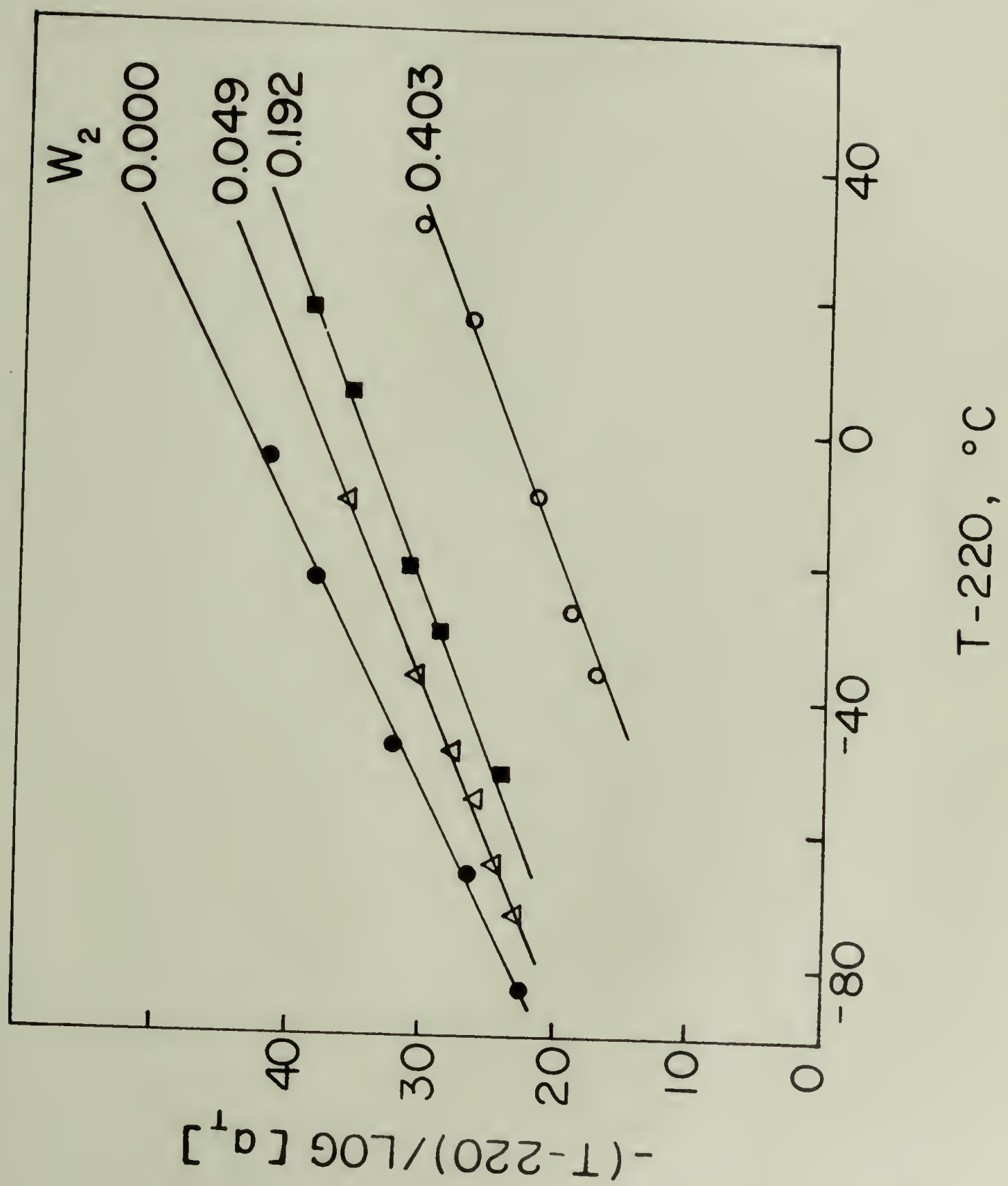

Figure 6

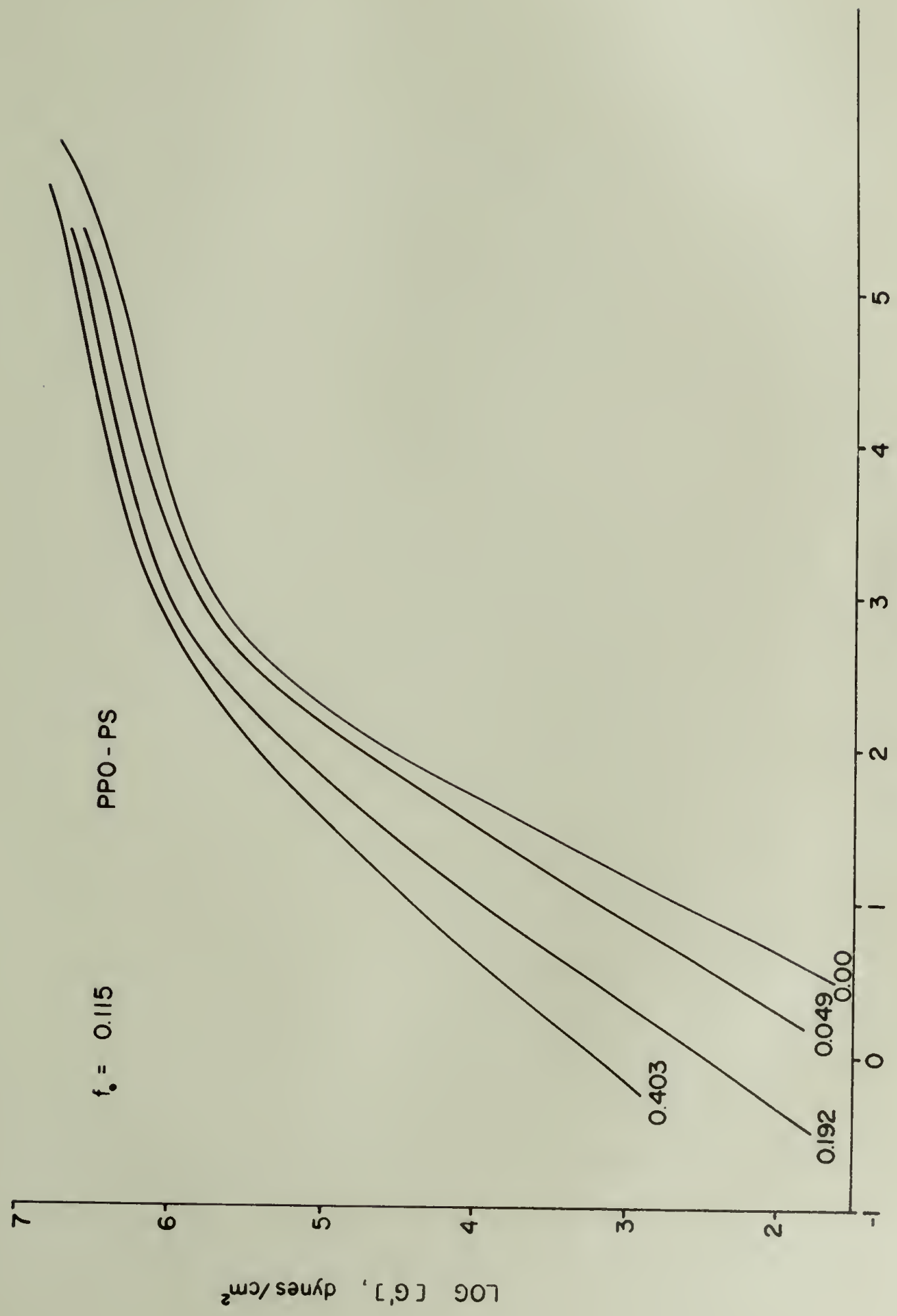
PPO-PS
f_o = 0.115
0.403
0.192
0.049
0.00
LOG [G'], dynes/cm²
LOG [ωa_T], LOG [$\dot{\gamma} a_T$] sec⁻¹
7
6
5
4
3
2
-1
0
1
2
3
4
5

Figure 7

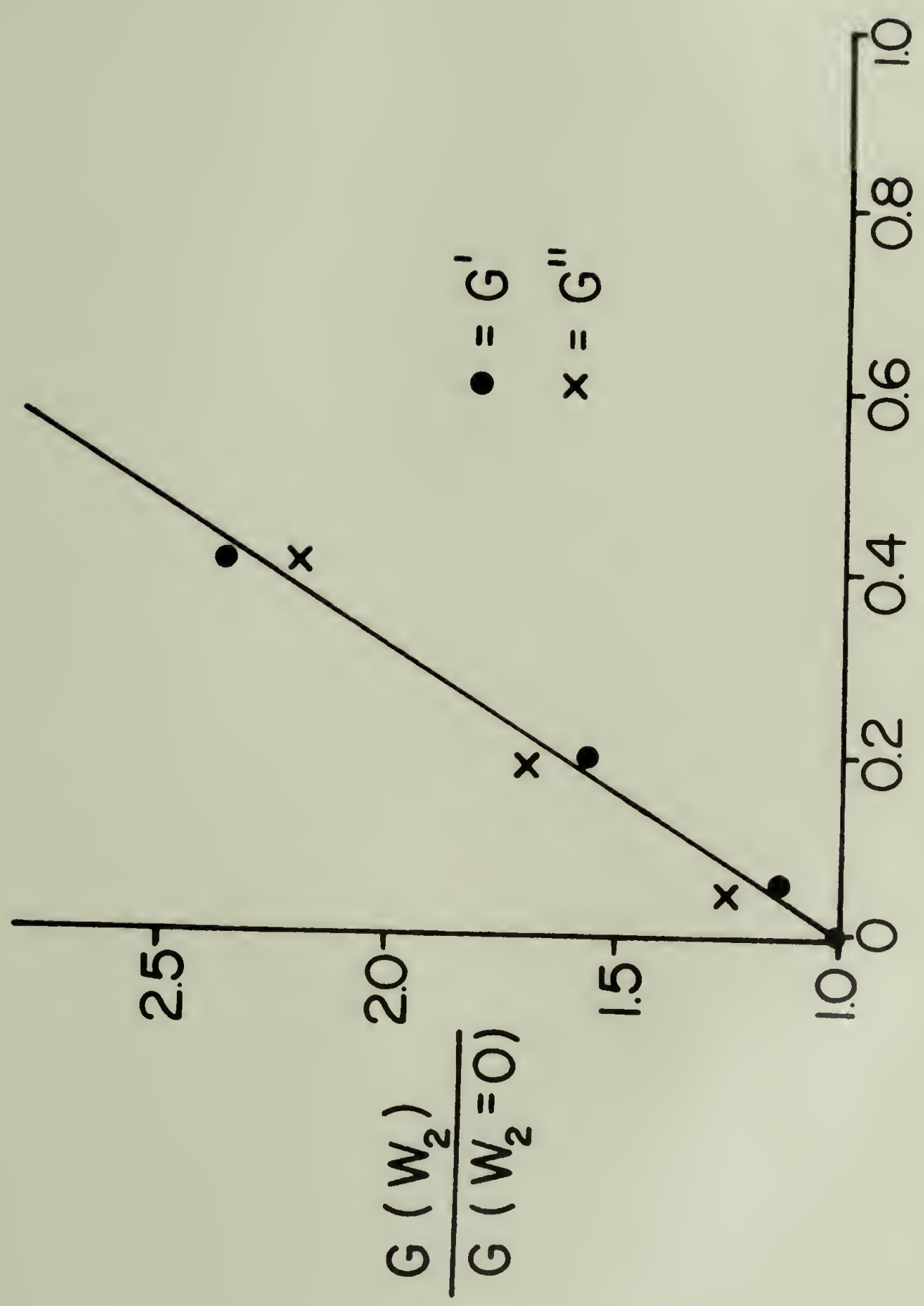

Figure 8

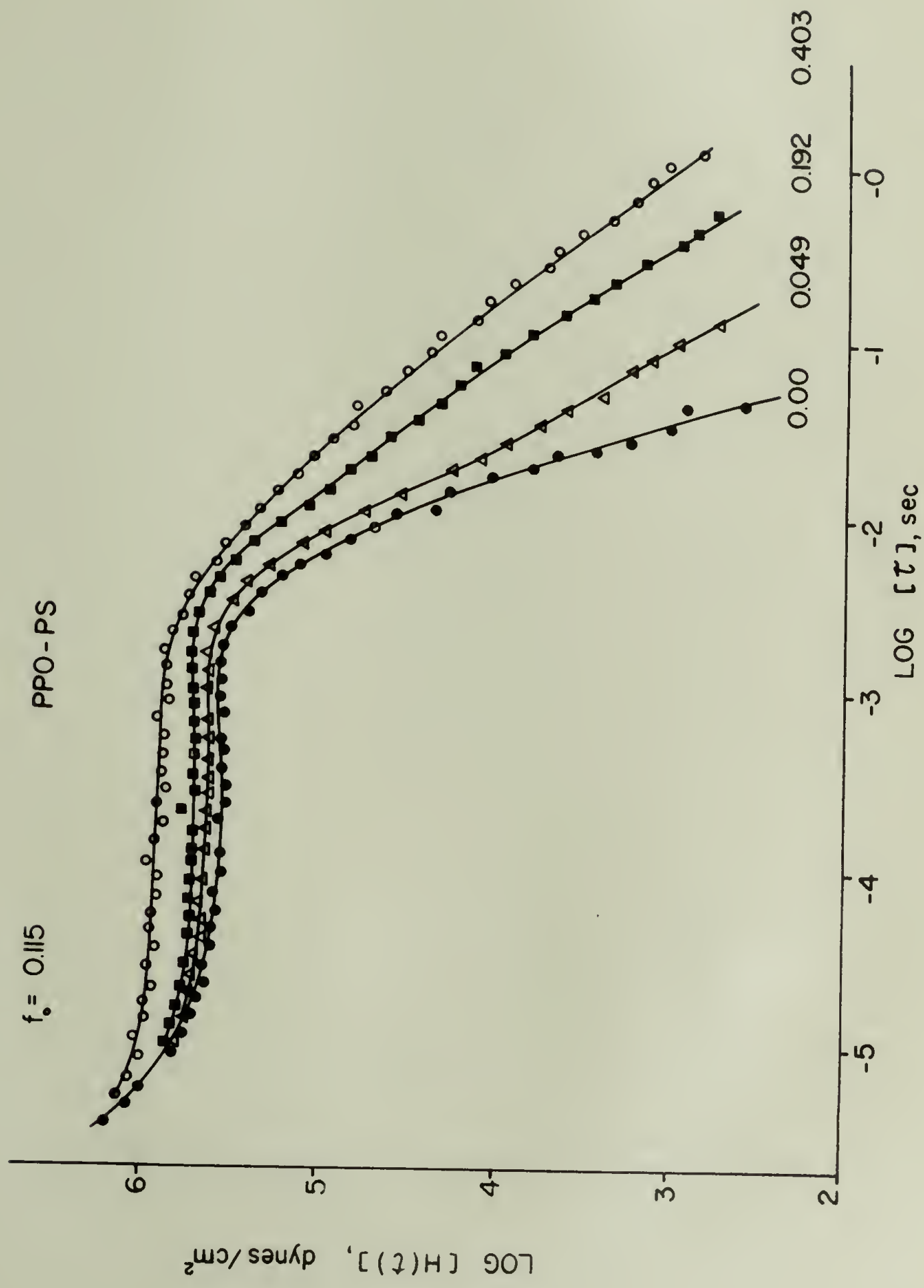

Figure 9

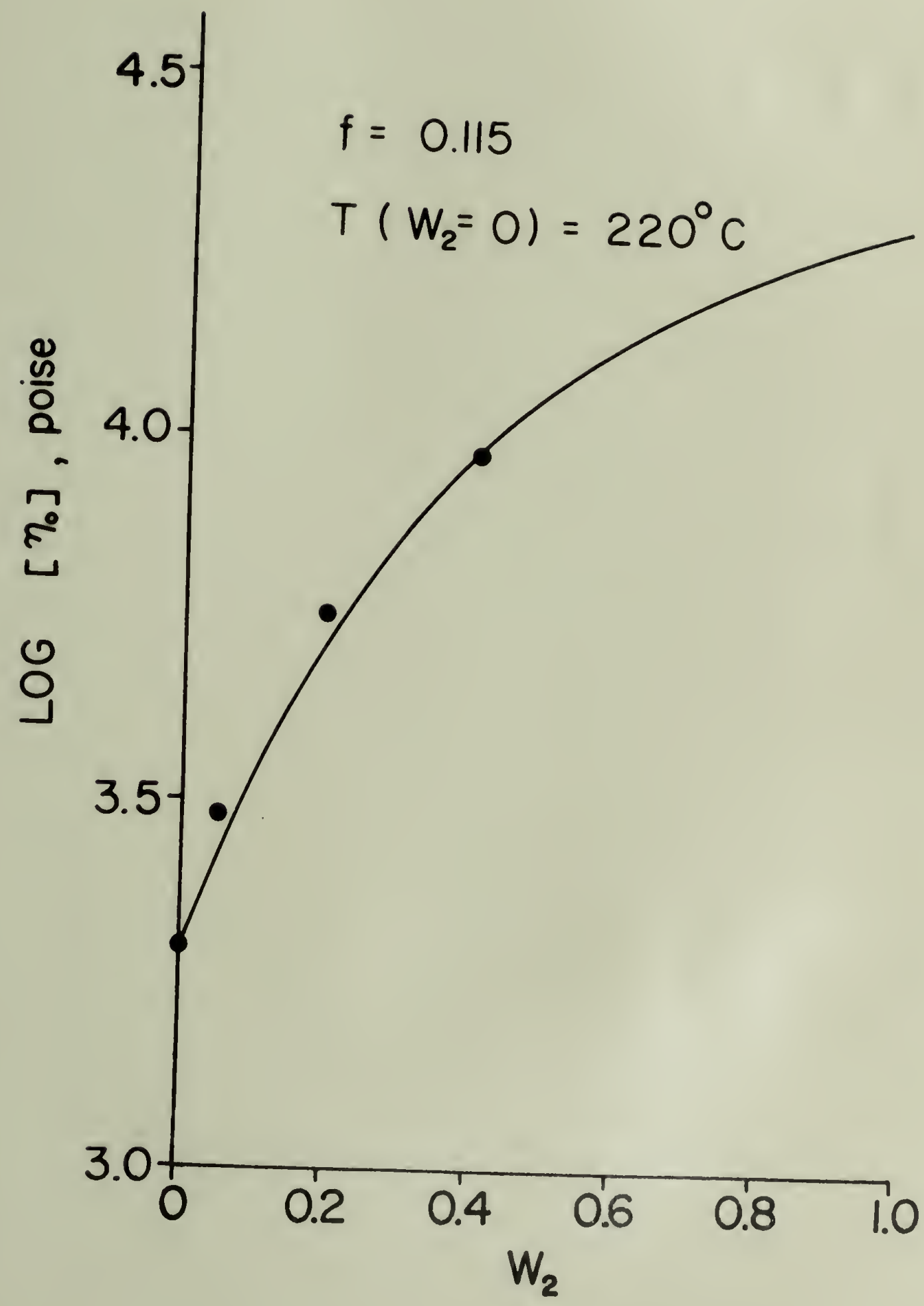

Figure 10

Chapter V

SUGGESTIONS FOR FUTURE STUDY

Critical Concentrations

The steady state shear compliance J_e^o, of blends of polymeric systems exhibits a maximum at low concentrations of the high MW component. In addition, changes in the relationships between other experimental quantities are observed in this concentration region. For example, log-log plots of the shift factors, λ_{ii}, versus the characteristic time, $\tau = \eta_{oB} J_{eB}^o$, and the weighting factors V_{ii} (see Chapter III) versus η_{oB} can be described by two lines which intersect in the neighborhood of the maximum of J_{eB}^o. It is proposed that these critical concentrations can be related to the molecular properties of the blend.

High MW blending experiments have shown that the initial concentration dependence of J_e^o (α w_2^{-2}) is independent of the MW of the lower MW component (1,2). The same concentration dependence is also observed when the low MW component is a solvent (3). Therefore, in terms of J_e^o, the low molecular weight component acts like a solvent even when it is a high MW entangled melt. This evidence implies that, over most of the concentration range, the elastic properties of polymer blends are controlled by just the elastic interactions between the molecules of the high MW component. This suggests that the maximum in J_e^o can be explained

in terms of a critical concentration for strong interactions between the high MW molecules. Two models for the critical concentration are given below.

Consider the experimentally observed MW dependence of the zero shear viscosity. A plot of log η_o versus log M_w yields two distinct linear regions with slopes approximately equal to 1 and 3.5. The MW at the intersection of these regions is defined as M_c. This represents the MW at which strong interactions between molecules first become apparent. Studies of the MW dependence of the viscosities of concentrated solutions of polymers have shown that $M_c = cM$ (4,5). This implies that strong interactions occur between high MW molecules above a critical concentration $c^* \equiv M_c/M$. Then, in perfectly mixed polymer-polymer blends, the molecules of the high MW component will interact strongly with each other for $w_2 \geq w_2^* \equiv M_c/M$. If, as suggested above, the elastic properties of the blend are controlled by just the interactions between the high MW components, then w_2^* should be related to the maximum in J_e^o.

A different proposal for the critical concentration has been given by Cornet (6). He defines this quantity as the concentration at which the segmental density of a polymer molecule becomes a constant. Calculations based on the packing of molecules with gaussian segmental distributions indicates that this condition is achieved when $c^{*2}M$ is a constant, approximately equal to 2700 (cgs) for PS in toluene. Daum and Wales (7) have shown that this relationship can be used to predict the concentration dependence of the

maximum in the reduced compliance, J_e^o M/cRT, which is observed in concentrated solutions of narrow MWD PS.

More experimental data is required to test either of the above predictions for the maximum of J_e^o in polymer-polymer blends. Unpublished results from this laboratory and data from the literature are presented in Figure 1 in hopes of stimulating further studies in this area.

Modified Spriggs - Rouse-Zimm Model

Several constitutive equations have been developed to describe the material functions of polymeric systems (8-12). Generally these can be used to represent experimental data over only limited ranges of shear rate and frequency. The Spriggs four-constant viscoelastic model (12) can describe the rheological response of polymer melts in both the low and high deformation rate regions (13). However, serious deviations from the experimental response are found at intermediate shear rates and frequencies.

The Spriggs' model uses the results of the Rouse (14) and Zimm (15) molecular theories to reduce the number of constants in the constitutive equations. The VE properties predicted by the Rouse-Zimm and the Spriggs' models is equivalent to the response of a sum of a set of Maxwell elements with modulus G and relaxation times τ_p. Spriggs assumes that the relaxation time of the system can be given by $\tau_p = \tau_1/p^a$, where a is an adjustable constant equal to 2 in the Rouse-Zimm model and p is a positive integer. The model

predicts that the high frequency slope, S, of a log-log plot of the viscosity, η, versus ω, is $(1 - 1/a)$. When a is approximately equal to 2, the predicted viscosities are smoothly varying functions of ω. However, when a is greater than 2.5, the predicted viscosities show small bumps in the intermediate ω region. These occur because the experimentally determined slopes effectively change the distribution of the relaxation times by changing the constant, a. As a increases, the spacing between the relaxation times increases. The sum over the relaxation times, required in the calculation of η, then begins to show the responses of each Maxwell element. As the spacing, a, increases, more elements become distinguishable and the resulting response appears to oscillate before the end slope is achieved.

This author believes that varying the parameter a is an unreasonable modification of the Rouse-Zimm theory becomes such a procedure, in effect, arbitrarily changes the characteristic values of the derived eigenvalue equations. It is suggested that, instead of changing the characteristic times (which have a theoretical basis), one considers changes in the modulus of each element. This suggestion is based on the following observations:

1. The Rouse-Zimm model, (a=2), adequately predicts the response of low molecular weight systems with narrow molecular weight distributions.
2. Changes in the VE response are found in high MW systems. These changes are believed to be caused by intermolecular interactions - sometimes referred to as entanglements.

3. The elastic response of high MW systems are found to be similar to the elastic properties of a cross-linked network.

The changes in the response of high MW materials may then be associated with changes in the elastic properties of the system. It is suggested that the modulus of each Maxwell element be considered to be a function of the relaxation time index, p. As an example, consider the case in which $G_p = G_1 p^b$. For this model it can be shown that the limiting slope S is equal to $(1 - \frac{(1-b)}{a})$. Values of a and b are given below as a function of S.

S	a(b=0)	b(a=2)
-0.4	1.67	+0.2
-0.5	2.0	0.0
-0.6	2.5	-0.2
-0.7	3.33	-0.4
-0.8	5.0	-0.6
-0.9	10.0	-0.8

Preliminary calculations of the VE response of this model, as a function of b with a=2, indicates that the intermediate time region is a smooth, non-oscillating function of ω. Therefore this approach yields a realistic prediction for the response of polymeric systems while retaining the formalism of the Rouse-Zimm theory.

These results demonstrate the practicality of the assumption of a variable modulus. Further studies should develop models for the MW and MWD dependence of the moduli associated with the longest relaxation times of entangled polymers.

Blends of High and Low MW Systems

Chapter III discussed the blending laws associated with the VE response of high MW polymer melts. By dealing solely with high MW components these studies eliminated effects that might be caused by changes in the free volume of the system. However, most commercial polymer systems contain significant quantities of low MW material. (i.e. $M < M_c$). These low MW components increase the available free volume in the melts and therefore change the time and temperature dependence of the relaxation processes. In addition, each low MW species has a much smaller compliance than the high MW components (1,16). The effects of blends of components with different compliances is not yet understood. It is suggested that the blending laws associated with the intermediate MW region, defined as blends of high and low MW materials, be investigated by the techniques described in Chapter II and III.

These blending experiments may be based on the existing narrow MWD polystyrene samples produced by the Pressure Chemical Company, Pittsburgh, Pa. The MW's of some of the available samples are:

$M < M_c$	$M > M_c$
10,300	97,200
20,400	200,000
	411,000
	670,000

The viscosities of these blends will be low enough to allow the complete characterization of each VE response without the problems associated with the thermal stability of high MW blends.

The analysis of the response of these blends must account for the change in the free volume of the systems. The resulting blending laws should require $H(\tau) \alpha \tau^{-1/2}$ in the iso-free volume transition region (see Chapters III and IV.) From this starting point it should be possible to incorporate free volume effects in the blending laws.

It is known that changes in free volume affect the viscosity of polymer systems through the segmental friction coefficient. The proposed study should be able to resolve the following related questions:

1. The free volume dependence of the modulus, if any.
2. The relative importance of the viscous and/or the elastic properties of each component in determining the MWD dependence of the shift factors, λ_{ii}.
3. The concentration and MW dependence of the weighting factors, V_{ii}.

Once the blending effects of low MW components are understood, these systems can be used as solvents to lower the viscosity of high MW blends. This will allow the experimental investigation of blending effects in very high MW materials.

Properties of Disperse Systems of Compatible Components

Chapter IV has shown that careful blending of PPO and PS will produce a single phase material. This compatibility is achieved only under special mixing conditions. It should therefore be possible to produce samples with compatible and incompatible regions and to

vary the relative size of these regions by making small changes in the mixing procedures. Previous rheological blending techniques required temperatures of at least 290°C to produce compatible PPO-PS systems (17,18). Therefore it may be expected that partially disperse blends will remain stable for rheological experiments conducted at much lower temperatures (≈200°C). Measurements on a series of these samples could be used to establish a rheological criteria for compatibility.

A parallel study could be performed on homopolymer blends. For example, blends of two different MW polystyrenes could be made by the crude mechanical mixing of performed pellets of each sample. The initial MW domain size could be controlled through the size of the blended pellets. The rheological properties of these systems would be expected to be a function of time and to approach the properties of a well mixed system. The time required for these changes would reflect the diffusion constants of each species and the mixing associated with the applied deformations.

Still another set of "compatible dispersions" could be made from polystyrene and crystalline PPO. The latter may be obtained by precipitating PPO from solution. The melting point of crystalline PPO is 262°C (19). By using low MW PS, it may be possible to mold samples at low enough temperatures to retain the crystallivity of the PPO component. The resulting system would contain hard crystalline regions loosely coupled to the amorphous PS component. The properties of these systems may be expected to be similar to the properties of incompatible copolymers such as styrene-butadiene-styrene.

Thermomechanical Analysis

The most intriging result of the thermomechanical penetration data presented in Figure 3 of Chapter IV is the ability of this type of experiment to detect the entanglement plateau of high MW systems. It would be extremely useful if this technique could be refined to measure the actual shape of the long time response of polymer melts. Initial experiments in this area should be performed on binary blends of high MW systems such as those studied in Chapters II and III. These blends exhibit a two step rubbery plateau which, in principle, can be resolved by the thermomechanical measurements. A useful starting point would be the 0.209/411/97.2 blend.

The sensitivity of the thermomechanical experiments to subtle changes in the VE response is expected to be increased as the applied loads and heating rates are reduced. The long time stability problems associated with low heating rates may be reduced by changing the temperature program during the run. For example a measurement may be conducted at a given heating rate until the rubbery plateau response is reached. Then the temperature may be held constant or a slower heating rate used to obtain the shape of the terminal response.

It should be possible to obtain the creep compliance J(t) of a system from thermomechanical measurements. This requires the reduction of data obtained at a given heating rate to the equivalent time dependent response at a given temperature. Relationships between the temperature and time scales can be obtained from the WLF equation (20).

In addition, displacements caused by the thermal expansion of the melt must be subtracted from the measured thermomechanical response. This correction may be measured with an expansion probe or by successive penetration measurements at different heating rates.

REFERENCES

1. W. M. Prest, Jr., J. Polym. Sci., A-2, 8, 1897 (1970).
2. T. Masuda, K. Kitagawa, T. Inoue, and S. Onogi, Macromolecules, 3, 116 (1970).
3. W. W. Graessley and L. Segal, Macromolecules, 2, 49 (1969).
4. T. G. Fox and S. Loshack, J. Appl. Phys., 26, 1080 (1955).
5. D. Gupta and W. C. Forsman, Macromolecules, 2, 304 (1969).
6. C. F. Cornet, Polymer, 6, 373 (1965).
7. U. Daum and J. L. S. Wales, Polymer Letters, 7, 463 (1969).
8. H. Markovitz, Trans. Soc. Rheol., 1, 37 (1957).
9. D. C. Bogue and J. O. Doughty, Ind. Eng. Chem. Fundamentals, 5, 243 (1966).
10. Ibid., 6, 388 (1967).
11. T. W. Spriggs, J. D. Huppler and R. B. Bird, Trans. Soc. Rheol., 10, 191 (1966).
12. T. W. Spriggs, Ph.D. thesis, Univ. Wisc., Madison (1965).
13. C. D. Denson, W. M. Prest, Jr., and J. M. O'Reilly, A.I.Ch.E. J., 15, 809 (1969).
14. P. E. Rouse, Jr., J. Chem. Phys., 21, 1272 (1953).
15. B. H. Zimm, J. Chem. Phys., 24, 269 (1956).
16. S. Onogi, T. Masuda, and K. Kitagawa, Macromolecules, 3, 109 (1970).
17. E. P. Cizek, U.S. Patent 3,383, 435 (May 14, 1968).
18. J. Stoehting, R. E. Kamasz, and W. J. MacKnight, Polym. Eng. Sci., 10, 133 (1970).

19. F. E. Karasz, H. E. Bair and J. M. O'Reilly, J. Polym. Sci., A-2, 6, 1141 (1968).

20. M. L. Williams, R. F. Landel, and J. D. Ferry, J. Amer. Chem. Soc., 77, 3701 (1955).

21. N. J. Mills and A. Nevin, J. Polym. Sci., A-2, 8, 1897 (1970).

22. G. Akovali, J. Polym. Sci., A-2, 5, 875 (1967).

FIGURE CAPTION

Figure 1 The steady state shear compliance, J_e^o, of blends of narrow molecular weight distribution polystyrenes as a function of the weight fraction of the high molecular weight component. The MW's of the components in thousands are indicated by the numbers. The 670/97.2 and the 411/97.2 blends were studied in this laboratory. Other blends were examined by Mills (21) 500/86.8 and Akovali (22) 267/125.

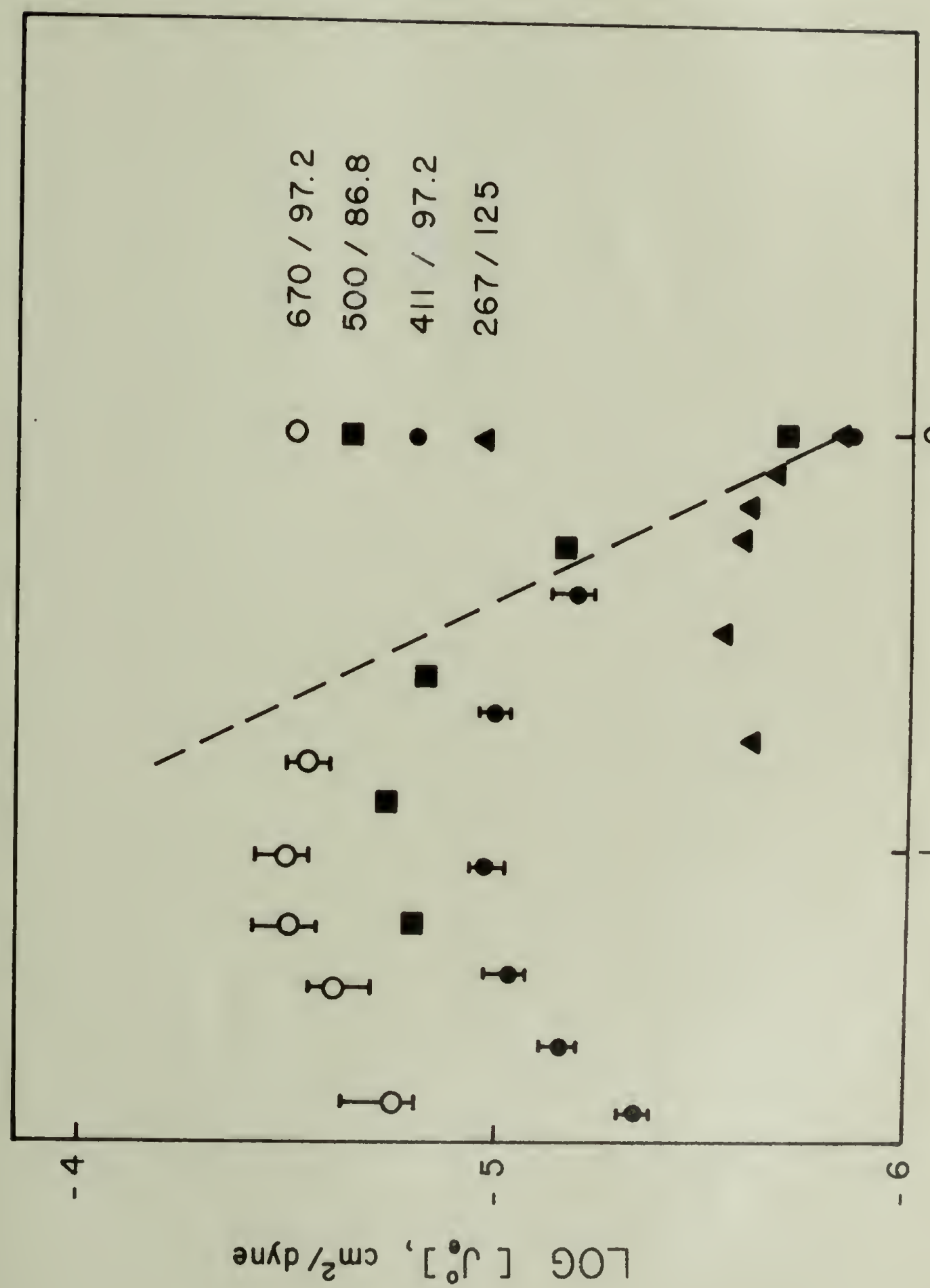

Figure 1

APPENDIX A

Comments on Approximations for the Relaxation Spectra of Polymer Melts

In general a property of a material, $g(\omega)$, is related to the relaxation spectrum $H(\tau)$ of the system by the integral transform

$$g(\omega) = \int_{-\infty}^{\infty} K(\omega,\tau)\ H(\tau)\ d\ \ln\ \tau \qquad (1)$$

where the kernal, $K(\omega,\tau)$, is the appropriate intensity function of $g(\omega)$. If the kernal contributes to the integral over only a portion of the integration and if $H(\tau)$ is approximately constant in this interval, then

$$H(\tau) \approx g(\omega) / \int_{-\infty}^{\infty} K(\omega,\tau)\ d\ \ln\ \tau \qquad (2)$$

If the kernal is a delta function, the relaxation spectrum is exactly equal to the material property. When the kernal of the material significantly contributes to the integral over a range of τ, the validity of equation 2 is a function of the shape of $H(\tau)$. The kernals associated with the loss modulus, G", and the storage modulus, G', are $(\omega\tau)^2/(1 + (\omega\tau)^2)$ and $\omega\tau/(1 + (\omega\tau)^2)$ respectively. Obviously these contribute to the integral over a wide range of τ. Therefore equation 2 is expected to be a poor approximation for the relaxation spectrum of the system, when $g(\omega)$ = G' or G".

Several techniques have been developed to improve the approximation of $H(\tau)$. (1-7). The results of several of these approaches have been given by Ferry (8). One approach (3-7) takes various linear combinations of G' (or G") and its derivatives as the function $g(\omega)$. A judicious

choice of $g(\omega)$ will narrow the interval over which $K(\omega,\tau)$ significantly contributes to the integral. This makes equation 2 less sensitive to the τ dependence of $H(\tau)$. Approximations based on this technique are given below in terms of the derivatives of the viscoelastic functions, $F' = \frac{dG'}{d\ln\omega}$, $S' = \frac{d^2G'}{d\ln\omega^2}$, $T' = \frac{d^3G'}{d\ln\omega^3}$, $F'' = \frac{dG''}{d\ln\omega}$, etc.

The Second Order Tschoegl Approximation (3)

$$H(\tau) = F' \pm \frac{S'}{2}; \qquad \tau_+ = 1/\omega\sqrt{2}, \ \tau_- = \sqrt{2}/\omega \tag{3}$$

$$H(\tau) = \frac{2}{\pi}\left(G'' \pm \frac{4}{3}F'' + \frac{S''}{3}\right); \qquad \tau_+ = 1/\omega\sqrt{5}, \ \tau_- = \sqrt{5}/\omega \tag{4}$$

where the + (-) signs are used when the slope of $H(\tau)$ is positive (negative).

Schwarzl and Staverman (SS) (4)

$$H(1/\omega) = F' - D'T' \tag{5}$$

$$H(1/\omega) = \frac{2}{\pi}(G'' - D''S'') \tag{6}$$

where $D' = \frac{1}{4}$ and $D'' = 1$.

Other approximations for $H(\tau)$ are very similar to equations 3-6. For example, Okano (7) and Fujita's (6) approximation for $H(\tau)$ from G', is equal to equation 3 multiplied by $\frac{e^2}{2}$ and evaluated at $\tau = 1/\omega$. Similarly Fujita's (6) approximation for $H(\tau)$ from G'' is $\frac{e^2}{8}$ times equation 6, again evaluated at $\tau = 1/\omega$.

Ninomiya and Ferry (5) have presented an approximation technique based on the numerical values of the VE function at equally spaced

values of log ω. For points separated by log a,

$$H(1/\omega) = \left[\frac{G'(a\omega) - G'(\omega/a)}{2 \ln (a)}\right] - \frac{a^2}{(a^2-1)^2}\left[\frac{(G'(a^2/\omega) - 2G'(a\omega) + 2G'(\omega/a) - G''(\omega/a^2)}{2 \ln (a)}\right] \tag{7}$$

and

$$H(1/\omega) = \frac{2}{\pi} G'' - \frac{2a}{\pi(a-1)^2}\left[G''(a\omega) - 2G''(\omega) + G''(\omega/a)\right] \tag{8}$$

The quantities in the brackets are the numerical approximations of the derivatives of G obtained from the differential difference equation (10) (see below). In terms of F, S, and T these become:

$$H(1/\omega) = F' - \left(\frac{a \ln a}{a^2-1}\right)^2 T_5' \tag{9}$$

$$H(1/\omega) = \frac{2}{\pi}\left(G'' - a\left(\frac{\ln a}{a-1}\right)^2 S_3''\right) \tag{10}$$

Therefore, the NF approximations are equal to equations 3 and 4 with $D' = \left[\frac{a \ln(a)}{(a^2-1)}\right]^2$ and $D'' = a\left[\frac{\ln(a)}{(a-1)}\right]^2$.

A different approach to the inversion of equation 1 makes use of the observation that $H(\tau)$ is a slowly varying function of τ for most polymer systems. Williams and Ferry (WF) (1,2) assume that $H(\tau) = K\tau^{-m}$ over some range of τ. Normalization factors calculated from equation 1 in terms of the negative slope of $H(\tau)$, m, are then applied to the first approximations of $H(\tau)$.

$$H(1/\omega) = A\,F' \quad ; \quad A = \frac{\sin(m\,\pi/2)}{m\,\pi/2} \quad \text{for } m < 1 \tag{11}$$

$$H(1/\omega) = A'[2G' - F'] \quad ; \quad A' = \frac{\sin(m\,\pi/2)}{\pi(1 - m/2)} \quad \text{for } 1 < m < 2 \tag{12}$$

$$H(1/\omega) = B\ G''[1 - F''] \ ; \qquad B = \frac{\sin(\frac{\pi}{2}(1 + |m|))}{\pi/2\ (1 - |m|)} \tag{13}$$

More involved techniques using interation procedures to approximate $H(\tau)$ have been discussed in a recent paper by Shroff (9).

The usefulness of any of the approximations for $H(\tau)$ depends on the accuracy of the calculated derivative. This in turn is a function of the experimental uncertainties in the data. Consider the numerical differentiation of the experimental VE functions. The j^{th} derivative can be given by the linear combination of equally spaced data points,

$$f^{(j)}(x) = \sum_{i=-\infty}^{\infty} C_i\ f(x+ih) \tag{14}$$

where h is the interval between points (10). For any desired approximation, the unknown coefficients, C_i, can be evaluated by expanding each data point in terms of a Taylor series about x.

$$f(x) = \sum_{i=-\infty}^{\infty} C_i \sum_{n=o}^{\infty} \frac{f^{(n)}(x)}{n!} (ih)^n \tag{15}$$

For example, consider the first derivative determined by three data points centered about x. The only non-zero terms in this approximation are: C_{-1}, C_0, and C_{+1}. Equating the coefficients in equation 14 and neglecting higher order derivatives yields

$$f_3^I = (f_{+h} + f_{-h})/2h - (h^2/6\ f^{III}) \tag{16}$$

where $f(x+ih) \equiv f_{ih}$ and the error in the approximation is proportional to the third derivative of f(x), f^{III}. Note that, in the limit as $h \to 0$, equation 16 is the definition of the first derivative of f_{-h}. The three

and five point central difference derivatives are given below.

Three point derivatives

$$F_3 \equiv f_3^I = \frac{f_{+1} - f_{-1}}{2h} - [\frac{h^2}{6} f^{III}] \quad (17)$$

$$S_3 \equiv f_3^{II} = \frac{f_{+1} - 2f_0 + f_{-1}}{h^2} + [\frac{1}{12} h^2 f^{II}] \quad (18)$$

Five point derivatives

$$F_5 \equiv f_5^I = \frac{-f_{+2} + 8f_{+1} - 8f_{-1} + f_{-2}}{12h} + [\frac{h^4}{30} f^V] \quad (19)$$

$$S_5 \equiv f_5^{II} = \frac{-f_{+2} + 16f_{+1} - 30f_0 + 16f_{-1} - f_{-2}}{12h^2} + [\frac{1}{90} h^4 f^{VI}] \quad (20)$$

$$T_5 \equiv f_5^{III} = \frac{f_{+2} - 2f_{+1} + 2f_{-1} - f_{-2}}{2h^3} - [\frac{h^2 f^V}{4}] \quad (21)$$

The error functions state that the numerical approximations for the derivatives may be improved by increasing the number of data points and decreasing the separation between these points. However this is only true for perfect data. In practice, uncertainties in the experimental measurements over ride the theoretically improvements in the approximations. For example, assume that the point f_0 is in error by an amount d. The resulting errors in the calculated second derivatives of the three point and five point approximations are $-2d/h^2$ and $-5d/2h^2$ respectively. In contrast the positive errors $1/h^2$ and $4/3h^2$ are associated with the derivatives of the neighboring points $f^{II}_{(\pm h)}$. Thus one poor experimental measurement produces oscillations in the calculated derivatives. This

general property of numerical differentiation is responsible for the fluctuations that usually appear in calculated relaxation spectra.

The effects of experimental errors may be reduced by increasing the separation between the data points. However, this technique makes the approximation less sensitive to actual, rapid changes in the experimental functions. The choice of a particular approximation is then controlled by the accuracy of the data and the shape of the experimental function. The relative practical importance of these considerations can be evaluated by calculating the numerical derivatives of experimental VE functions. In general the VE properties of polymer systems are slowly varying functions of frequency. However, relatively rapid changes in the VE response are observed for binary blends of components with narrow MWDs (10). These systems provide a critical test of the accuracy of the numerical derivatives as the function of the data interval, h. The VE properties of blends of this type were measured at several different temperatures. The data was superimposed to form a master curve representing the response of the system over five to seven decades of frequency. A smooth line was drawn through the master curve. Values of G' and G" were measured at intervals of $\log \omega = 0.1$ from this smooth line. It is estimated that these measured quantities differed from the smooth curve by no more then $\pm$ 1.5%. This procedure simulates the best data that may be experimentally obtained.

Certain generalizations can be made about the usefulness of the numerical derivative approximations, (equations 17-21) from this experimental data. The first derivative approximations, F_3 and F_5 yield essentially equal results for calculations over a given interval, h.

Generally the first derivatives are smooth functions, even for h = 0.1. However, small oscillations are evident when the first derivative is approximately a constant. These become important in the approximations for $H(\tau)$.

At a given h, the second and third derivative approximations are much more sensitive to experimental data than the first derivatives. Oscillations on the order of $\pm$ 20% occur in S_3 for h = 0.1. S_5 magnifies these oscillations, particularly in the regions where the slope of the second derivative is changing rapidly. The approximation for the third derivative is slightly more sensitive to experimental errors than S_3 and S_5. Doubling or tripling the interval to 0.2 or 0.3 significantly reduces the magnitude of the observed fluctuations for all derivative approximations. However, rather than improving the data, further increases in h tend to smooth out actual narrow transitions in the VE response. It is important to note that significant oscillations occur in the calculated second and third derivatives based on h = 0.1 for even carefully smoothed data. This problem is compounded as the accuracy of the data decreases. In general these oscillations are much greater than the errors associated with the information that is lost when too large an interval h is used. It is therefore desireable to choose a set of numerical derivatives which calculate the first, second, and third derivatives over progressively larger intervals of h. This procedure will reduce the effects of experimental errors while retaining a degree of sensitivity to actual, rapid changes in the data. As an example of this type of approximation, consider the simple set of numerical derivatives

defined by the repeated application of equation 17.

$$F_s = \frac{f_{+1} - f_{-1}}{2h} - [\frac{1}{6} h^2 f^{III}] \quad (22)$$

$$S_s = \frac{f_{+2} - 2f_0 + f_{-2}}{4h^2} + [\frac{1}{3} h^2 f^{IV}] \quad (23)$$

$$T_s = \frac{f_{+3} - 3f_{+1} + 3f_{-1} - f_{-3}}{8h^3} - [\frac{1}{2} h^2 f^{V}] \quad (24)$$

Note that equation 23 is equivalent to the three point central difference second derivative (equation 18) applied to an interval of 2h while equation 24 involves a slightly larger interval than equation 19. Table I compares the maximum errors of each type of approximation which results from an experimental uncertainty of +d. The errors associated with the single derivatives are proportional to d while the other approximations involve multiples of d. Calculations on VE data show that this improvement does not significantly decrease the absolute accuracy of the second and third derivatives.

Calculated Relaxation Spectra

The experimental VE response of binary blends of high MW polystyrene (10) were used to compare the different approximations for $H(\tau)$ given above. Each approximation was evaluated with the simple, the three point and the five point numerical derivatives. The interval between data points, $h = d \log \omega$, was varied from 0.1 to 0.6.

In the rubbery plateau region the first derivative of G' is found to be approximately independent of ω. Therefore the second and third derivatives should be negligible and all approximations for $H(\tau)$ equiv-

alent. This is observed for each of the derivative approximations when $h \geq 0.2$. It was stated above that small oscillations in the first derivative become noticeable when $h = 0.1$. These do not appreciably effect the simple derivative approximation for $H(\tau)$. However, these experimental errors are magnified by the three and five point approximations for S' and T' causing the higher order derivatives to contribute to $H(\tau)$. Relaxation spectra calculated with these derivations differ from the previously determined $H(\tau)$ by up to +20%.

In the terminal and near terminal regions, $G \alpha \omega^b$ where $b \approx 2$ for G' and $b \approx 1$ for G''. The derivatives of G are: $F = bG$, $S = b^2G$, and $T = b^3G$. The approximations for $H(\tau)$ are then proportional to the difference between two large and nearly equal numbers. Therefore, the use of the simple derivative approximations are preferred in this region because small errors in the numerical derivatives produce large fluctuations in the calculated $H(\tau)$.

The Tschoegl approximations produce the smoothest $H(\tau)$ in the near terminal region. This occurrs because the second (first) derivatives used in equations 3 and 4 are less sensitive to experimental errors than the third (second) derivatives required by equations 5, 6, 9, and 10. The Schwarzl and Staverman and the Ninomiya and Ferry approximations oscillate around the Tschoegl approximation, and become equal to it when the interval h is increased. The Williams and Ferry approximations are proportional to ratios of two numbers close to zero and thus are very sensitive to small fluctuations in the numerical first derivatives.

Similar results are obtained for the calculated relaxation spectra in the regions between the terminal and the rubbery plateau response.

Again the difference between the second and third derivatives make the Tschoegl approximations less subject to experimental errors than the SS and NF approximations. These converge to the Tschoegl approximation for h greater than 0.1 but less than some value which depends on the width of the transition. The initial decrease in $H(\tau)$ from the rubbery plateau response for narrow MWD polystyrenes were adequately reproduced with $h = 0.3$. Changes in the spectra become noticeable when $h > 0.4$. Most polymeric systems exhibit broader transitions than the narrow MWD polymers. Therefore, an interval, $h = 0.2 - 0.4$ should be sufficient for the determination of $H(\tau)$. However, sharper transitions are observed in binary blends of narrow MWD systems (10). These appear as shoulders in the terminal response of $H(\tau)$. Significant changes in the calculated spectra occur when the shoulder is narrower than 2h. Derivatives defined over larger intervals underestimate the actual changes in the shape of the VE functions. The resulting relaxation spectra approach an average of the spectra on either side of the transition. This loss of information obscures the shoulders in $H(\tau)$.

Each approximation for $H(\tau)$ indicated the presence of a shoulder in the relaxation spectra of the binary blends. Equivalent results were obtained with all but the WF approximations. This technique, (which is based on the assumption that $H(\tau)$ is a slowly varying function of τ) was unable to follow the sharp transition of the shoulders in $H(\tau)$.

The VE properties, G' and G'' were calculated by the numerical integration of equation 1 using the relaxation spectra defined by equations 3-12. This proved to be an insensitive test of the different approximations because the recalculated properties were generally equal to each other

and to the initial data. However, one important difference was consistently observed. At low stresses ($< 3 \times 10^3$ dynes/cm^2) the recalculated G' were slightly higher ($\approx$ 10%) than the actual G'. This was caused by erroneous non-zero contributions to $H(\tau)$ in the terminal response region.

Conclusions

The second order approximations for $H(\tau)$ proposed by Tschoegl (equations 3,4) were found to be the most practical method of calculating the relaxation spectrum of polymer melts. All of the approximations for $H(\tau)$ (equations 3-12) are found to be more sensitive to small errors in the experimental data than to inaccuracies in the numerical approximations of the derivatives. The set of simple numerical derivatives (equations 22-24) reduce these errors to acceptable levels.

REFERENCES

1. J. D. Ferry and M. L. Williams, J. Colloid Sci., 7, 347 (1952).
2. M. L. Williams and J. D. Ferry, J. Polym. Sci., 11, 169 (1953).
3. N. W. Tschoegl, Trans. Soc. Rheology, to be submitted; (reference 10, pps. 92, 94).
4. F. Schwarzl and A. L. Staverman, Appl. Sci. Research, A4, 127 (1953).
5. K. Ninomiya and J. D. Ferry, J. Colloid Sci., 14, 36 (1959).
6. H. Fujita, J. Applied Physics, 29, 943 (1958).
7. M. Okano, Busseiron Kenkyu, 3, 493 (1958).
8. J. D. Ferry, "Viscoelastic Properties of Polymers", John Wiley and Sons, Inc., New York, N.Y., 1961, 1970, Chapter 4.
9. R. N. Shruff, Trans. Soc. Rheology, 15, 163 (1971).
10. D. Greenspan, "Introduction to Numerical Analysis and Applications", Markham Publishing Co., Chicago, Ill., 1971, pp. 34-40.

Table I

Maximum Errors Of Derivatives For A Data Uncertainty Of $\pm$ d

Derivative	Simple	3 Point	5 Point
F	d/h	d/h	$3d/2h$
S	d/h^2	$4d/h^2$	$16d/3h^2$
T	d/h^3		$3d/h^3$

Computer Program To Calculate The Relaxation Spectrum Of Polymer Melts

1 - NAME H(TAU)

2 - INPUT

N:	Number of data points
TITLE:	Identification of sample
KO:	Multiple of initial data interval, h
K1:	1-simple derivatives
	2-three point central difference derivatives
	3-five point central difference derivatives
W1:	Log (ω)
G1:	G'
G2:	G"

3 - OUTPUT

TAU:	Log (τ)
H (TAU):	Relaxation spectrum at τ
GP:	Calculated G'
G2P:	Calculated G"

Approximations used -

1-Tschoegl second order

2-Swarzl and Staverman

3-Ninomiya and Ferry

4-Williams and Ferry

On each output page the first set of data is calculated from G', the second set from G", the third set is the input data and the calculated $1/J^1$.

```
      COMPUTER PROGRAM TO CALCULATE THE RELAXATION SPECTUM

       PROGRAM  H(TAU)
      DIMENSION W(60),GP(60),G2P(60),X(60),FGP(60,3),FG2P(60,3)
      DIMENSION SGP(60,3),SG2P(60,3),TGP(60,3),W1(60)
      DIMENSION TITLE(3) ,G1(60),G2(60)TH1(60,3),H2(60,3)
   10 READ 20,N,TITLE,K0,K1,K2
   20 FORMAT(I4,3A8,2X,I1,1X,I1,1X,I1)
   25 IF(N) 65,999,30
   30 M=N
      DO 50 I=1,M,2
   50 READ 60,W1(I),G1(I),G2(I),W1(I+1)TG1(I+1),G2(I+1)
   60 FORMAT(2(F10.2,2E10.2,10X))
   65 N=M/K0
      DO 70 LI=1,K0
      DO 70 L=1,N
      N1=L1+K0*(L-1)
      I=L+N*(L1-1)
      W(I)=W1(N1)
      GP(I)=G1(N1)
   70 G2P(I)=G2(N1)
      N1=N-1
      N2=N-2
      N3=N-3
      M3=M-3
      PRINT 80, TITLE
   80 FORMAT(1H1,40X,3A8,14HH(TAU) FROM GP//)
      B=2.3026
      C=2./3.1416
      DO 140 L1=1,K0
      DO 120 L=2,N1
      I=L+N*(L1-1)
      X(I)=(W(I+1)-W(I-1))*B/2.
      FGP(I,1)=(GP(I+1)-GP(I-1))/2./X(I)
      FG2P(I,1)=(G2P(I+1)-G2P(I-1))/2./X(I)
      FGP(I,2)=FGP(I,1)
  120 FG2P(I,2)=FG2P(I,1)
      DO 130 L=3,N2
      I=L+N*(L1-1)
      FGP(I,3)=(-GP(I+2)+8.*(GP(I+1)-GP(I-1))+GP(I-2))/12./X(I)
      FG2P(I,3)=(-G2P(I+2)+8.*(G2P(I+1)-G2P(I-1))+G2P(I-2))/12./X(I)
      SGP(I,1)=(FGP(I+1,1)-FGP(I-1,1))/2./X(I)
      SG2P(I,1)=(FG2P(I+1,1)-FG2P(I-1,1))/2./X(I)
      SGP(I,2)=(GP(I+1)-2.*GP(I)+GP(I-1))/X(I)**2
      SG2P(I,2)=(G2P(I+1)-2.*G2P(I)+G2P(I-1))/X(I)**2
      SGP(I,3)=(-GP(I+2)+16.*(GP(I+1)+GP(I-1))-30.*GP(I)-GP(I-2))/12./X(
     1I)**2
  130 SG2P(I,3)=(-G2P(I+2)+16.*(G2+(I+1)+G2P(I-1))-30.*G2P(I)-G2P(I-2))/
     112./X(I)**2
      DO 140 L=4,N3
      I=L+N*(L1-1)
      TGP(I,1)=(SGP(I+1,1)-SGP(I-1,1))/2./X(I)
      TGP(I,2)=(GP(I+2)-2.*(GP(I+1)-GP(I-1))-GP(I-2))/2./X(I)**3
  140 TGP(I,3)=TGP(I,2)
      J=K1
      DO 210 I=4,M3
      H1(I,J)=FGP(I,J)-SGP(I,J)/2.
  210 H2(I,J)=C*(G2P(I)-4.*FG2P(I,J)/3.+SG2P(I,J)/3.)
      PRINT 215,J
```

```
      GP1=0
      GP2=0
      G2P1=0
      G2P2=0
      L1=K2
      K4=1
      IF(K2) 999,811,812
  811 K4=K0
      DO 820 L1=1,K0
  812 DO 820 L=4,N3
      I=L+N*(L1-1)
      IF(H1(I,J))  813,814,814
  813 H1(I,J)=0
  814 IF(H2(I,J))  816,816,818
  816 H2(I,J)=0
  818 D3=10.**(T1+W(K)-W(I))
      E3=10.**(T2+W(K)-W(I))
      D2=D3/(1.+D3**2)
      D1=D3*D2
      E2=E3/(1.+E3**2)
      E1=E3*E2
      GP1=GP1+H1(I,J)*D1*X(I)/K4
      GP2=GP2+H2(I,J)*E1*X(I)/K4
      G2P1=G2P1+H1(I,J)*D2*X(I)/K4
  820 G2P2=G2P2+H2(I,J)*E2*X(I)/K4
      TAU1=10.**(T1-W(K))
      TAU2=10.**(T2-W(K))
      ETA1=ETA1+H1(K,J)*TAU1*X(K)/K4
      ETA2=ETA2+H2(K,J)*TAU2*X(K)/K4
      AG1=AG1+H1(K,J)*TAU1**2*X(K)/K4
      AG2=AG2+TAU2**2*H2(K,J)*X(K)/K4
      GG=GP(K)/(GP(K)**2+G2P(K)**2)
      T3=T1-W(K)
      T4=T2-W(K)
  830 PRINT 840,T3,H1(K,J),GP1,G2P1,T4,H2(K,J),GP2,G2P2,W(K),GP(K),G2P(K
     1),GG
  840 FORMAT(3(F10.2,3E10.2))
      AJE1=AG1/ETA1**2
      AJE2=AG2/ETA2**2
      PRINT 850,ETA1,AG1,AJE1,ETA2,AG2,AJE2
  850 FORMAT(//2(10X,3E10.2))
      GO TO (220,240,260,280),NR
  999 END


      SAMPLE DATA
54    97.2                          2 1
  -.2          1.0D+0       1.0D+0       1.0+0       -.1          4.50+1       6.00+3       3.55+3
```

```
215 FORMAT (1X,40X,35HH(TAU) FROM TSCHOLGL  DERIVATIVE =  ,I1)
    NR=1
    T1=0.151
    T2=0.349
    GO TO 800
220 CONTINUE
    T1=0
    T2=0
    DO 230 I=4,M3
    H1(I,J)=FGP(I,J)-TGP(I,J)/4.
230 H2(I,J)=C*(G2P(I)-SG2P(I,J))
    PRINT 235,J
235 FORMAT(1H1,30X,35HH(TAU)  FROM  SS   DERIVATIVE =     ,I1)
    NR=2
    GO TO 800
240 CONTINUE
    A=10.**(X(I)/R)
    A1=A*A/(A*A-1.)**2
    A2=A/(A-1.)**2
    DO 250 I=4,M3
    H1(I,J)=(GP(I+1)-GP(I-1)-A1*(GP(I+2)-GP(I-2)-2.*GP(I+1)+2.*GP(I-1)
   1))/2./X(I)
250 H2(I,J)=C*(G2P(I)-A2*(G2P(I+1)-2.*G2P(I)+G2P(I-1)))
    PRINT 255,J
255 FORMAT(1H1,30X,35HH(TAU)  FROM  NF   DERIVATIVE =     ,I1)
    NR=3
    GO TO 800
260 CONTINUE
    DO 270 L1=1,K0
    DO 270 L=4,N3
    I=L+N*(L1-1)
    DM=FGP(I+1,J)/FGP(I-1,J)
    DM=LOGF(ABSF(DM))/2./X(I)
    AF=C*SINF(DM/C)/DM
    H1(I,J)=AF*FGP(I,J)
    IF (DM-1.)  264,264,262
262 AF=C*SINF(DM/C)/(2.-DM)
    H1(I,J)=AF*(2.*GP(I)-FGP(I,J))
264 IF(DM-2.) 268,266,266
266 H(I,J)=0
268 DN=(G2P(I+1)-ABSF(FG2P(I,J)))/(G2P(I-1)-ABSF(FG2P(I-1,J)))
    DN= LOGF(ABSF(DN))/2./X(I)
    BF=C*SINF((1.+ABSF(DN))/C)/(1.-ABSF(DN))
270 H2(I,J)=BF*(G2P(I)-ABSF(FG2P(I,J)))
    PRINT 275,J
275 FORMAT(1H1,30X,35HH(TAU)  FROM  WF   DERIVATIVE=     ,I1)
    NR=4
    GO TO 800
280 GO TO 10
800 PRINT 810
810 FORMAT( 130H      TAU     H(TAU)      GP          G2P          TAU     H
   1(TAU)     GP          G2P          W(I)      GPP       G2P         JP
   I                //)
    ETA1=0
    ETA2=0
    AG1=0
    AG2=0
    DO 830 I1=1,K0
    DO 830 I2=4,N3
    K=I2+N*(I1-1)
```

APPENDIX B

Dynamic Testing with the Weissenberg Rheogoniometer

The use of the Weissenberg Rheogoniometer for dynamic testing has created a need for accurate low frequency phase measurements. The usual techniques rely on Lissajous patterns or compare signals on an ultraviolet recorder. These methods are both time consuming and of limited accuracy.

Meyer H. Birnboin of Mellon Institute has designed an Ultra Low Frequency Phase Meter[1] which measures the phase angle between two periodic signals and the amplitudes of perfect sine waves. It is capable of resolving angles to 10^{-4} radians and of operating at low frequencies, limited only by the stability of the input system. George Jernakoff of the General Electric Research and Development Center modified this phase meter for use with the Weissenberg Rheogoniometer. An improved version of this model, now in use in the polymer laboratories at the University of Massachusetts, was designed and built by Noel Mackisoc[2].

Phase Measurements

The meter records the time each signal exceeds a given trigger level. Referring to Figure 1a, the peak of signal A occurs at a time

$$T_A = t_{A_2} + \frac{t'_{A_2} - t_{A_2}}{2} = \frac{t_{A_2} + t'_{A_2}}{2} \qquad (1)$$

Likewise, the second signal peaks at $T_B = \frac{t_{B_2} + t'_{B_2}}{2}$. The time between the signal peaks is

$$\Delta t = T_B - T_A = \frac{1}{2}\left[(t_{B_2} - t_{A_2}) + (t'_{B_2} - t'_{A_2})\right] \qquad (2)$$

But $t_{B_2} - t_{A_2}$ is the time signal A is above trigger level V_{A_2}, while B is below V_{B_2}. Similarly, $t'_{B_2} - t'_{A_2}$ is the amount of time the level sensors see a B signal and not an A. The logic is set to record these times along with their half cycle counterparts. If T is the total time for one cycle, the phase angle is

$$\phi = \frac{A\bar{B} + B\bar{A}}{4T} \times 180° \qquad (3)$$

where $A\bar{B}$ indicates A and not B, and $B\bar{A}$ represents a B signal without A. (See Figure 2).

Amplitude Measurements

For a perfect sine wave, the time a signal is above the trigger levels is simply related to the amplitude. From Figure 1b,

$$V_{A_1} = A_o \sin \frac{2\pi}{T} t_{A_1} \qquad (4)$$

But

$$t_{A_1} = \frac{T}{4} - \frac{(t'_{A_1} - t_{A_1})}{2} \qquad (5)$$

or

$$V_{A_1} = A_o \sin \left[\frac{\pi}{2} - \frac{\pi}{T}(t'_{A_1} - t_{A_1})\right] = A_o \cos \frac{\pi}{T}(t'_{A_1} - t_{A_1}) \qquad (6)$$

Likewise for the other half cycle

$$V_{A_4} = A_o \cos \frac{\pi}{T}(t'_{A_4} - t_{A_4}) \qquad (7)$$

Then $$V_{A_1} - V_{A_4} = 2A_o \cos \frac{\pi}{T} \frac{(A_1 + A_4)}{2} \cos \frac{\pi}{T} \frac{(A_1 - A_4)}{2} \quad (8)$$

where $A_i = t'_{A_i} - t_{A_i}$ is the time the signal exceeds the trigger level V_{A_i}. Equation 8 is simplified when $A_1 = A_4$. This is achieved for symmetric signals when the electrical zero of the signal is equal to $(V_{A_1} - V_{A_4})/2$. If the signal is sinusoidal the amplitude is

$$A_o = V_{A_1} \sec \frac{\pi}{T} \frac{(A_1 + A_4)}{T} \quad (9)$$

Figure 3 demonstrates the measured time intervals ($A_+ = A_1$, $A_- = A_4$).

Phase Meter Operation

The time base of the phase meter is a 100 Khz oscillator equipped with decade countdown circuits. These allow slower clock rates for low frequency measurements. The clock output frequency is split in half, creating two sets of pulses, 180° out of phase. These provide the time bases for the top and bottom portions of the measured signals and allow proper counting in overlapping regions. Logic circuits controlled by the trigger levels present selected segments of the time bases to four counter inputs. These record the total counts during the measurement, T, the phase difference, Δt, and the counts proportional to the amplitudes of the signals, $A_1 + A_4$ and $B_1 + B_4$. Measurements can be averaged over several cycles to minimize errors due to non-coherent noise.

Phase Meter Modifications

Accurate amplitude measurements (equation 9) require that the times A_1 and A_4 be equal. The logic functions in the modified phase

meter, ΔA and ΔB, calculate $A_1 - A_4$ and $B_1 - B_4$ respectively. The condition for the amplitude measurements may then be satisfied by adjusting the DC bias of each transducer to make ΔA and ΔB negligible. Two variable gain DC amplifiers are incorporated in the input stage of the modified phase meter. These amplify the signals and thus, in effect, change the magnitudes of the trigger levels. The shape of the signal's waveform may be determined by comparing measurements conducted at different amplifications. This tests the assumption that the signals are sinusoidal. Small distortions in the input signals may be tolerated as long as the disturbances affect only a small portion of the wave. If this is the case, the trigger levels may be changed so the measurements are made in the undistorted region.

In the original phase meter, the trigger levels used to determine the phase angles, V_{A_2} and V_{A_3}, were a small fraction of the amplitude trigger levels V_{A_1} and V_{A_4}. This minimized the errors associated with each type of measurement. However much more significant errors will occur in the measured phase angle if the signal is distorted in the neighborhood of V_{A_2} or V_{A_3}. The modified phase meter was designed to allow either V_{A_2} and V_{A_3} or V_{A_1} and V_{A_4} to control the phase angle logic. This option, coupled with the variable gain input amplifiers, allow phase angle measurements to be made on any portion of the signal.

An analysis was made of the shape of the waveform produced by the model R-17 Weissenberg Rheogoniometer owned by the University of Massachusetts. A small perturbation, located at the maximum of

the input signal, was observed in the output response. This was associated with a slippage of approximately 1 micron in the oscillatory drive mechanism. This distortion, barely noticeable in the ultraviolet recordings of the response, could increase the measured phase angle by as much as 1°. The modified phase meter's capability of measuring phase angles over different portions of the signal eliminated this experimental problem. If the amplitude trigger levels, V_{A_1} and V_{A_4} are to be used for the phase measurements on signals with this type of perturbation, the operation of the meter requires Δt to satisfy the following requirements:

$$B - A < 2\,\Delta t < A + B \tag{10}$$

and

$$A < 2\Delta t$$

where $$A = A_1 + A_4 \quad \text{and} \quad B = B_1 + B_4 \tag{11}$$

Derivation Of The Dynamic Equations For The Cone And Plate Geometry

The oscillation input strains the sample at a frequency ω and amplitude θ'. The transmitted stress of amplitude θ'', measured by the torsion bar, leads the input stress by an angle ϕ.

$$\overline{\theta}' = \theta'_o\, e^{i\omega t} \tag{12}$$

$$\overline{\theta}'' = \theta''_o\, e^{i(\omega t + \phi)} \tag{13}$$

At any instant the deformation of the sample is the difference between the positions of the input and torsion bar platens. The strain, S, is uniform throughout the sample for the cone and plate geometry.

$$\bar{S} = \frac{r[\bar{\theta}' - \bar{\theta}'']}{r\,\alpha} \tag{14}$$

where α is the cone angle. Thus

$$\alpha\,\bar{S} = \theta'_o\, e^{i\omega t}\left[1 - \frac{\theta''_o}{\theta'_o}\, e^{i\phi}\right] \tag{15}$$

The magnitude of the strain is:

$$|\bar{S}| = \frac{\theta'_o}{\alpha}\sqrt{1 + \left(\frac{\theta''_o}{\theta'_o}\right)^2 - 2\,\frac{\theta''_o}{\theta'_o}\cos\phi} = \frac{\theta'_o}{\alpha}\, C_1 \tag{16}$$

where C_1 is Weissenberg's notation. The phase angle associated with the complex representation of the strain is

$$\phi_s = \sin^{-1}\left[\frac{\mathrm{Im}[\bar{S}]}{|\bar{S}|}\right] = -\sin^{-1}\left[\frac{\theta''_o}{\theta'_o}\,\frac{\sin\phi}{C_1}\right] \equiv C_2 \tag{17}$$

Therefore

$$\bar{S} = \frac{\theta'_o}{\alpha}\, C_1\, e^{i(\omega t + C_2)} \tag{18}$$

The torque transmitted by the sample is:

$$\bar{L} = \frac{2\pi R^3 \bar{P}_{12}}{3} \tag{19}$$

where $\bar{P}_{12}$ is the shear stress supported by the sample. This is balanced by the torsion bars spring constant, K, moment of inertia, I, and viscous loss term, U;

$$\bar{L} = K\bar{\theta}'' + U\,\dot{\bar{\theta}}'' + I\,\ddot{\bar{\theta}}'' \tag{20}$$

Then from equations 13, 19 and 20,

$$\bar{P}_{12} = \frac{3}{2\pi R^3}\,[K - \omega^2 I)\,\left[1 + \frac{i\,\omega\,U}{(K-\omega^2 I)}\right]\,\theta''_o\, e^{i(\omega t + \phi)} \tag{21}$$

or

$$\overline{P}_{12} = \frac{3}{2\pi R^3} [K - \omega^2 I] C_3 \theta''_o e^{i(\omega t + \phi - C_4)} \tag{22}$$

where

$$C_4 = - \tan^{-1} [\frac{\omega U}{K-\omega^2 I}] \tag{23}$$

The ratio of the stress to the strain is then

$$\frac{\overline{P}_{12}}{S} = \frac{3\alpha}{2\pi R^3} [K - \omega^2 I] \frac{C_3}{C_1} \frac{\theta''_o}{\theta'_o} e^{i(\phi - C_4 - C_2)} \tag{24}$$

The storage modulus G' and the loss modulus G" (=$\omega\eta'$) are given by the real and imaginary parts of equation 24.

$$\eta' = \frac{1}{\omega} \frac{\theta''_o}{\theta'_o} \frac{3\alpha}{2\pi R^3} (K - I\omega^2) \frac{C_3}{C_1} \sin (\phi - C_4 - C_2) \tag{25}$$

$$G' = \frac{\theta''_o}{\theta'_o} \frac{3\alpha}{2\pi R^3} (K - I\omega^2) \frac{C_3}{C_1} \cos (\phi - C_4 - C_2) \tag{26}$$

The "correction" terms C_1 and C_2 may be neglected if the amplitude ratio is small, but this unnecessarily limits the useful range of the equipment. The magnitude of the strain in the sample is $\theta'_o C_1$. This will be significantly different from the input amplitude θ'_o if the torsion head, θ''_o moves much at all. Likewise the phase between the sample's stress and strain, $[\phi - C_2]$ can be much bigger than ϕ. [C_2's greater than 80 degrees have been found.] This is shown in Figure 4, where C_2 is plotted as a function of the measured phase angle for different amplitude ratios ($A \equiv \frac{\theta''_o}{\theta'_o}$).

In normal use the Rheogoniometer is operated well below the resonant frequency of the torsion bar where $C_3 \approx 1$ and $C_4 \approx 0$.

In this region, the dynamic equations can be written in terms of the measured quantities A and ϕ.

$$\eta' = \frac{\zeta f(\omega)}{\omega C_1^2} A \sin(\phi) \tag{27}$$

$$G' = \frac{\zeta f(\omega)}{C_1^2} A [\cos(\phi) - A] \tag{28}$$

where $\zeta = \frac{3\alpha}{2\pi R^3} K$ and $f(\omega) = 1 - (\frac{\omega}{\omega_n})^2$.

Graphs of these functions (Figures 5 and 6) illustrate the accuracy problems which may be encountered for large amplitude ratios and/or small measured phase angles. Care should be taken in the selection of a torsion bar to avoid unnecessary excursions into these regions.

Calibration

The input amplifiers may be calibrated in the following manner:

1 - Feed mechanical sine wave (from input transducer) to both A and B inputs.

2 - Set the A and B gain controls to the same value. Record the number of A and B counts at the gain.

3 - Change the gain and repeat step 2.

The gain of the input amplifiers is proportional to the log of the numbers on the controls. It is therefore, advisable to vary the gains in logarithmic steps. A useful interval if 0.05. The values of the gain, A counts and B counts in order of increasing gain, are fed into the computer program as CAL.

The phase meter can be used to calibrate the Sangamo Twin Filter network. As explained by Bogie and Harris[3] each channel

of the filter system has its own attenuation and phase shift characteristics which, in general, are not equal. To determine these differences a measurement is made, the filter inputs and outputs reversed, and the measurement repeated. As seen by filter B, filter A adds ΔA to the true phase ϕ.

$$\phi_A = \phi + \Delta A \tag{29}$$

Likewise filter A sees B's measurement as

$$\phi_B = \phi + \Delta B \tag{30}$$

But, $\Delta A = -\Delta B$ since this is the same system. Thus

$$\phi_A - \phi_B = 2\Delta A \tag{31}$$

or the true phase

$$\phi = \frac{\phi_A + \phi_B}{2} = \phi_A + \Delta\phi \tag{32}$$

where $\Delta\phi = [\phi_B - \phi_A]/2.$ (33)

This procedure also yields the ratio of the attenuation constants. The phase meter records the amplitude of the signals as

$$A' = A_o \sec \frac{\pi}{2} \left[\frac{A}{T}\right] \tag{34}$$

and

$$B' = B_o \sec \frac{\pi}{2} \left[\frac{B}{T}\right] \tag{35}$$

Comparing the stable oscillation input signal as it passes through each filter makes $A' = B'$.

Thus

$$\frac{A_o}{B_o} = \frac{\cos \frac{\pi}{2} \left(\frac{A}{T}\right)}{\cos \frac{\pi}{2} \left(\frac{B}{T}\right)} \qquad (36)$$

The frequency dependent phase angle corrections, $\Delta\phi$, (equation 33) must be calculated for each gear box (GB) setting. These are inserted in the computer program as the quantities PI. The attenuation constant, equation 36, is the constant, TWIN. Large values of PI are found near the filter's cut off frequency. Best results are obtained if the 20hz filter is used for all GB equal to or greater than 0.7, the 50hz filter for GB = 0.3 to 0.6, and the 150hz filter for GB = 0.0, 0.1, and 0.2. The data corresponding to these filters, PI(I) with I = 10GB, is inserted into the program in order of increasing GB. Corrections for the 20hz filter for GB = 0.0 to 0.6 are stored as PI(50) to PI(56). Corrections for the 50hz filter for GB = 0.0 to 0.2 are stored in PI(57) to PI(59). Values of the average total counts AVET, correspond to the values of GB.

Each data card contains the variable FILT. FILT is left blank, except when a filter is used outside of its normal range. In these instances the frequency of the filter is used for FILT.

The entire system can be calibrated after the input amplifier and the twin filter corrections have been made. The following procedure eliminates any amplitude or phase errors caused by the transducers or the mechanical drive.

1-Clamp the top and bottom platens together. This is best accomplished by solidifing a sample, such as pitch, in the test region.

2-Detach the torsion bar.

3-Make a series of amplitude and phase measurements at low frequencies (GB ≈ 2.6).

The recorded amplitude ratio is the constant, SA, which is the relationship between the deflections of the input and output transducers. The measured phase angle, SB, is added to the phase angle corrections, PI, in the program.

Calculations

The rheological properties of each sample were calculated with the computer program given on pages 163-168. Equations 25 and 26 were used to obtain η' and G'. The steady state shear properties were obtained from the following equations (Program statements 300-310):

$$P_{12} = \frac{12\ L}{\pi\ d^3} \tag{37}$$

$$P_{11} - P_{22} = \frac{8\ F}{\pi\ d^2} \tag{38}$$

$$\dot{\gamma} = \frac{2\pi\ g}{\alpha} \tag{39}$$

where L is the measured torque, F is the total thrust, and g is the platens rotational speed in revolutions per second.

Computer Program For The Calculation Of The Steady State Shear And The VE Properties Of Polymer Melts With The Weissenberg Rheogoniometer

1 - NAME: UM RHEO

2 - INPUT:

CALIBRATION DATA

AVET:	Average number of total counts at each gear box setting
PI:	Phase angle corrections due to twin filters, (equation 33)
CAL:	Calibration of amplifiers: Gain, A counts, B counts

TITLE CARD

TITLE:	Identification of sample

CONSTANT CARD

L:	1-New output page 2-Same page - No titles 3-Exit from program
S:	Constants * - *
ALPHA:	Cone angle in degrees
DIAM:	Diameter of sample in cm
TWIN:	Ratio of twin filter attenuation constants (equation 36)
SA:	Ratio of output to input signal
SB:	Equipment phase angle error
FN:	Natural frequency of torsion bar
CKT:	Force constant of torsion bar

CKN:	Force constant of normal force spring
XAXIS:	Plot scale factor for X Axis
DEC:	Logarithmic decrement of torsion bar oscillations
SC:	Constants B-
PLOT CARD	Log of minimum value of plotted functions;
YS1(1), YS2(1)	η
YS1(2), YS2(2)	PN, or G'
YS1(3), YS2(3)	Shear stress or G"
YS1(4), YS2(4)	G or 1/J'
DATA CARD	
NEXT:	0-Normal data
	1-Self correction
	2-Calculated data
	3-Self calibration
	4-Plot
	5-Initialize plotter
GB:	Gear box setting
DT1:	Δt counts for trigger levels V_{A_2} and V_{A_3} or shear stress deflection ΔT
DT2:	Δt counts for trigger levels V_{A_1} and V_{A_4} or normal stress deflection ΔN
TOT:	Total counts
AA:	A counts
BB:	B counts
RGEA:	Range of A transducer

RGEB: Range of B transducer

AG: Gain of A amplifier

BG: Gain of B amplifier

FILT: Filter used if different from -

20cps for GB > 0.6

50cps for GB = 0.3, 0.4, 0.5

150cps for GB = 0.0, 0.1, 0.2

NP: Instruction for plot routine

0-Connect data point

1-Don't connect data point

3 - OUTPUT

ETASTAR: Complex dynamic viscosity or rotational viscosity

ETAP: Dynamic viscosity

GP: Storage Modulus

G2P: Loss Modulus

SHEAR RATE: Frequency or shear rate

JP: Storage compliance or $(P_{11} - P_{22})/2\ P_{12}$

1/JP: Reciprocal of JP

AMP: Amplitude ratio of output to input deflections

PHI1: Phase angle from DT1

PHI2: Phase angle from DT2

THETA: Corrected phase angle

FILT: Filter used

```
      COMPUTER PROGRAM FOR THE CALCULATION OF THE STEADY STATE SHEAR
      AND THE DYNAMIC VISCOELASTIC PROPERTIES OF POLYMER MELTS
      WITH THE WEISSENBERG RHEOGONIOMETER

      PROGRAM  UM RHEO
      DIMENSION AVET(60),PI(60),S(3),TITLE(10),ANG(2),CAL(3,24),V(2),
     1SC(3),YS1(2),YS2(2),YS3(2),YS4(2)
      READ 10, AVET,PI
   10 FORMAT (10F8.0)
      READ 15, CAL
   15 FORMAT(9F8.0)
      INDEX=0
      NEXT=8
      X=0
      L=5
   20 CALL XMPLOT(NEXT-3.,7.,YS2(2), .05,.05,.05,L,TITLE)
      IO=0
      READ 25, TITLE
   25 FORMAT(10A8)
   30 READ 35,L,S,ALPHA,DIAM,TWIN,SA,SB,FN,CKT,CKN,YAXIS,DEC,SC
   35 FORMAT(I1,3F1.0,6F10.0,4F10.0,I1,3X,3A1)
      IF(SA) 36,36,37
   36 SA=4.697
   37 ALPHA=ALPHA*0.01745
      CONST=12.*CKT/3.1416/DIAM**4*1.E08
      U=CKT/6.2832/FN/3.1416*DEC
      READ 38, YS1(1),YS2(1),YS3(1),YS4(1),YS1(2),YS2(2),YS3(2),YS4(2)
   38 FORMAT (8F10.0)
   40 GO TO (50,60,999),L
   50 PRINT 55
   55 FORMAT(1H1,32X,43HTHE WEISSENBERG RHEOGONIOMETER TEST RESULTS///,
     1 61H  ETASTAR      ETAP          GP          G2P      SHEAR RATE      JP,
     18X,45H 1/JP      AMP     PHI 1    PHI 2   DELTA  FILTER     )
   60 PRINT 65,TITLE
   65 FORMAT(/,33X,10A8,//)
  100 READ 110, NEXT,GB,DT1,DT2,TST,AA,BB,RCLA,RGLA,AC,BC,FILT,NP
  110 FORMAT(I1,F5.0,5F5.0,F4.0,3X,I1)
      X=DT1
      MODE=1
      MOD=1
  114 IF(DT1-DT2) 115,117,117
  115 X=DT2
      MODE=2
  117 IF(2*DT2-AA) 118,118,120
  118 MOD=2
      MODE=1
  120 IF(NEXT-3) 140,130,121
  121 ALPHA=ALPHA/0.01745
      PRINT 122, ALPHA,DIAM,TWIN,SA,SB,FN,CKT,CKN,DEC
  122 FORMAT(1H0,6F8.3,2F10.2,F8.3)
      GO TO 20
  130 DTR=X
      BBR=BB
      INDEX=1
      GO TO 100
  140 IF(BB) 999,300,150
  150 I=10.*GB+1.1
      RATIO=1.+TWIN/100.
      IF (FILT-20.) 170,165,160
```

```
160 I=I+7
165 I=I+50
170 COR=PI(I)+50
    IF(TOT) 999,171,176
171 TOT=AVET(I)*100.
172 TOT=TOT/10.
    IF(BB/TOT-.1) 172,172,176
176 IF(INDEX) 999,180,177
177 COR=(DTR-X)*TOT*10.
    RATIO = COSF((BOR/TOT)*1.5708)/COSF(BB/TOT*1.5708)
    INDEX=0
180 IF(NEXT-1) 200,190,185
185 PHI=X+COR
    VOLT=AA/BB*TWIN
    GO TO 210
190 AA=AA+2.*(DT2-DT1)
200 ANG(1)=DT1/TOT*100.+COR
    ANG(2)=DT2/TOT*100.+COR
    PHI=ANG(MODE)
201 IF(AG-CAL(2,1)) 202,206,202
202 CAL(2,1)=AG
    K=2
    J=1
204 J=J+1
    IF(CAL(K,1)-CAL(1,J)) 205,205,204
205 Y1=LOGF(COSF(CAL(K,J-1)*1.5708/CAL(1,1)))
    Y2=LOGF(COSF(CAL(K,J)*1.5708/CAL(1,1)))
    X1=LOGF(CAL(1,J-1))
    X2=LOGF(CAL(1,J))
    X3=LOGF(CAL(K,1))
    V(K-1)=EXPF((Y1-Y2)/(X1-X2)*(X3-X1)+Y1)
206 IF(BG-CAL(3,1)) 207,208,207
207 CAL(3,1)=BG
    K=3
    J=1
    GO TO 204
208 VOLT=COSF(BB/TOT*1.5708)/COSF(AA/TOT*1.5708)*V(1)/V(2)
210 AMP=VOLT*RGEA/RGEB*RATIO/SA
    FA=AA/TOT
    FB=BB/TOT
    FC=COSF(FA*1.5708)
    FD=COSF(FB*1.5708)
    TP=V(2)*RGEB/FD*0.802
    T2P=V(1)*RGEA/FC*0.802
    FE=FD*COSF(PHI*0.01745)+SQRTF(1.-FD*FD)*SINF(PHI*0.01745)
    MO=1
    IF(FC-FE) 212,211,211
211 MO=3
212 F=30.*10.**(-GB)
    FREQ=ABSF(1.-(F/FN)**2)
    SHEAR=6.2832*F
    C1=SQRTF(1.0+AMP*AMP-2.0*AMP*COSF(PHI*0.01745))
    C2=-ASINF(AMP*SINF(PHI*0.01745)/C1)*57.2958
    U1=SHEAR*U/CKT/FREQ
    C3=SQRTF(1+U1**2)
    C4=-ATANF(U1)
    THETA=PHI-C2+C4
    PHASE=THETA*0.01745
    IF(THETA-90.) 220,220,218
218 PHASE=1.57079
```

```
220 GSTAR=AMP*CONST*FREQ*C3/C1*ALPHA
    IF(GSTAR) 222,225,225
222 PRINT 223
223 FORMAT(14HG_STAR NEGATIVE)
    GSTAR=-GSTAR
225 GP=GSTAR*COSF(PHASE)
    G2P=GSTAR*SINF(PHASE)
    ETA=G2P/SHEAR
    ETAS=GSTAR/SHEAR
    CP=GP/GSTAR**2
    GM=1/CP
    K=2
    PN=GP
    PRINT 230,ETAS,ETA,GP,G2P,SHEAR,NEXT,CP,GM ,AMP,ANG(1),S(MODE),
   1ANG(2),S(MODE+1), S(MOD),S( ),TMETA,FILT,T2P,TP,FC,FD
230 FORMAT(4E11.3,F8.3,1X,I1,2E11.3,F*.4,F6.2,A1,F6.2,3A1,F6.2,F4.0,
   12F7.2,2F6.3)
    10=1+10
    ID=10
    GO TO 400
300 SHEAR=2.*3.1416/0.166/10.**GB/ALPHA
    G2P=CONST*DT1/50000.
    ETA=G2P/SHEAR
    PN=8.*CKN*DT2/3.1416/DIAM**2+0.000001
    GM=2.*(G2P)**2/PN
    CP=1/GM
    SR=PN/2./G2P
    K=1
    PRINT 310,ETA,PN,G2P,SHEAR,CP,GM,SR
310 FORMAT (E11.3,11X,2E11.3,F8.3,2X,2E11.3,F6.4)
400 X=2.*LOGF(SHEAR)/2.3026-2.*XAXIS
    Y1=2.*LOGF(ETA)/2.3026-2.*YS1(K)
    Y2=2.*LOGF(PN)/2.3026-2.*YS2(K)
    Y3=2.*LOGF(G2P)/2.3026-2.*YS3(K)
    Y4=2.*LOGF(GM)/2.3026-2.*YS4(K)
    CALL WMPLOT(1,X,Y1,Y2,Y3,Y4,K+2*NP,TITLE)
    GO TO 100
999 CALL WMPLOT(6,0.0,0.0,0.0,0.0,0.0,0.0,0.0,OT1,TITLE)
    STOP
    END
    SUBROUTINE WMPLOT(NEXT,X1,Y1,Y2,Y3,Y4,L,TITLE)
    RETURN
    END
```

```
    SAMPLE DATA
    0.5394/200    T= 214 C    2/9/71    25%
1* * 3.93 2.5  1.0 5.32 0.40 15.75 207.5      1330.
1.5       1.5       1.5       1.5       1.5       1.5       1.5       1.5
  1.6          29800.          32400.  34810.  200.  200.  800.  500.
  2.0 450.     4.
7     15.

3
```

Plot Routine To Use With UMRHEO

1 - NAME: UMPLOT

2 - INPUT

NEXT: 1-Store and order data

2-Store data-unordered

3-Plot data connecting points

4-Plot symbols-no connecting lines

5-Initialize program (L < 5) and plotter (L > 4)

X1: X data coordinate in inches

Y data coordinate in inches for symbol:

	L=1,3	2,4
Y1:		
Y2:		
Y3:		
Y4:		

TITLE: Sample indentification

```
      COMPUTER PLOT PROGRAM FOR USE WITH  GM RHEO

      SUBROUTINE WMPLOT(NEXT,X1,Y1,Y2,Y3,Y4,L,TITLE)
      DIMENSION TITLE(10)
      DIMENSION X(31,4),Y(120,4),LL(5),XM(27),YM(27),INT(4,4),IBUF(2500)
      N=ID-LL(L)
      GO TO (100,115,130,125,201,220),NEXT
  100 DO 112 I=N,ID
      IF(X1-X(I+1,L))111,114,114
  111 X(I,L)=X(I+1,L)
      DO 112 J=1,4
      K=I+(J-1)*ID
  112 Y(K,L)=Y(K+1,L)
      I=ID
  114 N=I
  115 X(N,L)=X1
      Y(N,L)=Y1
      Y(N+30,L)=Y2
      Y(N+60,L)=Y3
      Y(N+90,L)=Y4
      LL(L)=LL(L)+1
      RETURN
  125 NO=-1
  130 INT(1,1)=1
      INT(2,1)=0
      INT(3,1)=4
      INT(4,1)=9
      INT(1,2)=2
      INT(2,2)=5
      INT(3,2)=3
      INT(4,2)=10
      INT(1,3)=1
      INT(2,3)=0
      INT(3,3)=4
      INT(4,3)=9
      INT(1,4)=2
      INT(2,4)=5
      INT(3,4)=3
      INT(4,4)=10
      CALL PLOT7525(X1,0.,-3)
      ROT=90.+ROT
      IF(X1-12.) 132,131,131
  131 CALL AXIS(-4.,0.,15HLOG(SHEAR RATE),-15,9.,0.,-2.0,0.5)
      CALL AXIS(-4.,0.,11HLOG(STRESS),11,10.,90.,Y1,0.5)
      CALL SYMBOL(-3.9,10.,0.14,TITLE,0.0,80)
      ROT=0.0
  132 DO 200 K=1,4
      IF(LL(K)) 200,200,133
  133 IF(K-2) 136,136,134
  134 NO=-1
  136 DO 200 I=1,4
  144 N=ID+1-LL(K)
      INK=-1
      DO 200 J=N,ID
      MM=J+ID*(I-1)
      IF(10.-Y(MM,K)) 200,150,146
  146 IF(Y(MM,K)) 200,150,150
  156 CALL SYMBOL(X(J,K),Y(MM,K),0.07,INT(I,K),ROT,INK)
  160 INK=NO
```

```
200 CONTINUE
201 DO 210 K=1,4
    LL(K)=0
    DO 210 J=1,10
210 X(J,K)=0
    NO=-2
    IF(L-4) 215,215,217
215 RETURN
217 CALL PLOTS(IBUF,1000,6)
    CALL PLOT7525(0.,-15.,-3)
    CALL PLOT7525(0.,0.5,-3)
    ROT=-90.
    ID=30
    RETURN
220 CALL PLOT7525(12.,0.0,999)
    CALL EXIT
    END
```

REFERENCES

B-1. M. H. Birnboin, U.S. Patent #3,286,176 (November 15, 1966).

B-2. Noel Mackisoc, Tronotec, Boonton Ave., Kinnelon, N.J.

B-3. K. Bogie and J. Harris, Rheologica Acta, Band 5, Heft 3 (1966).

B-4. K. Weissenberg, The Testing of Materials by Means of the Rheogoniometer, Farol Research Engineers, Ltd., 1963.

FIGURE CAPTIONS

B-1. a) Trigger levels and times for phase angle measurement

b) Trigger levels and times for amplitude measurement

B-2. Phase angle measurement

B-3. Amplitude measurement

B-4. The dependence of the correction factor, C_2, on the measured phase angle, ϕ, as a function of the measured amplitude ratio, A.

B-5. The dynamic viscosity, η', as a function of the measured ϕ and A.

B-6. The storage modulus G', as a function of the measured ϕ and A.

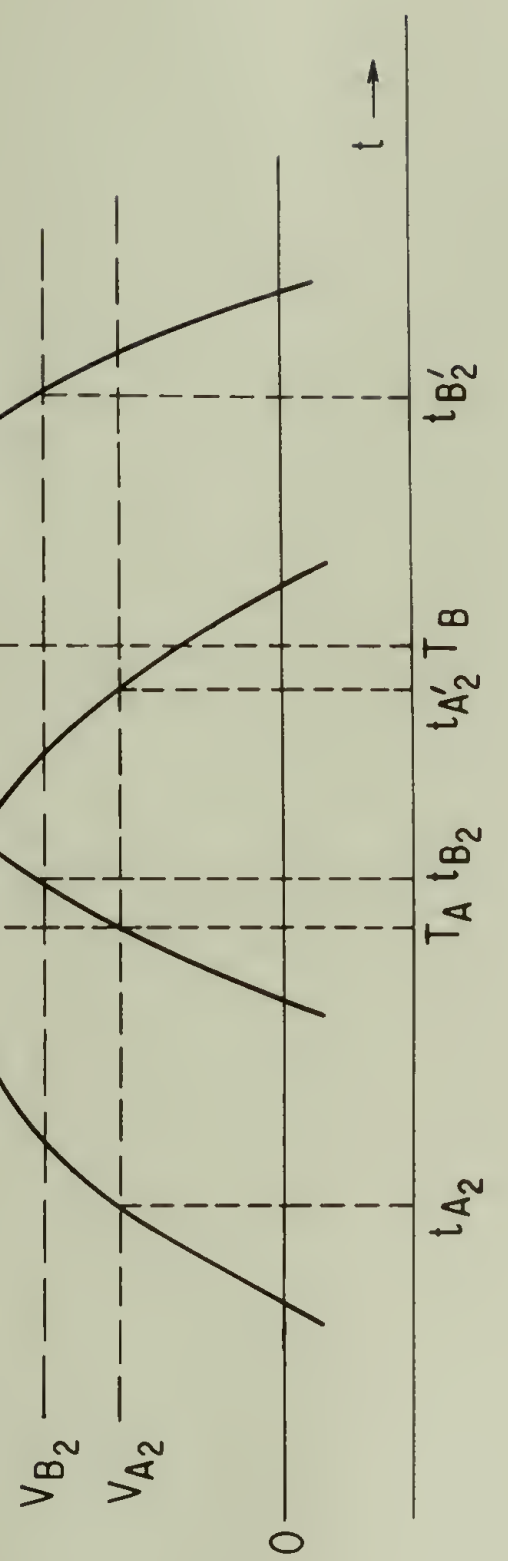

Figure B/a

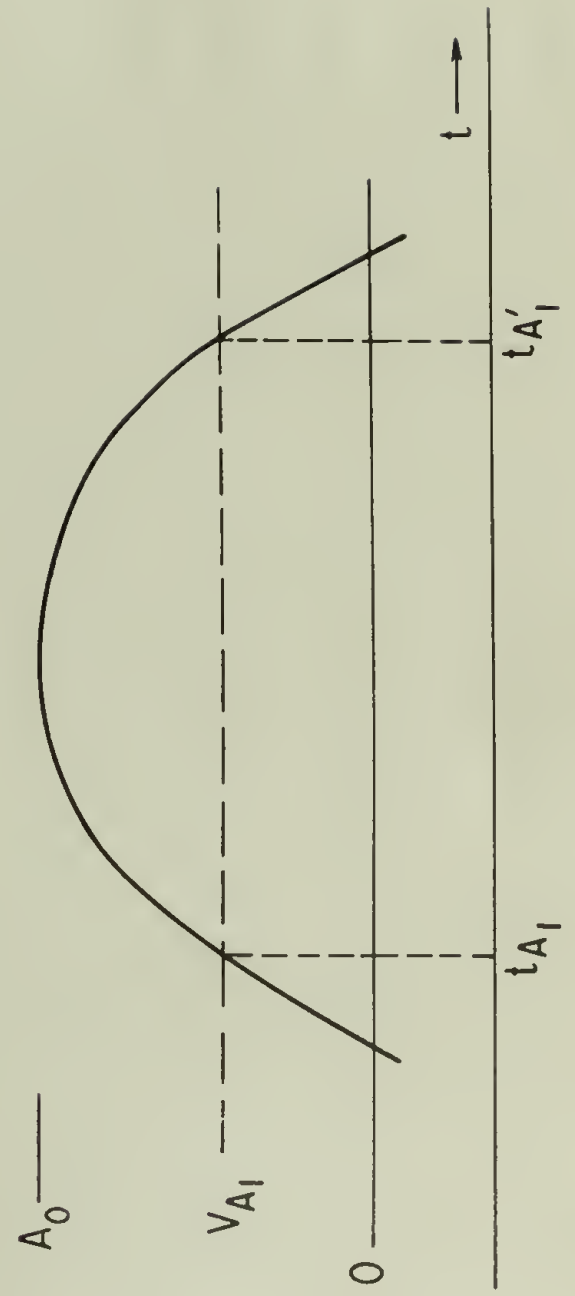

Figure b/b

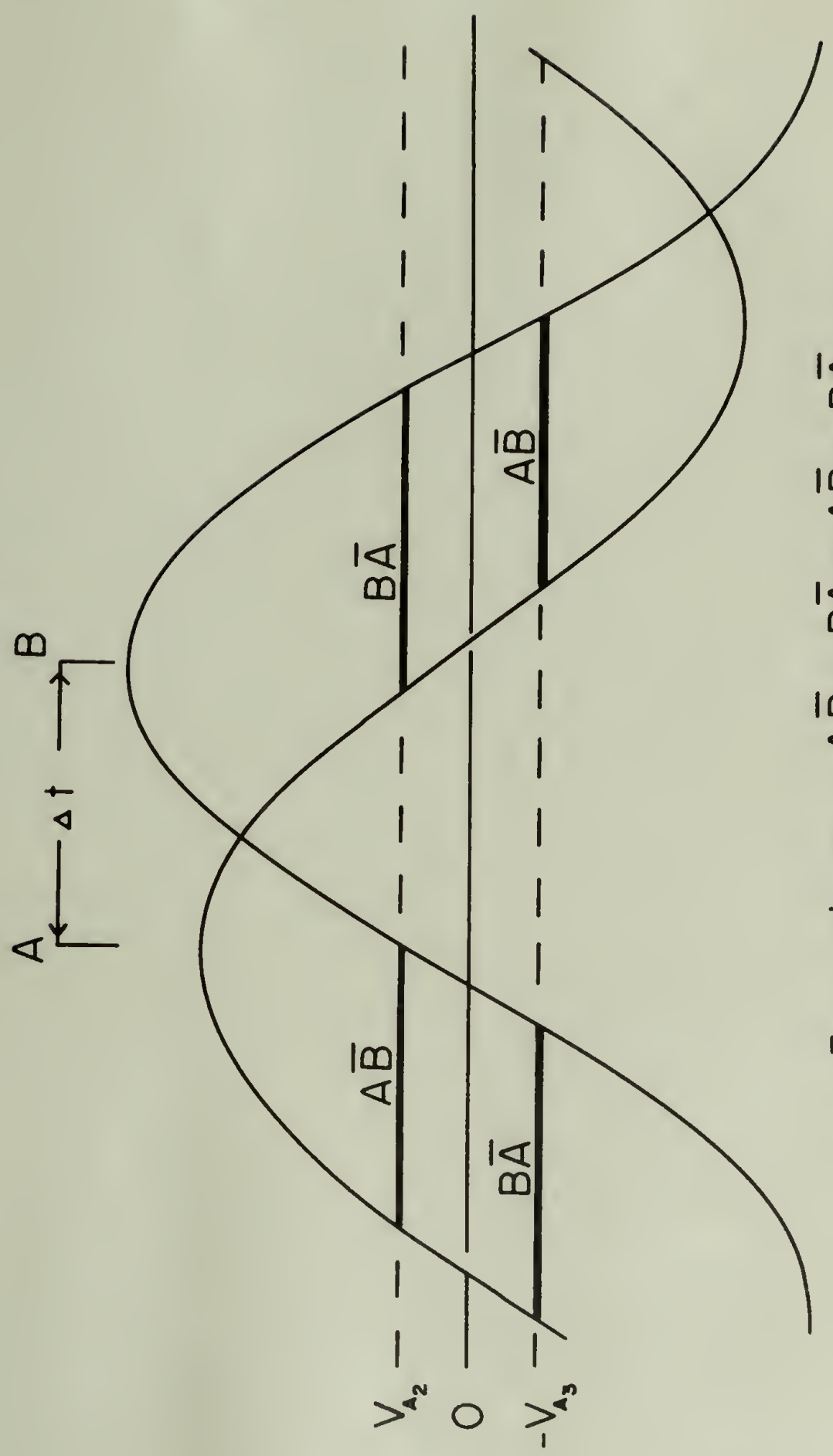
B
Δt
A
V_{A_2}
0
$-V_{A_3}$
$B\bar{A}$
$A\bar{B}$
$A\bar{B}$
$B\bar{A}$
$\Phi = \frac{\Delta t}{T}\pi = \frac{A\bar{B} + B\bar{A} + A\bar{B} + B\bar{A}}{4T}\pi$

Figure B-2

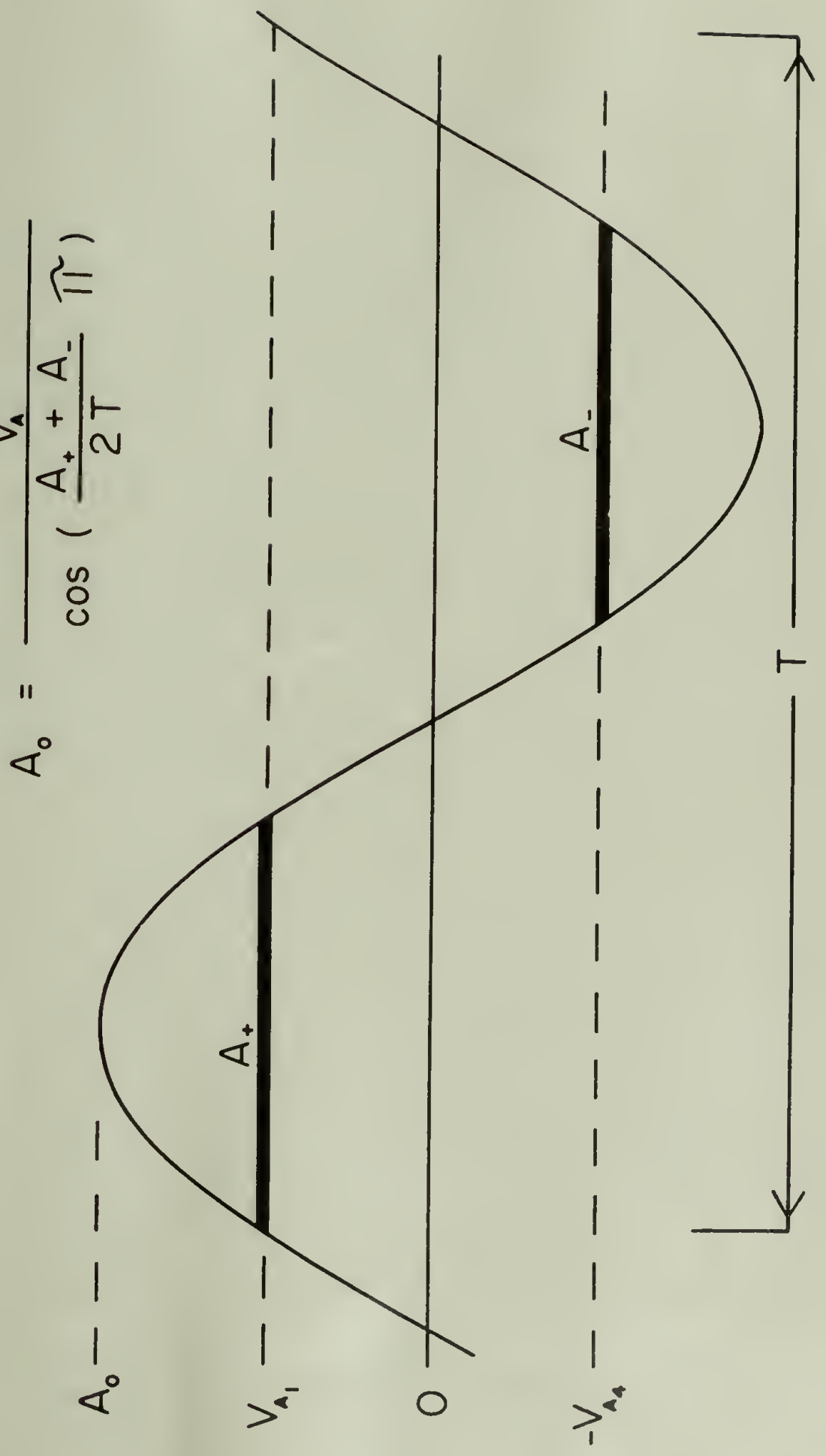

Figure B-3

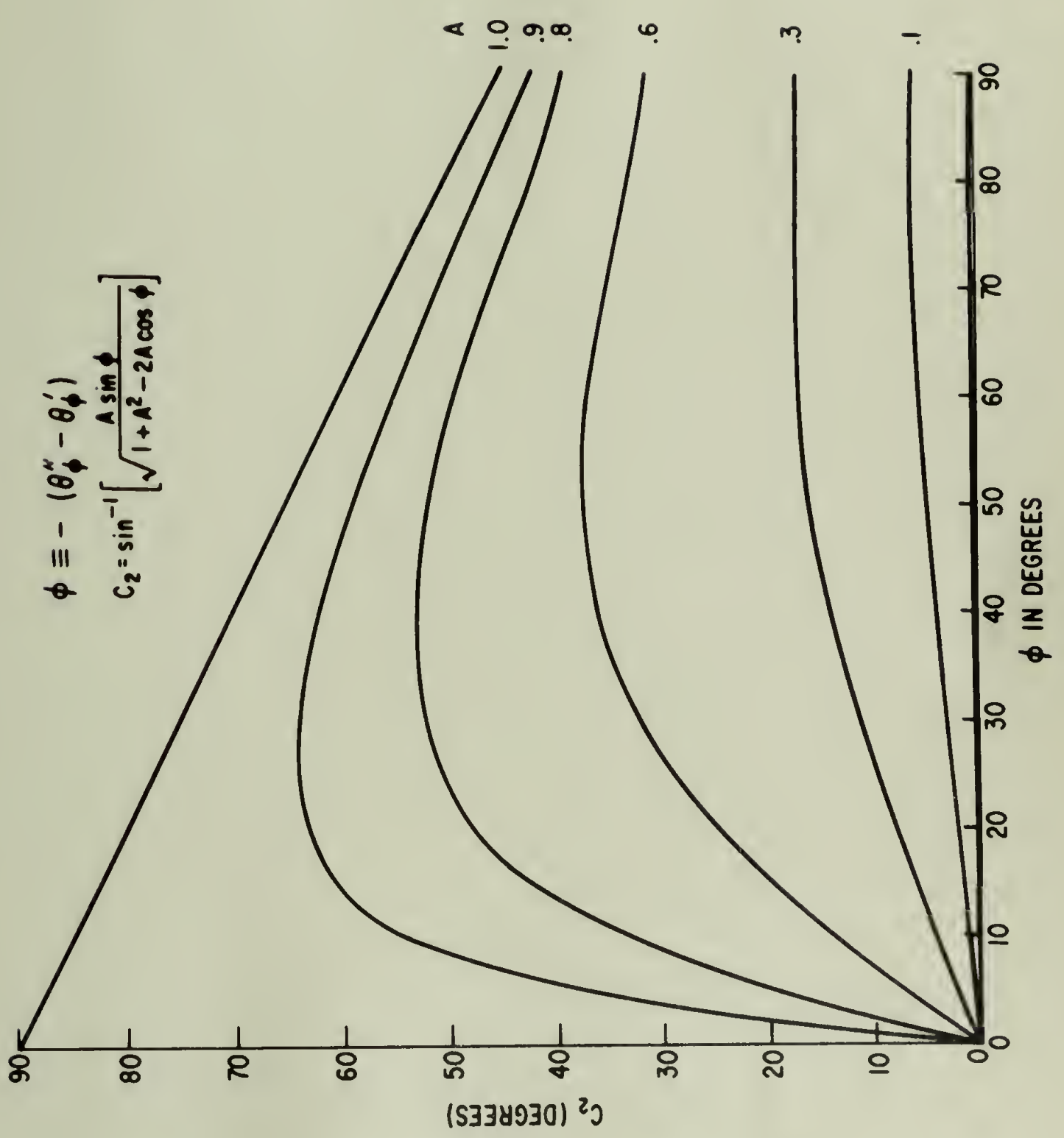
$\phi \equiv -(\theta''_\phi - \theta'_\phi)$
$C_2 = \sin^{-1}\left[\frac{A \sin\phi}{\sqrt{1+A^2-2A\cos\phi}}\right]$
A
1.0
.9
.8
.6
.3
.1
0
10
20
30
40
50
60
70
80
90
ϕ IN DEGREES
C_2 (DEGREES)

Figure B-4

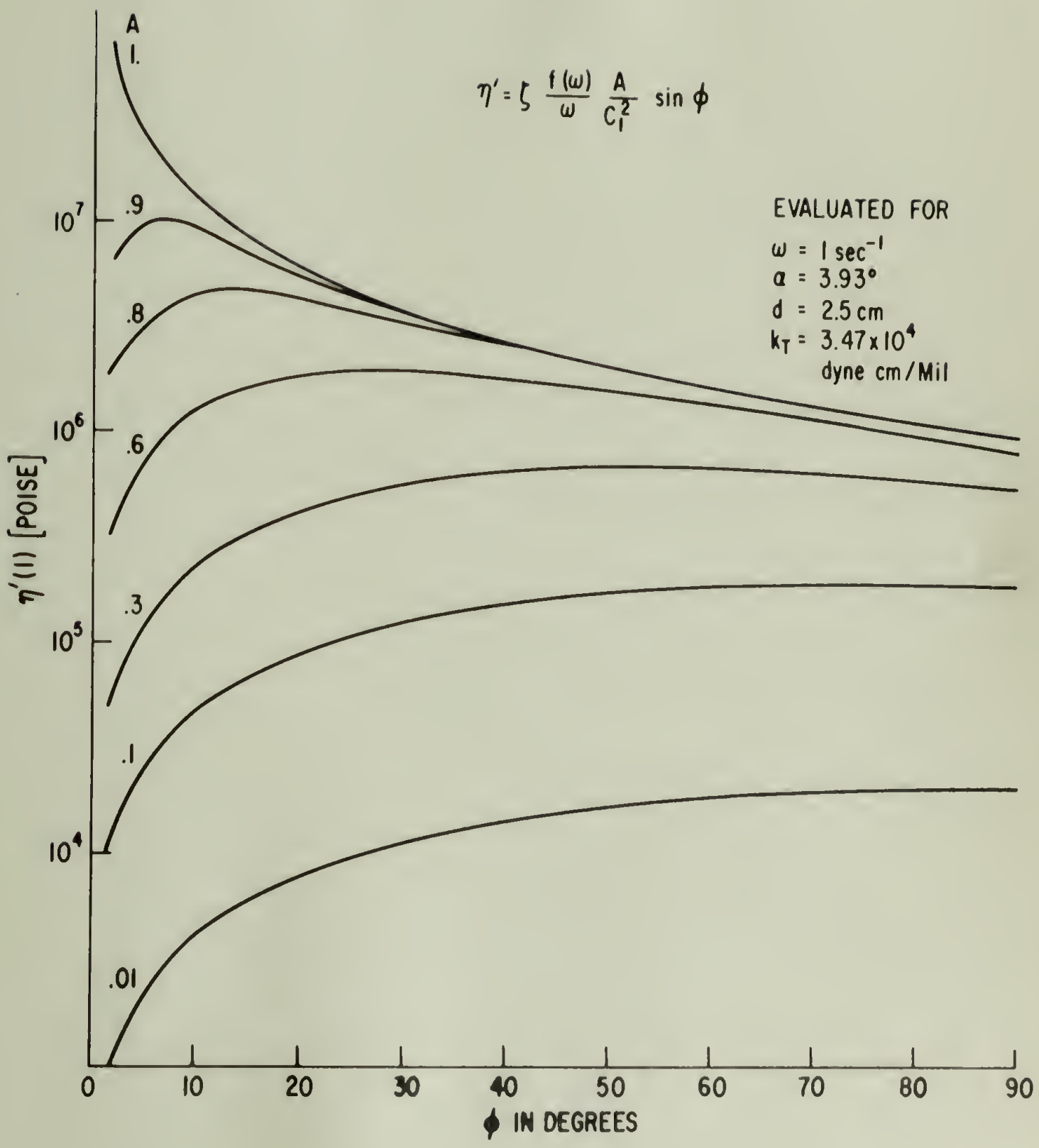
$\eta' = \zeta \frac{f(\omega)}{\omega} \frac{A}{C_1^2} \sin \phi$
EVALUATED FOR
ω = 1 sec^{-1}
α = 3.93°
d = 2.5 cm
k_T = 3.47 x 10^4 dyne cm/Mil
A
1.
.9
.8
.6
.3
.1
.01
10^7
10^6
10^5
10^4
$\eta'(1)$ [POISE]
0
10
20
30
40
50
60
70
80
90
ϕ IN DEGREES

Figure B-5

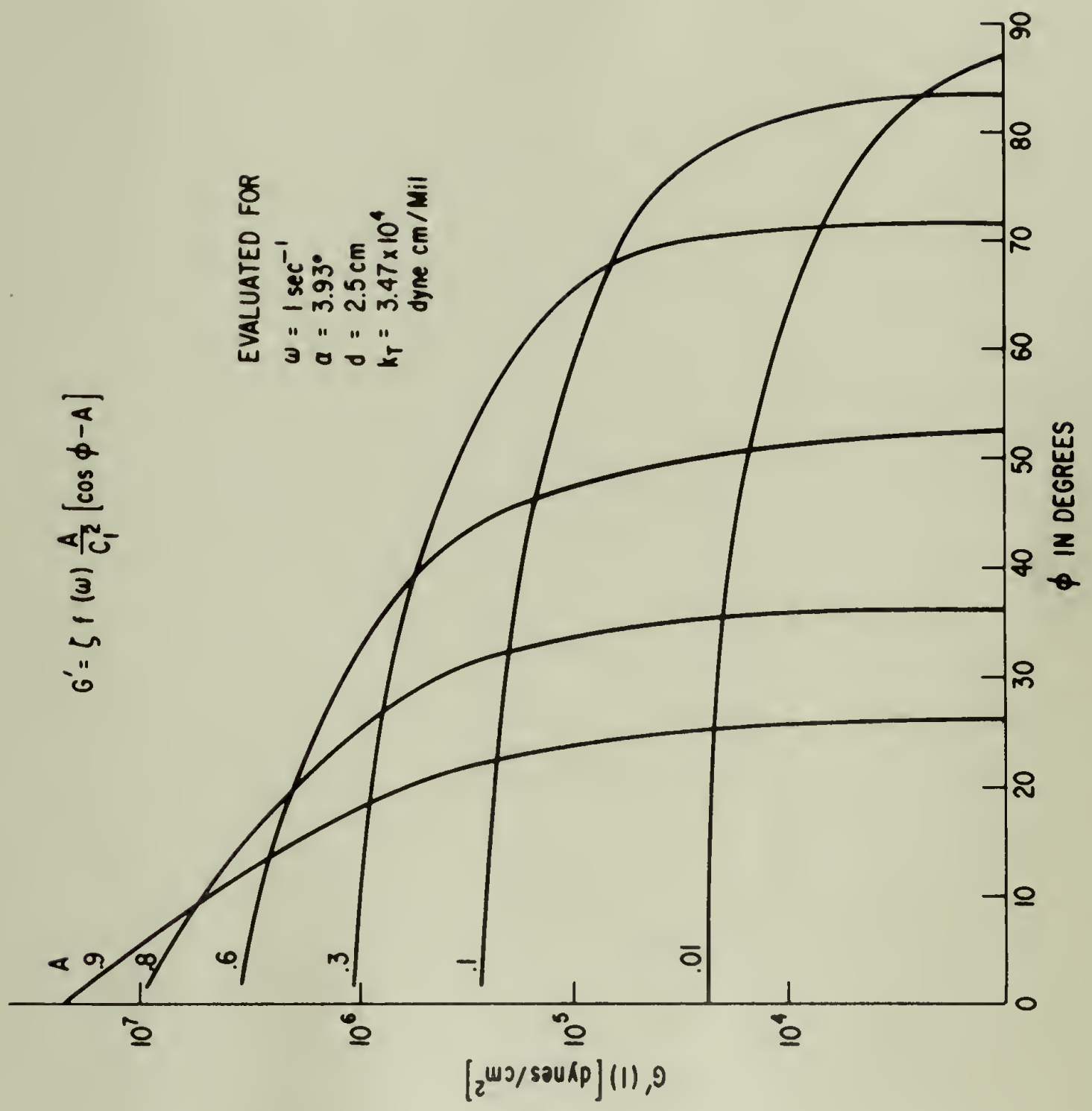
EVALUATED FOR
ω = 1 sec⁻¹
α = 3.93°
d = 2.5 cm
k_T = 3.47 x 10⁴ dyne cm/Mil
G' = ζ f (ω) A/C₁² [cos φ − A]
A
.9
.8
.6
.3
.1
.01
10⁷
10⁶
10⁵
10⁴
G' (1) [dynes/cm²]
0
10
20
30
40
50
60
70
80
90
φ IN DEGREES

Figure B-6

APPENDIX C

THEORY OF ENTANGLEMENTS

This appendix presents an unsuccessful theoretical attempt to explain the unusual elastic behavior observed in the viscoelastic response of high molecular weight polymer melts.

Several theories have been advanced which predict the viscoelastic response of polymeric systems by calculating the dynamics of the individual molecules as a function of the applied deformation rate. The Rouse-Zimm (1,2) model conceptually divides the molecule into Gaussian segments, each with a root mean square length, b. Displacements from this length are opposed by the statistical nature of the chain. The segments are the mechanical equivalent of springs with a force constant $\frac{3kT}{\langle b^2 \rangle}$. In a dilute solution the viscous drag forces exerted by the solvent on each segment, F_v, are balanced by the elastic forces, F_E and the force caused by the Brownian motion of the segments, F_B

$$F_v = F_B + F_E \tag{1}$$

If the viscous drag force, F_v, is assumed to be proportional to the velocity of the segment, $\dot{x}_j$, relative to that of the solvent, v_j, then the x component of F_v is

$$F_v = \frac{1}{B} (\dot{x}_j - v_j) \tag{2}$$

where B is the mobility of the segment. The elastic restoring force is equal to the force on j due to the displacement of points j + 1 and j - 1.

$$F_{Ej} = \frac{-3kT}{\langle b^2 \rangle} (-x_{j-1} + 2x_j - x_{j+1}) \tag{3}$$

The force due to the Brownian motion of the segments is:

$$F_B = \frac{-kT \, \partial \, \mathrm{Ln} \, \psi \, (x_j)}{\partial \, x_j} \tag{4}$$

where ψ is the distribution function of the segments in the molecule. A differential equation describing ψ may be obtained by solving the force balance for $\dot{x}_j$ and substituting this quantity in the continuity equation,

$$\frac{\partial \psi}{\partial t} = -\nabla(\psi \, \dot{x}_j) \tag{5}$$

Equation 5 is solved by transforming the spacial coordinates x_j to a set of normal coordinator, r_j. The complex viscosity of a dilute solution may then be calculated by averaging the energy dissipated by the molecule over all possible conformations, ψ.

$$\eta^* = \frac{-n}{\dot{\gamma}^2} \left\langle \sum F_j \cdot v_j \right\rangle \tag{6}$$

The model predicts that the steady state shear compliance, J_e^o, is proportional to molecular weight. In general this behavior is observed in dilute solutions of polymers. This model also successfully predicts the concentrated solution and melt response of low MW polymers with narrow MWD's.

However, at high MWs, intermolecular interactions become important. Experimentally, J_e^o becomes independent of M at high MWs. This change in the properties is attributed to the formations of an "entanglement network" in which the intermolecular interactions are thought to act as temporary cross links. These intermolecular interactions may be

incorporated in the Rouse-Zimm model of molecular motion. Initially an entanglement can be considered to be a frictional interaction which lowers the mobility of the involved segment. Chompff (3) has applied this idea to the Rouse-Zimm theory (1,2) by changing the mobility of the segment by δ at selected points along the molecule. The solution of the resulting equations gives the relaxation spectra of the molecule in terms of a sum of the relaxation spectra of sub-sections of this molecule, which in turn, are functions of the number of involved entanglements and the parameter δ. This experimental parameter can be obtained by fitting data to the prediction of the theory. In general, δ is found to be a very small number, typically of the order of 10^{-5} for high MW systems. Thus, in order to explain the experimental data, the Chompff theory (3) essentially eliminates the displacements of the entanglement point by, in effect, coupling all the drag forces of the entanglement network to this point.

The author believed that this approach not only overestimated the change in the mobility of an entanglement point, but also neglected the important elastic properties of the entanglement network. This appendix outlines an attempt to incorporate the viscous and elastic effects of the entanglement network into the Rouse-Zimm model, with the specific goal of obtaining an analytical expression for J_e^o.

Each connecting chain in the entanglement network is analogous to a segment in the Rouse-Zimm model (1,2). Independent motions of the entanglement points are opposed by both the statistical nature and the viscous drag forces associated with the network segment. If the equilibrium distance between entanglement points is b_e, the

effective force constant is $3kT/\langle b_e^2 \rangle$. Equation 3 then becomes

$$F_{E_j} = \frac{-3kT}{\langle b^2 \rangle} \left[-x_{j-1} + 2x_j - x_{j+1} + \chi \, (x_j - x_{jo}) \right] \tag{7}$$

where x_{jo} is the equilibrium position of the entanglement point and $\chi = \langle b^2 \rangle / \langle b_e^2 \rangle$. Completing the analogy, the viscous drag forces of the network segment may be considered to change the mobility of the entanglement point by a factor δ.

In matrix notation the time derivatives of the position vectors, x, are

$$\dot{x} = v_x - BkT\underline{H} \frac{\partial \ln \psi}{\partial x} - \frac{3kT}{\langle b^2 \rangle} B \, (\underline{H} \, (\underline{A} + \underline{E}) \, x - \underline{H} \, \underline{E} \, x_o) \tag{8}$$

with

$$\underline{H} = \begin{bmatrix} 1 & & & & & \\ & 1 & & & & \\ & & \delta & & & \\ & & & 1 & & \\ & & & & \ddots & \\ & & & & & \delta \\ & & & & & & 1 \end{bmatrix} \quad ; \quad \underline{A} = \begin{bmatrix} 1 & -1 & & & & \\ -1 & 2 & -1 & & & \\ & -1 & 2 & -1 & & \\ & & & & \ddots & \\ & & & & 2 & -1 \\ & & & & -1 & 1 \end{bmatrix}$$

$$\underline{E} = \begin{bmatrix} 0 & & & & & \\ & 0 & & & & \\ & & \chi & & & \\ & & & 0 & & \\ & & & & \ddots & \\ & & & & & \chi \\ & & & & & & 0 \end{bmatrix}$$

Substituting this into the continuity equation, the equations for laminar flow ($v_{xj} = \dot{\gamma} z_j$, $v_{yj} = v_{zj} = 0$) are

$$\frac{\partial \psi}{\partial t} = \sum_{u=x,y,z} -\dot{\gamma} \frac{\partial \psi}{\partial x^T} z + D \frac{\partial}{\partial u^T} \underline{H} \frac{\partial \psi}{\partial u} + \left[\frac{\sigma \partial \psi}{\partial u^T} + \sigma \psi \frac{\partial}{\partial u^T} \right] \left[\underline{H}(\underline{A}+\underline{E})u - \underline{H} \, \underline{E} \, u_o \right] \tag{9}$$

where $D = 3kT$ and $\sigma = \frac{3kTB}{\langle b^2 \rangle}$. The eigenvalues of the matrix $\underline{H}(\underline{A} + \underline{E})$ define a transformation matrix $\underline{Q}$ such that

$$\begin{pmatrix} x \\ y \\ z \end{pmatrix} = \underline{Q} \begin{pmatrix} r \\ s \\ t \end{pmatrix} \quad ; \quad \begin{pmatrix} \frac{\partial}{\partial x} \\ \cdot \\ \cdot \end{pmatrix} = \underline{Q}^{-1^T} \begin{pmatrix} \frac{\partial}{\partial r} \\ \cdot \\ \cdot \end{pmatrix} \tag{10}$$

and $\underline{Q}^{-1}\ \underline{H}(\underline{A} + \underline{E})\ \underline{Q} = 1_k$. (11)

The transformation of equation 9 to the normal coordinates r, s and q yields the two additional matrix combinations $\underline{Q}^{-1}\underline{H}\ \underline{Q}^{-1^T}$ and $\underline{Q}^{-1}\ \underline{H}\ \underline{E}\ \underline{Q}$. Since $\underline{H}$ and $(\underline{A} + \underline{E})$ are symmetric matricies and $(\underline{A} + \underline{E})$ has a distinct set of eigenvalues, these matricies are diagonal. Define the eigenvalues to be:

$$\underline{Q}^{-1}\ \underline{H}\ \underline{E}\ \underline{Q} = E_k \tag{12}$$

$$\underline{Q}^{-1}\ \underline{H}\ \underline{Q}^{-1^T} = N_k \tag{13}$$

The normal coordinate equations for ψ in laminar flow then become:

$$\frac{\partial \psi}{\partial t} = -\dot{\gamma}\ \frac{\partial \psi}{\partial r^T} \cdot s + \sum_{u=r,s,q} [N_k\ D\ \frac{\partial^2 \psi}{\partial u^2} + \sigma\ \ell_k [\frac{\partial \psi}{\partial u^T} + \frac{\partial}{\partial u^T}] u \tag{14}$$

$$- \sigma\ E_k [\frac{\partial \psi}{\partial u^T} + \psi\ \frac{\partial}{\partial u^T}]\ u_o]$$

If $E_k = 0$, equation 14 is Zimm's differential equation for ψ, with $\underline{H}$ representing the effects of the change in mobility due to an

entanglement point, instead of the hydrodynamic interactions. The last term in equation 14 adds the elastic effects of entanglements in terms of the normal coordinates of the equilibrium positions u_o. In an advanced treatment the motion and slippage of an entanglement point may be analyzed by considering u_o to be a function of time and the normal coordinates of the system. In the following analysis u_o is assumed to be a fixed point in space.

The complex viscosity of the system can be calculated by equation 5. This requires a series of integrals involving various products of ψ, u and $\partial\psi/\partial u$. These integrals may be evaluated by multiplying equation 14 by appropriate combinations of u and integrating over all space. This yields a series of first order time dependent differential equations. If the shear rate $\dot{\gamma}$ is assumed to be sinusoidal and transient terms are neglected the complex viscosity becomes

$$\eta^* = \eta' - i\,\eta'' = nkT \sum_j \left[\frac{\tau_j(1 - i\omega\tau_j)}{(1 + \omega^2\tau_j^2)} + C_j \frac{2\tau_j(1 - i\omega 2\tau_j)}{(1 + 4\omega^2\tau_j^2)}\right] \qquad (15)$$

where $\tau_j = \dfrac{1}{2\sigma\ell_j}$ and $C_j = \dfrac{\sigma}{D} \dfrac{E_j^2 r_{jo}^2}{\ell_j N_j^2}$

As expected, the first term in equation 15 is the result of the Rouse-Zimm model. The elastic properties of the entanglement network add a second set of relaxation times which include the mobility parameter δ.

Evaluation of the eigenvalues yields

$$C_j = \frac{n_e^2}{\pi^2 j} \qquad j \leq n_e \tag{16}$$

$$C_j = 0 \qquad j > n_e \tag{17}$$

where n_e is the number of entanglements per molecule, $\frac{M}{M_e}$.

The relaxation times τ_j, also depend on n_e. In terms of the reduced mobility coefficient, δ, and the longest relaxation time, τ_1 they become

$$\tau_j = \tau_1/\delta j^2 \qquad j \leq n_e \tag{18}$$

$$\tau_j = \tau_1/j^2 \qquad j > n_e \tag{19}$$

The goal of the preceeding analysis was to obtain an analytical expression for the steady state shear compliance of high MW systems. This quantity may be calculated from the real and imaginary components of the complex viscosity given in equation 15.

$$J_e^o = \frac{M}{\rho RT} \frac{\sum_{j=1}^{n_e} \frac{1}{j^4\delta^2}\left(1 + \frac{4n_e^2}{\pi^2 j}\right) + \sum_{j=n_e+1}^{n} 1/j^4}{\left[\sum_{j=1}^{n_e} \frac{1}{j^2\delta}\left(1 + \frac{2n_e^2}{\pi^2 j}\right) + \sum_{j=n_e+1}^{n} 1/j^2\right]^2} \tag{20}$$

When $n_e = 0$ equation 20 reduces to the Rouse prediction for the steady state shear compliance:

$$J_e^o = \frac{Z(4)}{Z(2)} \frac{M}{\rho RT} \tag{21}$$

where

$$Z(a) = \sum_{j=1}^{\infty} 1/j^a \tag{22}$$

The functions Z(a) converge rapidly when $a \geq 2$. Therefore, the compliance of high MW systems, (i.e., large n_e) becomes

$$J_e^o \approx \frac{M}{\rho RT} \frac{Z(4)}{Z(2)} \frac{[1 + 4n_e^2 Z(5)/\pi^2 Z(4)]}{[1 + 2n_e^2 Z(3)/\pi^2 Z(2)]^2} \tag{23}$$

Thus, this model predicts that the compliance of high MW systems is independent of the mobility of the entanglement points and is proportional to M^{-1}. This latter prediction is in disagreement with the experimentally observed MW independence of J_e^o.

A more basic deficiency in the model becomes apparent when the parameter δ is evaluated. Following Rouse, the characteristic time τ_1, can be related to the zero shear viscosity of low MW systems, η_{oL}. In terms of the zero shear viscosity of high MW systems, η_{oH}, the parameter δ becomes:

$$\delta = \frac{\eta_{oL}}{\eta_{oH}} [1 + 2 \frac{Z(3)}{Z(2)} n_e^2] \tag{24}$$

Under the assumption that $\eta_{oL}/\eta_{oH} = M/M^{3.5}$, equation 15 requires the entanglement mobility coefficient δ to be proportional to $M^{-1/2}$. The frequency dependence of the entanglement relaxation processes is controlled by the intensity function $1/[1 + (\omega\tau_1/\delta)^2]$ (see equation 15). Therefore, while η_o has been forced to be proportional to $M^{3.5}$, the frequency dependence of the predicted VE functions changes only by $M^{1/2}$. However, this time scale change is experimentally found to have the same

MW dependence as η_o. Thus the proposed model not only predicts an unobserved MW dependence of J_e^o, but also requires an unreasonably low MW dependence of the entangled relaxation processes.

Therefore the explicit incorporation of the elastic effects of entanglements in the Rouse-Zimm theory does not explain the unusual elastic properties of high MW polymer melts.

REFERENCES

1. P. E. Rouse, Jr., J. Chem. Phys., 21, 1272 (1953).

2. B. H. Zimm, J. Chem. Phys., 24, 269 (1956).

3. A. J. Chompff and W. Prins, J. Chem. Phys., 48, 235 (1968).